



University of Kentucky
UKnowledge

Theses and Dissertations--Plant and Soil
Sciences

Plant and Soil Sciences

2016

PROBING THE PLANT CELL WALL WITH HERBICIDES: A CHEMICAL GENETICS APPROACH

Chad B. Brabham

University of Kentucky, chadbrabham@gmail.com

Digital Object Identifier: <https://doi.org/10.13023/ETD.2016.453>

[Right click to open a feedback form in a new tab to let us know how this document benefits you.](#)

Recommended Citation

Brabham, Chad B., "PROBING THE PLANT CELL WALL WITH HERBICIDES: A CHEMICAL GENETICS APPROACH" (2016). *Theses and Dissertations--Plant and Soil Sciences*. 83.

https://uknowledge.uky.edu/pss_etds/83

This Doctoral Dissertation is brought to you for free and open access by the Plant and Soil Sciences at UKnowledge. It has been accepted for inclusion in Theses and Dissertations--Plant and Soil Sciences by an authorized administrator of UKnowledge. For more information, please contact UKnowledge@lsv.uky.edu.

STUDENT AGREEMENT:

I represent that my thesis or dissertation and abstract are my original work. Proper attribution has been given to all outside sources. I understand that I am solely responsible for obtaining any needed copyright permissions. I have obtained needed written permission statement(s) from the owner(s) of each third-party copyrighted matter to be included in my work, allowing electronic distribution (if such use is not permitted by the fair use doctrine) which will be submitted to UKnowledge as Additional File.

I hereby grant to The University of Kentucky and its agents the irrevocable, non-exclusive, and royalty-free license to archive and make accessible my work in whole or in part in all forms of media, now or hereafter known. I agree that the document mentioned above may be made available immediately for worldwide access unless an embargo applies.

I retain all other ownership rights to the copyright of my work. I also retain the right to use in future works (such as articles or books) all or part of my work. I understand that I am free to register the copyright to my work.

REVIEW, APPROVAL AND ACCEPTANCE

The document mentioned above has been reviewed and accepted by the student's advisor, on behalf of the advisory committee, and by the Director of Graduate Studies (DGS), on behalf of the program; we verify that this is the final, approved version of the student's thesis including all changes required by the advisory committee. The undersigned agree to abide by the statements above.

Chad B. Brabham, Student

Dr. Seth Debolt, Major Professor

Dr. Arthur Hunt, Director of Graduate Studies

PROBING THE PLANT CELL WALL WITH HERBICIDES: A CHEMICAL
GENETICS APPROACH

DISSERTATION

A dissertation submitted in partial fulfillment of the
requirements for the degree of Doctor of Philosophy in the
College of Agriculture at the University of Kentucky

By
Chad Brandon Brabham

Lexington, Kentucky

Director: Dr. Seth Debolt, Professor of Horticulture

Lexington, Kentucky

2016

Copyright © Chad Brandon Brabham 2016

ABSTRACT OF DISSERTATION

PROBING THE PLANT CELL WALL WITH HERBICIDES: A CHEMICAL GENETICS APPROACH

The primary cell wall is a highly organized multi-layered matrix of polysaccharides (cellulose, hemi-cellulose, and pectin). The ability of the rigid cell wall to sufficiently loosen to allow growth is a complex process that differs considerably between grasses monocots and dicots. Cellulose is the major structural component required for anisotropic cell expansion and is synthesized by CELLULOSE SYNTHASE A (CesA) proteins. Here, our objectives were two-fold: 1) dissect cell walls and cellulose biosynthesis in dicots and grasses using chemical biology and reverse genetic approaches 2) characterize and classify the inhibitory mechanisms of cellulose biosynthesis inhibitors (CBIs). A reverse genetics TILLING experiment was conducted to study *CesAs* in the model grass *Brachypodium* (Bd). New mutant alleles of *BdCesA1* and *BdCesA3* were identified and characterized. On average, *Bdcesa1*^{S830N} and *Bdcesa3*^{P986S} mutants had 15% and 8% less cellulose than wild type plants, respectively. No obvious vegetative growth phenotypes were detected in mutants. However, at reproduction, inflorescence stems of *cesa1*^{S830N} were 62% shorter than that of the wild type while *cesa3*^{P986S} mutants were 20% longer. To classify CBIs, time-lapse confocal microscopy data were used to categorize CBIs based on how they disrupted the normal tracking and localization of fluorescently labeled *CesAs*. Furthermore, biochemical and confocal microscopy data were used to characterize the putative CBI, indaziflam. Three different inhibitory mechanisms were discovered within the CBI mode of action. Next, CBIs were used as molecular probes to study grass cell walls. However, grasses were found to be inherently tolerant to isoxaben and other *CesA* targeting CBIs. Isoxaben-tolerance was investigated but could not be explained by target and non-target site mechanisms. Thus, it was hypothesized mixed linkage glucans (MLGs), a unique grass cell wall polysaccharide, have cell wall strengthening characteristic and may partially compensate for reduced cellulose content. *Bdcslf6* mutants deficient in MLGs were 2.1 times more susceptible to isoxaben than wild type plants indicating MLGs do have a structural role in expanding cells, but likely cannot explain tolerance. These data, collectively, support a conclusion that the non-cellulosic fraction of grass primary cell walls has more load-bearing capacity than dicot cell walls.

KEYWORDS: cellulose biosynthesis inhibitors, Brachypodium, indaziflam, isoxaben, cellulose synthase, cell walls

Chad Brabham

12/7/16

PROBING THE PLANT CELL WALL WITH HERBICIDES:
A CHEMICAL GENETICS APPROACH

By

Chad B. Brabham

Dr. Debolt

Director of Dissertation

Dr. Hunt

Director of Graduate Studies

12/7/16

TABLE OF CONTENTS

LIST OF TABLE	v
LIST OF FIGURES	vi
Chapter 1 : Chemical Genetics to Examine Cellulose Biosynthesis.....	1
1.1 Introduction.....	1
1.2 Chemical Genetics To Dissect Cellulose Biosynthesis	2
1.3 Classifying Inhibitor Phenotypes on CesaA in Living Tissue.....	3
1.3.1 CesaA Clearing From Plasma Membrane	5
1.3.2 Stopping of CesaA Plasma Membrane Mobility	6
1.3.3 Modifying CesaA Trajectory	7
1.4 Chemical Genetics: Resistance or Hypersensitivity Loci	8
Chapter 2 : Cellulose Biosynthesis Inhibitors - A Multifunctional Toolbox.....	11
2.1 Introduction	11
2.2 Cellulose Biosynthesis in Plants	12
2.3 Cellulose Biosynthesis Inhibitors	13
2.4 How to Identify a CBI and its MOA.....	14
2.5 Recently Characterized CBIs.....	15
2.6 CBI Classification System	20
2.7 Difference in Sensitivity to CBIs Seen in Monocotyledons Versus Dicotyledons	24
2.8 CBIs and the Across Kingdom View of Cellulose Synthesis	25
2.9 Conclusion	27
Chapter 3 Indaziflam herbicidal action: a potent cellulose biosynthesis inhibitor	28
3.1 Abstract.....	28
3.2 Introduction.....	29
3.3 Results.....	30
3.3.1 Indaziflam Treated Seedlings Exhibit CBI Symptomologies	30
3.3.2 Indaziflam Inhibits Cellulose Biosynthesis	32
3.3.3 Isoxaben- and Quinoxiphen-Resistant Plants Are Not Cross-Resistant to Indaziflam	32
3.3.4 Indaziflam Caused Reduced Particle Velocity and Increased Accumulation of CESA Particles at the PM Focal Plane	34
3.3.4 Reduced CESA Velocity After Indaziflam Treatment is CSI1 Independent	37
3.4 Discussion.....	37
3.5 Materials and Methods.....	43
Chapter 4 TILLING Brachypodium Cellulose Synthase A Genes	46
4.1 Introduction.....	46
4.2 Results.....	48
4.2.1 Identification of Brachypodium Primary Cell Wall CesAs.	48

4.2.2 Targeting and Identification of BdCesA1 and BdCesA3 TILLING Mutants	50
4.2.3 Cellulose Content and Digestibility in Bdcesa3 ^{P986S} and Bdcesa1 ^{S830N} Mutants	50
4.2.4 Phenotype of Bdcesa3 ^{P986S} and Bdcesa1 ^{S830N} TILLING Mutants	53
4.2.5 Non-Cellulosic Cell Wall Composition	55
4.3 Discussion	55
4.4 Materials and Methods	60
Chapter 5 Probing Plant Cell Wall Biology in Grasses: A Function of Chemical Genetics and Herbicide Selectivity	65
5.1 Introduction	65
5.2 Results	67
5.2.1 Grasses Are Tolerant to a Chemical Diverse Subclass of CBIs.	67
5.2.2 Brachypodium Does Not Sufficiently Metabolize Isoxaben.	70
5.2.3 Known Resistance Conferring Point Mutations Are Not Found in BdCesAs.	70
5.2.4 CSLF6 Mutants are Hypersensitive to Isoxaben.	72
5.3 Discussion	74
References	86
Vita	105

LIST OF TABLE

Table 4.1 Total number and location of mutations identified in.....	51
Table 4.2 Quantification of non-cellulosic TFA soluble sugars and acetyl bromide soluble lignin content in the stem, sheath, and leaf of wild type and TILLING mutants.....	57
Table 5.1 List of primers used in all experiments.....	83

LIST OF FIGURES

Figure 1.1 The chemical toolbox for dissecting cellulose biosynthesis via live-cell imaging.	4
Figure 2.1 CBI screening and characterization..	16
Figure 2.2 A Venn diagram depicting the three groups of CBIs and the complex nature of the classification system.	19
Figure 2.3 Mutations in Cesa confer resistance to CBIs	23
Figure 3.1 Indaziflam is a fluoroalkyltriazine-containing compounds that inhibits elongation in seedlings of <i>P. annua</i> and <i>Arabidopsis</i>	31
Figure 3.2 Indaziflam treatments quantitatively inhibited the production of cellulose.	33
Figure 3.3 Indaziflam dose response and GR ₅₀ values of light-grown <i>Arabidopsis</i> genotypes.	35
Figure 3.4 Indaziflam treatment induced a higher density of CesAs at the PM.	38
Figure 3.5 Indaziflam reduced the velocity (particle movement rate) of YFP:CesA6	38
Figure 3.6 Indaziflam treatment decreased the net colocalization between MTs and YFP:CesA6 at the PM.	40
Figure 4.1 Characterizing relative transcript abundance of <i>Brachypodium</i> Cesa genes in 3-4 day old roots, shoots, and coleoptiles to determine primary cell wall Cesa.	49
Figure 4.2 Gene structure, protein topology, and TILLING region of BdCesA1 and BdCesA3.	52
Figure 4.3 Cellulose content in leaf, sheath, and stem from senesced wild type, <i>cesa3</i> ^{P986S} , and <i>cesa1</i> ^{S830N}	54
Figure 4.4 Comparing the growth characteristics of wild type, <i>cesa3</i> ^{P986S} , and <i>cesa1</i> ^{S830N} mutants.	56
Figure 5.1 Isoxaben root growth inhibition curves of <i>Brachypodium</i> , annual bluegrass, <i>Arabidopsis</i> , and soybean seedlings after 7 days on treatment.	69
Figure 5.2 <i>Brachypodium</i> does not sufficiently metabolize radiolabeled isoxaben after 72 hours of treatment.	71
Figure 5.3 The putative isoxaben targets in <i>Brachypodium</i> do not contain expected resistance conferring point mutations found in <i>Arabidopsis</i>	73
Figure 5.4 Characterization of <i>Brachypodium cslf6</i> mutants gene expression, glucose content, and susceptible to isoxaben.	75

Chapter 1 : Chemical Genetics to Examine Cellulose Biosynthesis

1.1 Introduction

A chemical inhibitor approach utilizes bioactive small molecules instead of genetic lesion to disrupt protein function and have been applied to answer many fundamental questions in plant science (Zhao et al., 2003; Armstrong et al., 2004; Surpin et al., 2005; Rojas-Pierce et al., 2007; Bassel et al., 2008; De Rybel et al., 2009; Park et al., 2009; Santiago et al., 2009; Ovecka et al., 2010; Drakakaki et al., 2011). There are some exploitable differences between chemical and traditional genetics. Small molecules can be employed to help circumvent lethal loss-of-function mutations. Alternatively, an inhibitor can overcome genetic redundancy that results in masking of the mutant phenotype by targeting a clade of common gene products with a single mechanism of action (Robert et al., 2009; Toth and van der Hoorn, 2009). However, challenges can arise with compounds that display broad inhibitor activity on a large class of structurally similar proteins that function in subtly different ways or where the mechanism of action has not fully been elucidated making it difficult to appropriately interpret plant response. In an ideal setting a small molecule can provide experimental flexibility allowing for use at precise temporal points for rapid, yet reversible inhibition of a target pathway.

Drug dose rates are generally tuneable, which allows for a range of phenotypes to be observed over various concentrations. For example, a tuneable gradient could be used to generate a dose that barely compromises or completely inhibits growth. The mid range dose, named the lethal dose 50 (LD50). This tuneable nature of inhibitors can then be combined with mutagenesis studies in plants to isolate mutants that are resistance to the LD50 or hyper- sensitive to a dose that barely compromises plant growth. The hypothesis is that a resistant or hypersensitive mutant will provide new genetic elements involved in a target pathway.

***This chapter was originally published as: Brabham, C and Debolt, S. 2013.**

Chemical genetics to examine cellulose biosynthesis. *Frontiers in Plant Sci.* 3:309.

Copyright permission was granted by the authors for inclusion in this dissertation.

Frontiers is an open access journal and authors own content.

Examples of this type of experimental design will be referred to for cellulose biosynthesis inhibition. The overarching challenge has been to isolate a genetic mutation that confers resistance in an ethyl methane sulfonate treated population, which are often missense mutations. Map-based cloning is then needed, which traditionally required hundreds if not thousands of segregating individuals (Scheible et al., 2001). With the advent of next-generation sequencing it is now feasible to map single base pair mutations using a small number of homozygous individuals within a mapping population (around 20). This will reduce the raw material requirements of map-based cloning efforts to hours rather than months (see Vidaurre and Bonetta, 2012 for further information). Moving from a drug-induced phenotype to a genetic component required a substantial resource investment. As we review herein, the use of cell biology to examine cellulose biosynthesis inhibitors (CBIs) has been a valuable intermediary that allows the researcher to explore the mechanism by which cellulose synthase A (CESA) responds to the drug, and secondly learn more about CESA behavior in living cells. The current mini-review provides an overview of the developing toolbox of compounds that perturb cellulose biosynthesis.

1.2 Chemical Genetics To Dissect Cellulose Biosynthesis

In plants, anisotropic cell growth is facilitated by a rigid, yet extensible cell wall, which acts to collectively constrain internal turgor pressure. Cellulose forms the central load-bearing component of cell walls and is necessary for plant cell expansion. Hence, inhibiting cellulose biosynthesis causes radially swollen tissues in seedlings providing a robust phenotype for genetic screens. In contrast to the Golgi-fabricated hemicellulose and pectin carbohydrate units in the cell wall matrix, plants synthesize cellulose at the plasma membrane by a globular, rosette-shaped, protein complex, collectively referred to as cellulose synthase complex (CSC; Mueller and Brown, 1982; Haigler and Brown, 1986; Brown, 1996). The CSC contains a number of structurally similar CESA catalytic subunits (Pear et al., 1996; Saxena and Brown, 2005) that extrude *para*-crystalline microfibrils. Microfibrils are made up of multiple, unbranched, parallel (1,4) linked β -D-glucosyl chains. The predicted membrane topology of a typical plant CESA

has a cytoplasmic N-terminal region with a zinc-finger domain followed by two transmembrane domains (TMDs), a large cytoplasmic domain containing the catalytic motifs, and finally a cluster of six TMDs at the C-terminus. Hypothetical models based on this topology suggest that eight TMDs anchor the monomeric protein in the plasma membrane and create a pore through which a polymerizing glucan chain extrudes (Delmer, 1999).

Experimental evidence for the dynamic behavior of CESA in living plant tissue has arisen via the use of live-cell imaging (laser spinning disk confocal microscopy; Paredez et al., 2006). Trans- genic *Arabidopsis* plants carrying a fluorescent protein reporter on the N-terminal of CESA6 or CESA3 have demonstrated quantifiable behaviors of the CSC at the plasma membrane such as relatively constant velocity of the CSC at the plasma membrane focal plane ($\sim 250 \text{ nm}\cdot\text{min}^{-1}$). Furthermore, the presence of the CESA reporter has been aligned with a suite of intercellular compartments (Paredez et al., 2006; Crowell et al., 2009; Gutierrez et al., 2009). Examination of CESA behavior in combination with CBI treatments can provide a platform to ask questions of the cell biology and will be examined herein. Unfortunately, plant CESA proteins have not been crystallized, nor has a functional CSC been purified *in vitro*, therefore the precise associations between CBIs and CESA are correlative. Nevertheless, the use of these inhibitors, as detailed below, has been of use in obtaining rational theories regarding the mechanism of delivery, activation, movement, and array organization during cellulose biosynthesis.

1.3 Classifying Inhibitor Phenotypes on Cesa in Living Tissue

Three principle responses to chemical inhibition have been documented via live-cell imaging thus far, and inferences can be made beyond live-cell imaging to cluster compounds into similar response groups. Each of the response phenotypes will be discussed independently below and are broadly summarized as (1) clearing of CESA from the plasma membrane focal plane, (2) stopping the movement of CESA, and (3) modifying the trajectory of CESA to or in the plasma membrane (Figure 1). Other CBI compounds have been characterized, but experiments with real-time confocal imaging of fluorescently tagged CESA have not been performed and are not discussed, accordingly.

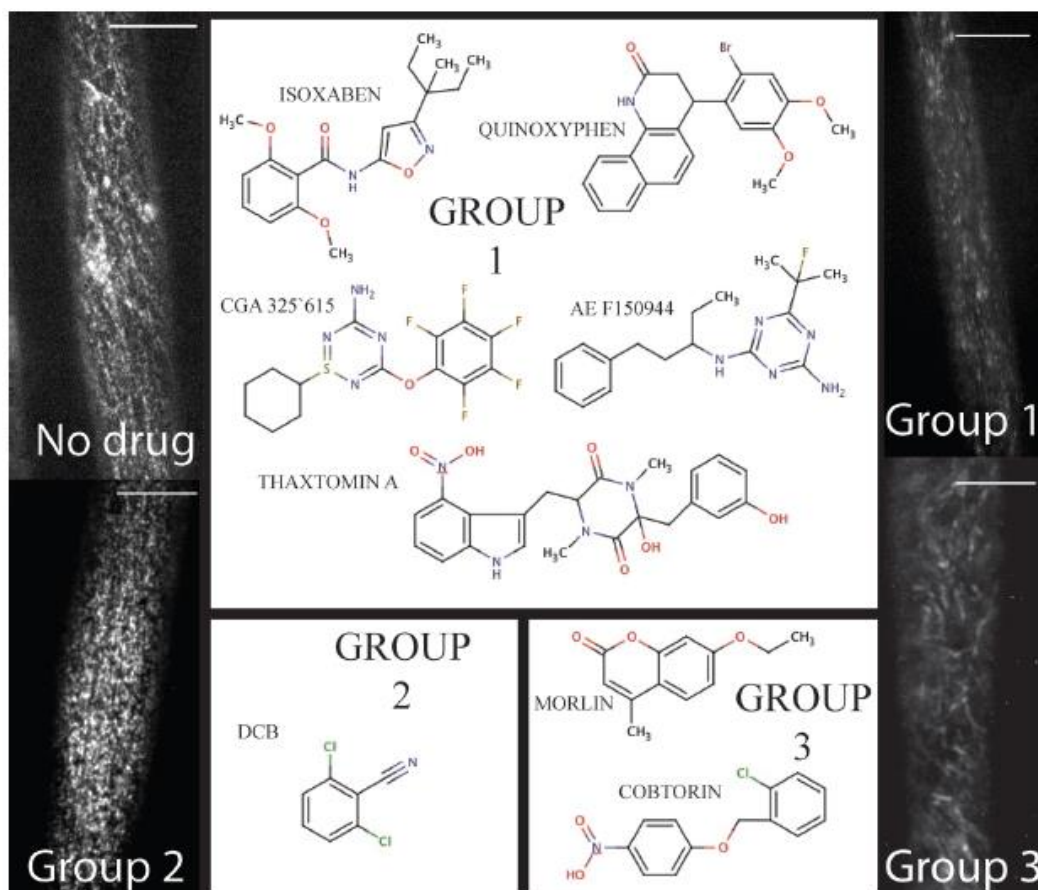


Figure 1.1 The chemical toolbox for dissecting cellulose biosynthesis via live-cell imaging. Group 1 includes compounds such as isoxaben and tanxtomin A that induce clearance of CesA from the plasma membrane. By contrast, Group 2 is comprised of DCB, which causes a syndrome of reduced CesA velocity and hyperaccumulation at the plasma membrane. Finally, morlin and cobtorin (Group 3) induce the plasma membrane localized CesA to move with aberrant trajectory and cause reduced CesA movement. For each example, the scale bar =10uM

1.3.1 Cesa Clearing From Plasma Membrane

The first group includes compounds that deplete the CSC from the plasma membrane (Figure 1 – Group 1). CBIs in this group include isoxaben (N-[3-(1-Ethyl-1-methylpropyl)-5-isoxazolyl]-2,6-dimethoxybenzamide), thaxtomin A ((4-nitroindol-3-yl- containing 2,5-dioxopiperazine), AE F150944 (N2-(1-ethyl-3-phenylpropyl)-6-(1-fluoro-1-methylethyl)-1,3,5-triazine-2,4-di- amine), CGA 325'615 (1-cyclohexyl-5-(2,3,4,5,6-pentafluorophe-noxyl)-1λ4,2,4,6-thiatriazin-3-amine), and quinoxiphen (4-(2-bromo-4,5-dimethoxy-phenyl)-3,4-dihydro-1H-benzo-quinolin-2-one) (Paredes et al., 2006; Bischoff et al., 2009; Crowell et al., 2009; Gutierrez et al., 2009; Harris et al., 2012). All of the com- pounds are synthetically derived, except for thaxtomin A, which is a phytotoxin produced by *Streptomyces* species pathogenic to potato and other taproot crops (Scheible et al., 2003). Forward genetic screens have identified point mutations that confer resistance to isoxaben in CESA3 and CESA6 (Heim et al., 1989; Scheible et al., 2001; Desprez et al., 2002), and quinoxiphen-resistance in CESA1 (Harris et al., 2012). This data further supports the notion that CESA1, 3, and 6 interact to form a functional CSC required for primary cell wall biosynthesis, since both compounds affect YFP-CESA6 similarly in susceptible seedlings (Baskin et al., 1992; Persson et al., 2007; Gutierrez et al., 2009; Harris et al., 2012). Moreover, quinoxiphen-resistance mutation was mapped to Ala903Val in *A. thaliana* CESA1, which has recently been aligned with Tyr455 in TMD6 of BCSB (Morgan et al., 2012). These authors demonstrate that Tyr455 forms a hydrogen bond to the translocating glucan during cellulose synthesis. Thus, quinoxiphen-resistance mutations are consistent with quinoxiphen action being inhibition of translocation rather than catalysis during cellulose biosynthesis.

Subsequent live-cell imaging (>20 min) after aforementioned drug treatment reveals that the plasma membrane eventually is devoid of CESA and fluorescently labeled CESAs accumulate in static and/or erratically moving cytosolic CESA containing compartments (SmaCC/MASC; Crowell et al., 2009; Gutierrez et al., 2009). Several possible scenarios may result in the clearance phenotype. For instance, the activity of the CBI leading to CESA depletion from the plasma membrane might modify vesicular trafficking and stop CESA cargo from reaching the site of synthesis. Further, CBI activity could target many processes in the endomembrane system, changing the speed of

cycling, or modify CESA localization. It is also not possible to rule out that depletion of CESA from the plasma membrane is the result of natural protein turnover ($< GhCESA1$ half life < 30 min; Jacob-Wilk et al., 2006). Alternatively, drug treatment could cause disassembly of CSCs and induce CESA endocytosis. For instance, freeze-fracture images of AE F150944 treated *Z. elegans* tracheary elements provide data showing that the few detectable plasma membrane rosettes are destabilized (control diameter 24 nm vs treated 30 nm; Kiedaisch et al., 2003). Decoding how and why CESA is cleared from the plasma membrane is a keenly awaited result.

Cellulose biosynthesis inhibitors that clear the plasma membrane of CESA may be used to monitor non-CESA proteins associated with cellulose biosynthesis. For instance, clearance CBIs have been used to garner guilt by association logic for co-clearance of CESA and CESA-interacting proteins such as GFP:KOR1 (KORRIGAN1, Robert et al., 2005) and GFP:CSII (CELLULOSE SYNTHASE INTERACTING1, Bringmann et al., 2012). Although this alone fails to prove association, it adds to the usefulness of CESA clearance compounds outside of studying CESA behavior.

1.3.2 Stopping of Cesa Plasma Membrane Mobility

The second CESA response phenotype is increased accumulation and cessation of CSC movement in the plasma membrane (Herth 1987; DeBolt et al., 2007b). Currently this group consists of one compound, DCB (2,6-dichlorobenzonitrile; Figure 1 – Group 2). DCB, another synthetic herbicide marketed since the 1960s, is second only to isoxaben as an experimental probe (Sabba and Vaughn, 1999).

2,6-Dichlorobenzonitrile exhibits a broad range of activity on species with terminal complexes, regardless if it is in lower species with a linear-complex or the rosette form found in higher plants (Mizuta and Brown, 1992; Orologas et al., 2005; DeBolt et al., 2007b). This suggests that DCB targets cellulose synthesis in a range of organisms, however, in species with linear-terminal complex such as the red alga *Erythrocladia subintegra*, treatment resulted in disappearance from the plasma membrane (Orologas et al., 2005). An early clue toward the molecular function of DCB was discovered when an DCB analog was found to bind a small protein of 12 or 18 kDa from suspension-cultured tomato cell extracts or cotton fiber extracts, respectively (Delmer et al., 1987). The

amount of bound protein seemed to increase significantly at the onset of secondary cell wall synthesis in cotton fibers. Recently, the same DCB analog target using a biochemical approach was identified in hybrid aspen (*Populus tremula* × *tremuloides*) and found to be MAP20 (Rajangam et al., 2008). Microtubule-associated proteins (MAPs) have been shown to bind to microtubules (MTs) and play a role in the synthesis of the secondary cell walls in *Arabidopsis*, as the FRAGILE FIBER1 (FRA1) and FRA2 kinesin like proteins influence cellulose microfibril patterning in the inner wall of interfascicular fibers (Zhong et al., 2002; Burk et al., 2007). *In lieu* of this data, Wightman et al. (2009) used the confocal technique FLIP (fluorescence loss in photobleaching) to observe that DCB treatment also slowed CSC tagged YFP:AtCESA7 needed for secondary wall deposition. This could indicate that MAPs are necessary for primary and secondary cell wall development.

1.3.3 Modifying Cesa Trajectory

The third disruption mechanism of the CSC is co-disturbance of both CESA and cortical MT. The molecular rail hypothesis (Giddings and Staehelin, 1988), suggests that MTs act as a guidance mechanism for the CSC. Using dual labeled CESA and MT reporter lines this can be visualized in real time showing that coincident MT and CESA arrays are often perpendicular to the axis of elongation during expansion (Paredez et al., 2006). Interestingly, when MTs are pharmacologically depolymerized via the drug oryzalin, YFP-CESA6 plasma membrane trajectory (organization of direction) but not velocity was altered (Paredez et al., 2006; DeBolt et al., 2007a). The velocity or positional change over time suggests that the CSC is moving the plasma membrane while making cellulose (Paredez et al., 2006). Interpretation of this evidence implies that the force of glucan chain polymerization is responsible for CSC movement in the plasma membrane rather than MTs or MT motor proteins. Within this group of compounds that we clustered based on modifying CESA trajectory, some do not cause depolymerization of MTs. These compounds were identified in forward chemical genetic screens for compounds affecting cell wall synthesis and morphology (DeBolt et al., 2007a; Yoneda et al., 2007). The first of two compounds is a coumarin derivative, named morlin (7-ethoxy-4-methyl chromen-2-one; Figure 1 – Group 3). Analysis using live-cell imaging

of fluorescently labeled MAP4 (microtubule-associated protein-4) revealed that morlin caused a defect in cytoskeleton organization that actually hyper-bundled the MTs. The CESA arrays were also disorganized compared to control cells, but instead of clearing CESA from the plasma membrane, morlin treated cells displayed reduced CESA velocity that was independent of MTs. Likewise, in a similar screen looking for a swollen cell phenotype in tobacco BY-2 cells, cobtorin (4-[(2-chlorophenyl)-methoxy]-1-nitrobenzene) (Figure 1 – Group 3) was identified as a potent compound that distorts the behavior of both CESA and MT (Yoneda et al., 2007, 2010), not dissimilar to that of morlin. It was further discovered that pectin methylation mutants could decrease the effectiveness of cobtorin. Further elucidation of the feedback between CSCs and MTs in multiple cell types and growth phases will provide important data for pinpointing the mechanisms of cell shape acquisition and it is evident that small molecule inhibitors will be valuable tools in this endeavor.

1.4 Chemical Genetics: Resistance or Hypersensitivity Loci

As additional chemical screens are completed and new compounds are identified that target the cell wall, it is imperative that they be followed up with forward resistant or hypersensitive screenings for detection of new molecular players in cell wall biosynthesis. An example of a resistant screen was recently performed for the quino- line derivative, quinoxiphen. The resistant locus for this drug was determined through a map-based approach in *Arabidopsis* to *CESA1* (Harris et al., 2012). The quinoxiphen-resistant mutant also shows a growth phenotype only slightly reduced to that of wild-type, thus representing a viable, non-conditional mutation in *CESA1*. This screen followed the logic generated in the screen for isoxaben-resistant (*ixr*) mutants (Heim et al., 1989). Here, the loci conferring resistance to isoxaben were mapped to *cesa3^{ixr 1}* and *cesa6^{ixr 2}* (Scheible et al., 2001; Desprez et al., 2002). The mutations conferring resistance to isoxaben and quinoxiphen are not found near the putative active site for *CESA1*, *CESA3*, or *CESA6*. Rather, the resistance conferring mutations are located in the C-terminal TMD of these gene products. The TMD region mutations individually caused a reduction in the degree of crystallinity created by the inter- and intra chain hydrogen bonding between glucan chains comprising cellulose in the mutant plants (Harris et al., 2012). In turn, this

resulted in greater conversion of the cellulose within the biomass to fermentable sugars. This information may prove to be a significant finding for the lignin-cellulosic biofuel field. Further studies are needed to determine the usefulness of such mutations under field situations and to determine the biochemical rationale for such mutations.

While no resistant mutant has been identified for AE F150944 or CGA 325'615, a forward genetics resistance screen to thaxtomin A in *Arabidopsis* identified the gene *TXR1* (*THAXTOMIN RESISTANCE-1*) that encodes a novel small protein most likely involved in the regulation of a transport mechanism and thus may provide resistance by reducing plant uptake of thaxtomin A (Scheible et al., 2003). Specifically, N- and C-terminal GFP fusions to TXR1 were localized in the cytoplasm of tobacco leaf protoplasts, suggesting that the protein acts as a cytosolic regulator of a membrane protein rather than being a permanent component of a transporter complex. The focus of future studies will be to determine whether the GFP fusions correctly reflect the localization of TXR1 and with which proteins TXR1 interacts (Scheible et al., 2003). The identification of mutants of this nature are good examples of how resistance to a small molecule is not always target-site based and may occur by preventing the drug from reaching the site of action via metabolism, reduced uptake, or altered translocation. In the future, if forward resistance screens are successful toward AE F150944 or CGA 325'615, it will be interesting to learn whether the resistance loci map to CESA or to new molecular players in cellulose biosynthesis.

An example of an opposite screen, hypersensitivity, was performed using an EMS-mutagenized *Arabidopsis* population to the compound flupoxam (1-[4-chloro-3-[(2,2,3,3,3-pentafluoropropoxy)methyl]phenyl]-5-phenyl-1H-1,2,4-triazole-3-carboxamide) (Austin et al., 2011). Flupoxam is a characterized CBI as has not been examined using live-cell imaging (Hoffman and Vaughn, 1996). Two mutants were identified through the use of next-generation-mapping technology as *flupoxam hypersensitive 1* and 2 (*fph1*, *fph2*). The loci were identified as *ECTOPIC ROOT HAIR3* (*ERH3*) for the *fph1* locus and *OLIGOSACCHARIDE TRANS-MEMBRANE TRANSPORTER* (*OST3/OST6*) for the *fph2* locus. Neither *ERH3/FPH1* nor *ST3/OST6/FPH2* encoded known cell wall biosynthetic enzymes and consequently this screen identified potential regulators of cell wall composition (Austin et al., 2011).

Resistant- or hypersensitive-mutants to the compounds that perturbed the parallel alignment of pre-existing cortical MTs and nascent cellulose microfibrils have not been decoded for morlin however, success has been made with cobtorin. The target proteins are likely to have an important role in the relationship between MTs and microfibrils. Yoneda et al. (2007) employed the *Arabidopsis* FOX hunting library, an activation tagging technology that makes use of full-length cDNAs that create gain-of-function mutants. From approximately 13,000 FOX lines, three cobtorin-resistant lines were identified and mapped to a lectin family protein, a pectin methylesterase (AtPME1) and a putative polygalacturonase (Yoneda et al., 2010). This study goes on to show some important features of pectin in relation to the formation and orientation of cellulose microfibrils, which depends on the methylation ratio of pectin and its distribution (Yoneda et al., 2010), which has recently been experimentally explored by ^{13}C solid-state magic-angle-spinning NMR (Dick- Perez et al., 2011).

As described, identification of drug targets linked to novel mechanisms of action can delineate information that is difficult to obtain via classical reverse genetics and are powerful tools in elucidating the dynamics of plant cell walls. It is fully expected that additional inhibitory mechanisms exist and academia and industry are keenly waiting for them to be identified. We apologize to the authors of other papers that have provided significant information to this field, as it was not possible to discuss the entire range of chemical agents and experimental results.

Chapter 2 : Cellulose Biosynthesis Inhibitors - A Multifunctional Toolbox

2.1 Introduction

The primary cell wall is an elaborate matrix of polysaccharides interwoven among a relatively small amount of proteins and aromatic compounds (Vogel, 2008; Carpita, 2011). The interaction, rearrangement, and biochemical changes between these components give the cell wall its rigid, yet extensible architectural characteristic. The strongest element in the plant cell wall is a network of coalesced long linear chains of β -1, 4 linked glucose molecules, called cellulose microfibrils. Cellulose has evolved to serve as the structural reinforcement of the cell wall. As a chain of sugar units, cellulose displays a surprisingly high tensile strength (Somerville et al., 2004). Cellulose microfibrils are organized in respect to the growth state of a cell. For example, in cells undergoing rapid expansion, microfibrils are often aligned perpendicular to the axis of growth (Baskin, 2005). Disruption of cellulose biosynthesis or alteration of microfibril alignment in the cell wall causes loss of directional cellular expansion, resulting in cells becoming radially swollen and growth organs becoming dwarfed. In this review, recent advances in our understanding of cellulose chemical perturbation and regulation by small molecules will be discussed. Chemicals that inhibit plant growth are globally referred to as herbicides, but are also referred to as drugs, small molecules or chemical inhibitors. For simplicity, we use the term herbicide or cellulose biosynthesis inhibitor (CBI). Particular attention is paid to the use of advanced live cell imaging microscopy techniques and screening platforms for CBIs.

***This chapter was originally published as:** Tatento, M., **Brabham¹**, C., and Debolt, S. 2015. Cellulose biosynthesis inhibitors- A multifunctional toolbox *Journal of Experimental Botany* 67: 533-542. Copyright permission was granted by the authors and Oxford University Press for inclusion in this dissertation.¹ **First author and wrote the majority of paper with Dr. Debolt.**

2.2 Cellulose Biosynthesis in Plants

It is important to convey to the reader that cellulose biosynthesis is complex, particularly when considering potential CBI targets. Therefore, we will briefly review the process of cellulose biosynthesis before focusing on CBIs. Cellulose is synthesized at the plasma membrane (PM) by a multi-protein complex referred to as the cellulose synthase complex (CSC). CELLULOSE SYNTHASE A proteins (CESA) are the processive glycosyltransferases responsible for catalyzing the conversion of UDP-glucose to cellulose (Kimura et al., 1999). The CSC is likely pre-assembled in the Golgi (Haigler and Brown, 1986) and transported to the PM via the trans-Golgi network and ultimately by cortical micro-tubule-assisted vesicle trafficking (Paredes et al., 2006; Crowell et al., 2009; Gutierrez et al., 2009). A series of genetic experiments have shown that three different CESAs are needed to form a functional CSC (Taylor et al., 2003; Desprez et al., 2007; Persson et al., 2007). Furthermore, freeze fracture electron microscopy images have revealed that the PM bound CSC is a hexameric rosette-shaped complex (Saxena and Brown, 1997). It is believed that the CESA proteins in each subunit organize into a heterotrimeric complex (Desprez et al., 2007) that possibly involves a stoichiometry of 1:1:1 between these three different CESA subunits (Gonneau et al., 2014; Hill et al., 2014). Rationalizing the number of active CESAs in a CSC has been guided by estimates of the numbers of glucan chains in a microfibril. However, this is still an area of debate and has been revised from a commonly cited 36 glucan chains in a microfibril to an estimate of 18 (Fernandes et al., 2011) and more recently, ‘at least’ 24 (Wang and Hong, 2015).

Numerous accessory proteins are required for cellulose biosynthesis in plants, such as KORRIGAN, COBRA and CELLULOSE SYNTHASE INTERACTING protein 1 (CSI1/POM2), and CSI3. KORRIGAN, an endoglucanase (Roudier et al., 2005), physically interacts with the CSC (Mansoori et al., 2014; Vain et al., 2014) and is thought to offer an editing role for the arising cellulose strands. COBRA, a glycosyl-phosphatidyl inositol-anchored protein, is also required for cellulose biosynthesis (Lane et al., 2001). While COBRA’s catalytic role remains unclear it has recently been found that it is critical to maintaining cellulose structure (Sorek et al., 2014). Interestingly, KORRIGAN, COBRA, and CESA respond to CBI application in an analogous

manner, suggesting they are cognate members of a CSC. In addition, the microtubule-CSC binding protein complex CSI-1/POM2 and CSI3, which is thought of as a molecular cross linker (Gu et al., 2010; Bringmann et al., 2012; Li et al., 2014) was also found to interact with the CSC (Gu et al., 2010; Bringmann et al., 2012). Another such group of microtubule interacting accessory proteins that were recently described are the Companion of Cellulose synthase (CC) proteins (Endler et al., 2015). The catalytic function for the CCs is still under investigation but it appears to be a marker for micro-tubule recovery from salt stress.

As it relates to the potential targets for a CBI, an interesting facet of the cellulose biosynthetic process is its complexity. Aside from the catalytic CESAs, each of these accessory proteins are plant specific and are valid targets for a CBI herbicide. Post-translational modifications such as phosphorylation have also been identified and found to influence cellulose biosynthesis (Chen et al., 2010) and therefore it remains possible that targeted kinase inhibitors may induce a CBI-like mode of action.

2.3 Cellulose Biosynthesis Inhibitors

Group L herbicides have a mode of action that inhibits cell wall (cellulose) biosynthesis, as classified by the Herbicide Resistant Action Committee (HRAC), and are further subdivided by their structural chemistry. As chemical inhibitors of cellulose biosynthesis, cellulose biosynthesis inhibitors (CBIs) are useful for weed control in agriculture and are particularly used as pre-emergent herbicides in recreational lawns, golf courses, orchards, vineyards, and railroad tracks with a combined multi-billion dollar value. CBIs are of increasing importance in agriculture at present due to problematic rates of weed resistance to known herbicides and the development of resistance management strategies that involve multiple modes of action (MOAs). CBIs have no reported field resistance (Heap 2012), which makes them attractive in such strategies. However, Arabidopsis mutants have been generated that confer resistance (or at least tolerance) to CBIs (e.g. Heim et al., 1989; Harris et al., 2012). It is not clear why field resistance is not more prevalent. One possibility is that these resistance loci were isolated from populations of intentionally mutagenized Arabidopsis seed and are associated with a fitness penalty (Harris et al., 2009,

2012). While field resistance has not been observed to date, it appears quite possible that it could arise and a strategy of resistance management would be needed in any application regimen.

2.4 How to Identify a CBI and its MOA

For a compound to be classified as a CBI, it must meet three criteria: 1) treated seedlings exhibit characteristic CBI symptomology of stunted growth and radial swelling in rapidly expanding tissue (Fig. 1A, B) where ectopic lignification is sometimes evident (as shown in Fig. 1A-inset in red); 2) reduced cellulose content in a dose-dependent manner; and 3) rapidly (<2 h) inhibit the incorporation of ^{14}C -glucose into the cellulose fraction of cell walls (Fig. 1C). As stated above, the complexity of cellulose biosynthesis makes it difficult to further elucidate the potential inhibitory mechanisms of CBIs. A considerable breakthrough in examining cellulose biosynthesis was achieved almost a decade ago with the functional complementation of the *procuste-cesa6* mutant with a translational fusion between YFP and CESA6, driven by its native promoter (Paredes et al., 2006). This, along with advanced laser scanning (or spinning disc) confocal imaging systems, enabled the quantitative assessment of CESA behavior in living cells (Fig. 1D).

Live cell imaging of cellulose biosynthesis can also be applied to CBI MOA. Plants expressing the fluorescent protein reporter tagged CESA (CESA6, CESA3, and CESA5) are imaged within a 1–2 h period after exposure to a CBI/herbicide at a saturating rate (Fig. 1D). It is therefore assumed that the disruption is a direct result of the MOA rather than a pleiotropic effect. Short duration movies (5–10 min in length comprising 60–100 frames) of live plants expressing YFP:CESA6 are generated and compared between CBI treated and untreated tissue (Paredes et al., 2006; DeBolt et al., 2007b). Using qualitative and quantitative assessments of behavior of the CESAs, the MOA were then characterized. Interestingly, but perhaps not surprising considering the multiple proteins involved in cellulose biosynthesis, different CBIs caused markedly different symptoms. To try and use this advanced imaging data to classify CBIs, we developed a categorization system based on how a given CBI disrupts the normal

mobility and localization of fluorescently labeled CESA particles, both individually and in array (Brabham and DeBolt, 2012). The three different classification groups that have been proposed are CBIs that 1) cause clearance of CESA particles from the PM; 2) increase CESA accumulation in at PM accompanied by arrested (or slowed) CESA movement in the PM; and 3) induce modified CESA trajectory to PM and CESA speed at the PM focal plane. Recently, new CBIs have been discovered and characterized such as CESTRIN, indaziflam, and acetobixan (Brabham et al., 2014; Xia et al., 2014; Worden et al., 2015). Below we elaborate on the classification system and its potential use in understanding newly identified CBIs and complexity of cellulose biosynthesis.

2.5 Recently Characterized CBIs

Indaziflam

One of the interesting CBIs to be added to both the commercial and research space was indaziflam. Indaziflam, a member of the alkylazine family is active at μM concentrations and has a long soil residual making it an outstanding pre-emergent herbicide. The alkylazine scaffold has shown to be an excellent lead compound for CBI discovery and optimization. This group includes indaziflam, triaziflam, and AE F150944 (Grossman et al., 2001; Kiedaish et al., 2003; Brabham et al., 2014). However, relating structure to MOA within this group has been difficult as the inhibitory mechanism of triaziflam, AE F150944, and indaziflam do not appear to match (Grossman et al., 2001; Kiedaish et al., 2003; Gutierrez et al., 2009; Brabham et al., 2014). Interestingly, indaziflam treatment induced an increase in the number of fluorescently labeled CESAs particles at the PM (~30%), but these particles exhibited reduced velocity (by approximately 66%) in comparison to the untreated control CESAs (Brabham et al., 2014). Colocalization rates between microtubules and CESAs were nearly abolished upon indaziflam treatment (53% compared with 70% in untreated), but this could be partially attributed to the increase in CESA particles at the PM. Since this phenotype was quite similar to CESA behavior observed in *csi1-3* mutants (Gu et al., 2010; Lei et al., 2012), the authors asked whether indaziflam treatment phenotypes would be visible in the *csi1-3*

mutant background. No discernable differences were detected between the behavior of CESAs in wild type or *csi1-3*. It was concluded that the inhibitory mechanism of indaziflam does not require a functional CSII, however, this does not exclude

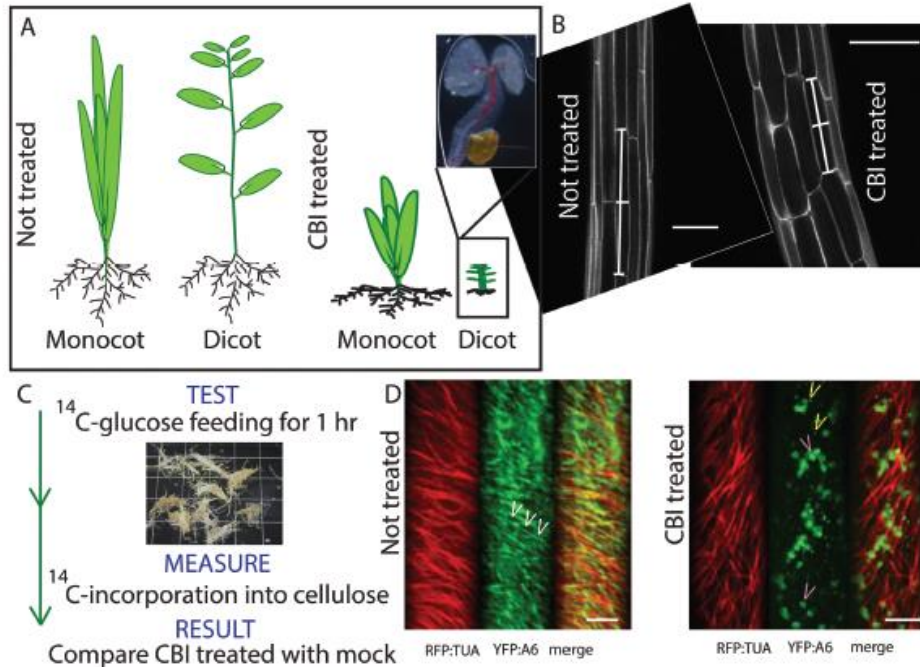


Figure 2.1 CBI screening and characterization. (A) Representation of the effect of CBIs on monocots and dicots as compared with their untreated counterparts. CBI treatment manifests itself in a dwarfed phenotype with ectopic lignification (see insert above CBI treated dicot). (B) CBI treated plant cells become radially swollen and irregularly shaped, which is visualized microscopically using a PIP:GFP (plasma membrane reporter) and laser scanning confocal microscopy (Xia et al. 2014). Scale bar=10uM. (C) The use of radioisotope tracer studies to track the amount of incorporation into cellulose is common in define a CBI. Here a CBI treated and untreated batch of seedlings are examined by ^{14}C glucose uptake and incorporation into cellulose. Inset is a batch of dark grown 7 day old etiolate seedlings that were grown in liquid culture prior to spiking with ^{14}C glucose and a CBI or no CBI (scale is indicated by the 1 cm squares on dish). (D) CBI elects behavioral change in population of CesA particles at the plasma membrane, cortex, or Golgi. Here, laser scanning or spinning disc confocal microscopy is used to image plant expressing RFP:TAU (red) and YFP:CesA6 (yellow) in CBI treated and untreated plants. As I shown in the left versus right panel comparisons, the treated results in the clearance of the CesA particles at the PM create linear tracks (white carats). By contrast in the treated panel where PM bound CesA is absent, the intracellular compartments are localized as either Golgi (pink carats) or SMACCs (yellow carats).

the potential requirement of CSI3 on CESA PM velocity. CSI3 is a homolog to CSI1 that also associates with the primary CSC and like CSI1 is required for normal velocity of the CSC as it moves along the microtubule tracks (Lei et al., 2013). The exact role of CSI3 is unknown and while it is not redundant with CSI1 it is dependent on it for its proper function (Lei et al., 2013). It would be of interest to see the effects of indaziflam on the *csi1 csi3* double mutant.

In contrast to indaziflam, AE F150944 (Kiedaish et al., 2003) appears to cause different subcellular symptomologies than indaziflam. AE F150944 treatment induced clearance of CESA particles from the PM focal plane with no noticeable influence on microtubule association (Gutierrez et al., 2009). Furthermore, freeze fracture electron microscopy images showed AE F150944 treatment caused the relatively few CSC observed at the PM to become fractured (Kiedaish et al., 2003), possibly a prelude to endocytosis and clearance from the PM. For triaziflam, no confocal or freeze fracture TEM images exist (Grossman et al., 2001).

CESTRIN

Another newcomer to the CBI family is CESTRIN (CESA Trafficking Inhibitor) (1-[2,6-dinitro-4-(trifluoromethyl) phenyl]-2-[6-methyl-4-(trifluoromethyl)pyridin-2-yl]hydrazine). CESTRIN was identified (Drakakaki et al., 2011; Worden et al., 2015) and found to be an efficacious CESA exocytosis inhibitor (Worden et al., 2015) that altered CSC trafficking in etiolated *Arabidopsis* hypocotyl cells from a screen of known pollen germination or endocytosis inhibitors (Drakakaki et al., 2011). Worden and authors (2015) showed that CESTRIN is not a broad trafficking disruptor, but is specific to the proteins associated with CSC trafficking. CESTRIN largely reduced the number of CSCs in the PM and those that were present displayed reduced movement. Accompanying these phenotypes, CESTRIN treatment preferentially increased the abundance of CESAs in Syntaxin of Plants 61 (SYP61) intercellular labeled compartments. SYP61 is involved in the trafficking of vesicles from the trans-Golgi network to the PM (Sanderfoot et al., 2001; Drakakaki et al., 2012). SYP61 has been found to co-localize with intercellular compartmentalized CSC (Crowell et al., 2009; Gutierrez et al., 2009) and through proteomic analysis of proteins found in SYP61 labeled vesicles (Drakakaki et al., 2012). As described

above, CESTRIN also influenced the PM population of CSC particles. After CESTRIN treatment, most of the CSC particles were cleared from the PM but some CSCs remained visible (Worden et al., 2015). However, the appearance of some CESAs at the PM can possibly be attributed to the relatively low rate used in this study (~3X) in comparison to other CBI studies (> 50X; X = rate reducing growth by 50%) (Crowell et al., 2009; Gutierrez et al., 2009). It is interesting that the MOA caused a slowdown in the remnant CSC particle movement at the PM. This may indicate a requirement for a specific CSC delivery rate or density to achieve normal movement. Alternatively, it may be that isoxaben and other CBIs that induce clearance (discussed in Group 1 below) all cause a slowdown of CSCs in the PM prior to complete clearance, which will be interesting to test experimentally.

Acetobixan

Acetobixan was discovered using subtractive metabolic fingerprinting from bacterial secretions (Xia et al., 2014). Specifically, the lead compound was isolated from a library of complex bacterial secretions and refined to one that induced synergistic reduction in root growth in the *AtcesA6^{prc1-1}* mutant compared with wild type seedlings (with and without treatment). Similar to several other CBI compounds described below as clearance compounds (Group 1), acetobixan caused clearance of YFP:CESA6 particles from the PM (Fig. 1D). Interestingly, mutants conferring resistance to quinoxiphen (Harris et al., 2012) or isoxaben (Scheible et al., 2001) were not cross resistant to acetobixan. These data infer that these CBIs may differentially disrupt the cellulose biosynthesis process.

Below, we explore the CBI classification system focusing on live cell confocal microscopy imaging of CESAs upon CBI treatment (Fig. 2A, B). We explore the potential to use confocal microscopy to study newly identified CBIs MOA, assess similarity between CBIs MOAs, and provide insights into the complexity of cellulose biosynthesis.

B. Classification system of CBIs

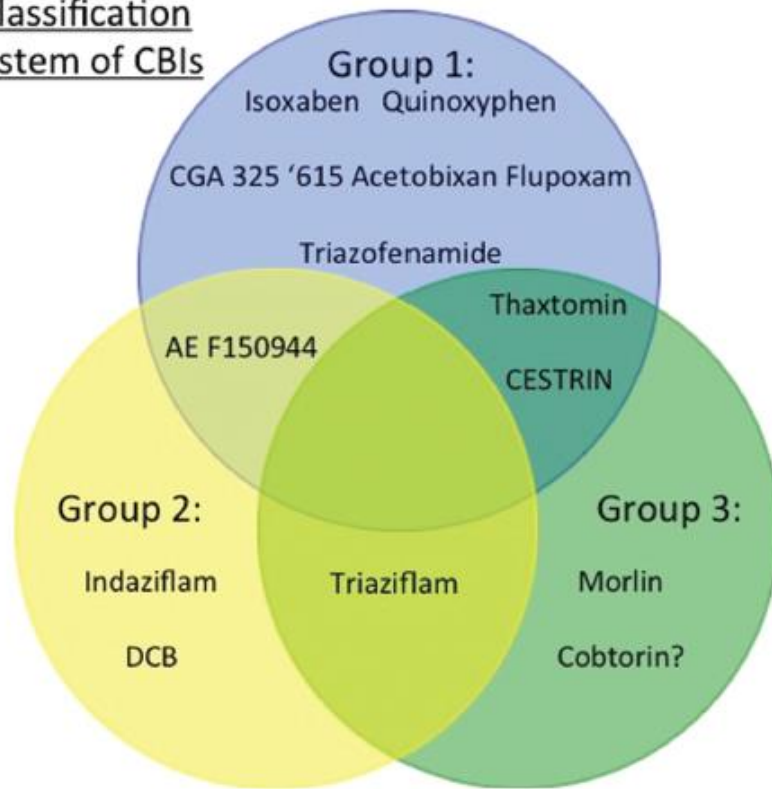


Figure 2.2 A Venn diagram depicting the three groups of CBIs and the complex nature of the classification system. The overlapping regions represent how a CBI can show a range of MOA that can pose a challenge to their classification. Not the question mark next to cobtorin indicates that while Yoneda et al. 2007 found evidence for irregular cellulose deposition trajectories, live cell imaging of CesA-reporter is needed to validate this classification.

2.6 CBI Classification System

Group 1: clearance of CSC from the PM focal plane

Compounds in Group 1 are based on the phenotype (cellular MOA) of fluorescently labeled CESA-containing CSCs being depleted from the PM focal plane and concomitantly accumulate in cytosolic vesicles. It is likely that all members of this group in fact elicit this phenotype but may do so by different mechanisms.

Furthermore, fluorescently labeled CESAs are visually being produced in the Golgi (donut-shaped fluorescence in images), but in one way or another fail to reach and be inserted into the PM. This was demonstrated clearly for the well studied CBI isoxaben (Paredes et al., 2006; Gutierrez et al., 2009). Compounds in this group include isoxaben (Gutierrez et al., 2009), quinoxiphen (Harris et al., 2012), AE F150944 (Gutierrez et al., 2009), CGA 325'615 (Crowell et al., 2009), thaxtomin A (Bischoff et al., 2010) and two new compounds CESTRIN (Worden et al., 2015) and acetobixan (Xia et al., 2014).

The molecular target of some members of Group 1 has been directly associated with CESAs (Fig. 3). Here, forward genetic screens are conducted using ethyl methyl sulfonate (EMS) mutagenized populations of Arabidopsis seed to look for resistance to CBIs among hundreds of thousands of individuals. From these screens, researchers have mapped resistance to multiple point mutations in AtCESA1, three or, six that confer resistance to isoxaben (Scheible et al., 2001; Desprez et al., 2002; Sethaphong et al., 2013) or quinoxiphen (Harris et al., 2012; Sethaphong et al., 2013) (Fig. 2). Resistance to the triazole carboxamides, triazofenamide and its more potent derivative flupoxam, has also been mapped to point mutation in AtCESA1 and AtCESA3 (Austin et al., 2011; Shim, 2014). Although, flupoxam and triaxofenamide meet the criteria to be classified as CBIs (Heim et al., 1998; Kudo et al., 1999; García-Angulo et al., 2012), their effect on fluorescently labeled CESAs is unknown. It will be interesting to examine their MOA by confocal microscopy in the future to determine their influence on CESA.

An alternative scenario where the PM can become devoid of CESAs is a result of severe alteration in the trafficking of CESA-containing vesicles between the trans-Golgi network and the PM (Drakakaki et al., 2011; Worden et al., 2015).

Delivery of CESA-containing vesicles to the PM is a highly coordinated process and is facilitated by microtubules and cargo transport proteins. Several advances have recently been made in this research area (Crowell et al., 2009; Gutierrez et al., 2009; Gu et al., 2010; Drakakaki et al., 2012; Bashline et al., 2013; Lei et al., 2013). Cortical microtubules, CSI1, CSI3, an adaptin protein μ 2, and the SYP61 have all been shown to partially coincide with CESA-containing vesicles indicating their importance in CESA trafficking and therefore could be viable CBI targets. Thaxtomin A is a CBI identified from necrotrophic *Streptomyces* spp. Resistance to thaxtomin A was previously mapped to a protein of an unknown function (Scheible et al., 2003). This protein was recently identified and characterized as the mitochondrial inner membrane protein import motor subunit called PAM16 (Huang and Fu, 2013). The authors concluded the loss of AtPAM16 limited the over-accumulation of reactive oxygen species required for cell death and thus provided resistance to *Streptomyces* spp. but not necessarily thaxtomin A (Huang and Fu, 2013). Therefore, it was likely the CBI tolerance was a secondary effect. Questions about the CBI activity of thaxtomin A and the internalization of PM bound CESAs remain unanswered. One possible theory is thaxtomin A activates the early endocytosis CESA-related pathway that has been associated with SYP61 and other accessory proteins (Zhu et al., 2002; Robert et al., 2008; Crowell et al., 2009; Gutierrez et al., 2009; Drakakaki et al., 2012; Luo et al., 2015). To corroborate this, supplementing treated plant with auxin-like compounds has been shown to ameliorate the toxicity of thaxtomin A (King and Calhoun, 2009; Tegg et al., 2013). Interestingly, auxin transport proteins (PIN2) have also been shown to be endocytosed by the SYP61-trafficking complex (Robert et al., 2008). Further research is needed to see if SYP61-sensitive proteins, for example BRI1 and PIN2, are sensitive to thaxtomin A induced internationalization.

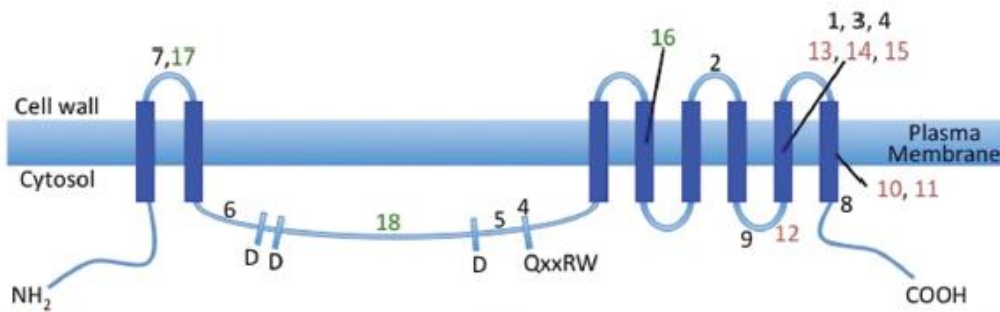
Group 2: increased CESA in PM and slowed or arrested movement

The second CESA classification group contains DCB (2,6-dichlorobenzonitrile) and indaziflam (Fig. 2B). The CESA phenotype induced by these CBIs is interesting in that more CESA particles accumulate at the PM (Herth,

1987; DeBolt et al., 2007b). Accompanying this increase in CESA abundance is an almost complete reduction of CSC velocity (DeBolt et al., 2007b), and while indaziflam (Brabham et al., 2014) too accumulated more PM bound CESA particles it elicits some interesting differences. DCB caused increased accumulation at specific foci at the PM focal plane resulting in brighter and brighter fluorescent ‘dots’ over a time series of 2 h. By contrast, indaziflam induced a more even distribution of particles across the PM. Another variation from DCB was that indaziflam treatment resulted in a reduction rather than cessation of CESA particle movement at the PM. Obtaining resistant mutants using a mutagenesis approach has been unsuccessful for both. To date, we have screened at least 20-times the number of mutagenized seed for indaziflam resistance than used to isolate several quinoxiphen resistant mutants (Harris et al., 2012; Brabham and DeBolt, unpublished). Similarly, no DCB resistant mutants have been identified despite similar efforts. A modestly tolerant (2–4X) DCB mutant DH75 was reported by Heim and coworkers (1989), which would be interesting to examine further.

Group 3: modifying CESA trajectory to and at the PM

No additional CBIs that fall under the designation of compounds that alters the trajectory of CESA particles to and at the PM have arisen in the past few years. The main CBI in this group is morlin (7-ethoxy-4-methyl chromen-2-one) (DeBolt et al., 2007a). Notably, morlin has the potential to elicit its primary influence on microtubules, which could in turn influence trajectories of CSCs at the PM. While indirect evidence also exists for another CBI named cobtorin (4-[(2-chlorophenyl)-methoxy]-1-nitrobenzene) (Yoneda et al., 2007, 2010), it has not been used in combination with YFP::CESA6 or other live cell CSC reporter. Cobtorin alters the methylation ratio and the distribution of pectin in the cell wall and was hypothesized to act by interfering with cellulose pectin associations. Resistance to cobtorin was also conferred by overexpressing a pectin biosynthetic gene (Yoneda et al., 2007, 2010). We tentatively place cobtorin as a Group 3 CBI based on existing cellulose and microtubule imaging data (Yoneda et al., 2007) but further work is



number	mutation	CBI	number	mutation	CBI
1	<i>cesa3</i> ^{ixr1-1} G ₉₉₈ D	isoxaben	10	<i>cesa3</i> ^{fp1-1} S ₁₀₄₀ K	flupoxam
2	<i>cesa3</i> ^{ixr1-2} T ₉₄₂ I	isoxaben	11	<i>cesa3</i> ^{fp1-2} S ₁₀₃₇ F	flupoxam
3	<i>cesa3</i> ^{ixr1-3} G ₉₉₈ S	isoxaben	12	<i>cesa3</i> ^{fp1-3} S ₉₈₃ F	flupoxam
4	<i>cesa3</i> ^{ixr1-4} R ₈₀₆ K	isoxaben	13	<i>cesa1</i> ^{fp2-1} G ₁₀₁₃ F	flupoxam
5	<i>cesa3</i> ^{ixr1-5} L ₇₉₇ F	isoxaben	14	<i>cesa1</i> ^{fp2-2} P ₁₀₁₀ L	flupoxam
6	<i>cesa3</i> ^{ixr1-6} S ₃₇₇ F	isoxaben	15	<i>cesa1</i> ^{fp2-3} G ₁₀₀₉ D	flupoxam
7	<i>cesa3</i> ^{ixr1-7} R ₂₇₆ H	isoxaben	16	<i>cesa1</i> ^{aegeus} A ₉₀₃ V	quinoxypfen
8	<i>cesa6</i> ^{ixr2-1} R ₁₀₆₄ W	isoxaben	17	<i>cesa1</i> ^{P2P5} R ₂₉₂ C	quinoxypfen
9	<i>cesa6</i> ^{ixr2-2} S ₁₀₀₂ F	isoxaben	18	<i>cesa1</i> ^{P3P4} G ₆₂₀ E	quinoxypfen

* The numbers on the figure depicts the approximate location of the various mutations

Figure 2.3 Mutations in CesaA confer resistance to CBIs (A) Plant CesaA diagram depicting the predicted eight transmembrane helices and the cytosolic catalytic region. (Note: diagram not to scale). The diagram is a visual representation of the location for the multiple published point mutations that have been demonstrated to confer resistance to CBIs within the primary cell CesaA (Cesa1,3,6) (Heim et al. 189; Scheible et al. 2001; Desprez et al. 2002; Harris et al. 2012; Sethaphong et al. 2014; Shim, 2014). The number on the diagram corresponds to the tabular listing of mutations below the schematic, to help the reader identify the exact location of the point mutation.

needed to examine it in Arabidopsis cells expressing YFP:CESA6 and compare its MOA with morlin.

2.7 Difference in Sensitivity to CBIs Seen in Monocotyledons Versus Dicotyledons

There has been a general trend for CBIs to inhibit dicot root elongation at lower rates as compared with monocots (Corio- Costet et al., 1991; Sabba and Vaughn, 1999).

This peculiarity could be due to a number of reasons such as seed size, metabolism, sequestration, herbicide uptake and translocation, or differences in the genetic composition. While seed size and metabolic differences are valid rationales, studies in plant tissue cultures have shown that tolerance to isoxaben in soybean nor wheat callus could not be explained simply by its metabolism or metabolic fate (Corio- Costet et al., 1991).

Alternatively, could the composition of the cell wall also influence CBI tolerance? For example, the primary cell wall composition varies between certain plants with dicots and liliaceous monocots having type I cell walls while type II cell walls are found only in the Poales (grasses) and related commelinid monocots (Carpita and Gibeaut, 1993; Carpita and McCann, 2008). When maize tissue and barley cultures (calli) are habituated in DCB and their cell wall analyzed, it was found that it was reduced in cellulose content, but increased in mixed linkage glucans or glucuronoarabinoxylan (GAX) and arabinoxylans, and it was hypothesized that the increase in cell wall phenolics could be a compensation mechanism for the 'cellulose impoverished cell wall' (Shedletzky et al., 1992; Mérida et al., 2010). If the cellulose biosynthetic carbon sink is halted, where does the metabolic pool destined for cellulose production go? ^{14}C glucose uptake studies suggest that it can be diverted to pectin and hemicelluloses (García-Angulo et al., 2012). This could be signifying a compensation mechanism in which the excess glucose is being utilized for hemi- cellulose (xyloglucan, heteroxylan) production in grasses and pectin production in dicots. With the notable differences in cell wall composition in the grasses, this diversion to alternative cell wall polysaccharides caused by the CBIs could differentially influence the response. Understanding this divergence will be interesting for the cellulose biosynthesis research community but also the broader weed science community.

2.8 CBIs and the Across Kingdom View of Cellulose Synthesis

The terminal complex extruding cellulose has significantly evolved overtime from a single linear array in the prokaryote *Gluconacetobacter xylinus* (Ross et al., 1991) to the solitary, hexagonal, rosette-shaped complex in land plants (Tsekos, 1999). We postulate that this divergence possibly explains the selectivity of CBIs towards plants, except for the non-selective nature of DCB on cellulose producing eukaryote (Mizuta and Brown, 1992; Orologas et al., 2005; DeBolt et al., 2007b). Another class of CBIs, the carboxylic acid amides (CAAs), has been commercialized to control cellulose producing oomycetes, for example *Phytophthora infestans* (Blum et al., 2010). There are no freeze fracture electron microscopy images of the terminal complex in oomycetes, but the C-terminus of PiCESAs has a similar predicted protein topology to plant CESAs (Somerville, 2006; Grenville-Briggs et al., 2008). Point mutations conferring resistance to CAAs have been mapped to the C-terminus of CESA3 in several oomycetes (Blum et al., 2012).

In cellulose producing prokaryotes, BcsA (bacterial CESA) is ‘activated’ with the binding of the allosteric agonist cyclic-di-GMP (Amikam and Galperin, 2006; Morgan et al., 2014). In the absence of cyclic-di-GMP, the catalytic pocket is blocked by interface helices 3 (IF3) (between trans-membrane helices 6 and 7 in BcsA) referred to as the gating loop, and is sterically hindered by the cytosolic C-terminus of BcsA. This inhibition is removed by a conformational change in the C-terminus upon cyclic-di-GMP binding (Morgan et al., 2014). However in eukaryotic CESAs, the cyclic-di-GMP binding site has been lost along with the majority of the cytosolic C-terminus, but the gating loop core sequence has remained fairly conserved (the amino acid residues FxVTxK in the IF between transmembrane helices 5 and 6 in *Arabidopsis*) (Slabaugh et al., 2014). The presence of such a gating loop has yet to be established in eukaryotic CESAs and may not exist. The clustering of CAA- and Group 1 CBI-resistant point mutations in the putative pore-forming trans-membrane domains of CESA orthologs (Blum et al., 2012; Sethaphong et al., 2013) begs the question of whether CESAs are under allosteric control (in the absence of CBIs) and what is the ligand?

CBIs and their subsequent resistant point mutations have proved useful in examining question in the absence of a crystallized plant CESA. For instance, the putative gating loop region (Slabaugh et al., 2014) has been shown to be required for AtCESA1 function. Here, an amino acid substitution from the conserved Phe to a Leu at position 954 in the gating loop resulted in dysfunctional CSCs (Slabaugh et al., 2014). This was further supported with live cell imaging of the mutated variant showing fluorescently labeled AtCESA1^{F954L} was not found to accumulate at the PM focal plane. It is important to note that null mutations in AtCESA1 are lethal and therefore transformations and experiments had to be performed at restrictive temperatures in the temperature sensitive *rws1* mutant background. Furthermore, in AtCESA3 a Thr to Ile substitution at position 942 in the conserved region of the gating loop confers a high level resistance to isoxaben. While a T942I in AtCESA3 does not disrupt protein function, it does have a significant effect on cellulose crystallinity (Harris et al., 2012; Griffiths et al., 2015).

The putative gated loop region appears important for CESA function. Could this region be important for the inhibitory mechanism of Group 1 CBIs? Analysis of computational data suggests that this region exists in a binary state as either 'up' or 'down' (Slabaugh et al., 2014). The two amino acid substitutions examined influence the preferred position, with the F954L favoring the conformational 'down' state, while T942I favored an 'up' state (Slabaugh et al., 2014). Based on this information, one possibility is that Group 1 CBIs act as steric inhibitors by preventing conformational change of CESAs from a 'off' to an 'on' state. This could explain why treatment with Group 1 CBIs results in a PM devoid of CSC as the complex is in an 'off' state. On the other hand, if this region is constitutively down or 'on' then a given CBI i.e. isoxaben may not bind to its cognate target. However, such mechanisms remain purely speculative and perhaps may be best aided by molecular dynamic simulations of the plant CESAs (Sethaphong et al., 2013) since no crystal structures are available.

2.9 Conclusion

Combining genetics with CBIs will continue to assist in elucidating the basic mechanisms of cellulose and cell wall biogenesis, and continued development of new and current CBIs is expected to be driven by their utility in cellulose biosynthesis research but also as weed control agents. The capacity for new inhibitory mechanisms of action in the broad CBI grouping is particularly of interest due to the lack on new herbicidal MOAs developed in the past decades. Additionally, breakthroughs in advanced cellular imaging techniques will also facilitate the use of CBIs as research tools to disrupt cellulose biosynthesis in a targeted way. Beyond cellulose, using chemical genetics to dissect other cell wall processes is anticipated. We highlight that screening natural compounds for future CBIs (Bischoff et al., 2010; Xia et al., 2014) may also be valuable to identify new MOAs.

Chapter 3 Indaziflam herbicidal action: a potent cellulose biosynthesis inhibitor

3.1 Abstract

Cellulose biosynthesis is a common feature of land plants. Therefore, cellulose biosynthesis inhibitors (CBIs) have a potentially broad acting herbicidal mode of action and are also useful tools in decoding fundamental aspects of cellulose biosynthesis. Here, we characterize the herbicide indaziflam as a CBI and provide insight into its inhibitory mechanism. Indaziflam treated seedlings exhibited the CBI-like symptomologies of radial swelling and ectopic lignification. Furthermore, indaziflam inhibited the production of cellulose within < 1 hour of treatment and in a dose dependent manner. Unlike the CBI isoxaben, indaziflam had strong CBI activity in both a monocotyledonous (*Poa annua* L.) and a dicotyledonous plant (*Arabidopsis thaliana* L.). *Arabidopsis* mutants resistant to known CBIs, isoxaben or quinoxiphen, were not cross resistant to indaziflam suggesting a different molecular target for indaziflam. To explore this further, we monitored the distribution and mobility of fluorescently labeled CELLULOSE SYNTHASE A (CESA) proteins in living cells of *Arabidopsis* during indaziflam exposure. Indaziflam caused a reduction in the velocity of YFP:CESA6 particles at the plasma membrane (PM) focal plane when compared to controls. Microtubule (MT) morphology and motility were not altered after indaziflam treatment. In the hypocotyl expansion zone, indaziflam caused an atypical increase in the density of PM localized CESA particles. Interestingly, this was accompanied by a cellulose synthase interacting 1 (CSI1) independent reduction in the normal coincidence rate between MT and CESA. As a CBI, for which there is little evidence of evolved weed resistance, indaziflam represents an important addition to the action mechanisms available for weed management.

***This chapter was originally published as: Brabham¹, C., Lei, L., Gu, Y., Stork, J., Barrett, M., and DeBolt, S. 2014. Indaziflam herbicidal action: A potent cellulose biosynthesis inhibitor. *Plant Physiology* 166: 1177-1185. Copyright permission was granted by the authors and *Plant Physiology*® for inclusion in this dissertation.¹ Co-First author- designed, conducted, and wrote manuscript. Confocal work was done by Lei Lei.**

3.2 Introduction

Cellulose is a composite polymer of β -1,4 linked glucan chains and is the main load bearing structure of plant cell walls (Jarvis, 2013). While cellulose is a relatively simple polysaccharide molecule, its synthesis is quite complex. The principle catalytic unit is a plasma membrane (PM) localized protein-complex referred to as the cellulose synthase complex (CSC) (Davis, 2012). In plants, the CSC, visualized with freeze fracture microscopy, is a solitary, hexagonal rosette shaped complex (Herth and Weber, 1984; Delmer, 1999) and at least three of the catalytic CELLULOSE SYNTHASE-A (CESA) proteins are required in each CSC for the production of cellulose (Desprez et al., 2007; Persson et al., 2007). In addition to CESAs, several accessory proteins have been discovered to be necessary for the production and deposition of cellulose, such as KORRIGAN (Lane et al., 2001), COBRA (Roudier et al., 2005) and CELLULOSE SYNTHASE INTERACTING-1 (CSI1) (Gu et al., 2010) and several others that have yet to be identified. The loss of function in any of the aforementioned proteins causes complete or partial loss of anisotropic growth in cells undergoing expansion resulting in radial swelling. Severe radial swelling in rapidly expanding tissue is also a common symptomology observed in seedlings treated with cellulose biosynthesis inhibitors (CBIs). Therefore, numerous potential herbicidal targets exist (mechanisms of action) for the broad group of known CBIs.

Classification of a herbicide to the CBI designation was traditionally achieved by short-term [^{14}C] radioisotope tracer studies focused on the incorporation of glucose into cellulose (Heim et al., 1990; Sabba and Vaughn, 1999). More recently, time-lapse confocal microscopy of reporter tagged CESA proteins (Paredes et al., 2006) has been used to further classify CBIs. CBIs can be classified into at least three primary groups based on how treatment disrupts the normal tracking and localization of fluorescently labeled CESAs (reviewed by Brabham and DeBolt, 2013). The disruption is assumingly the result of the inhibitory mechanism of the CBI. In the first group, isoxaben and numerous other compounds cause YFP:CESAs to be depleted from the PM and concomitantly accumulate in cytosolic vesicles (SmaCCs/MASC) (Paredes et al., 2006; Crowell et al., 2009; Gutierrez et al., 2009) The second group, consisting only of dichlobenil (DCB), causes YFP:CESAs to become immobilized and hyper-accumulated

at distinct foci in the PM (Herth, 1987; DeBolt et al., 2007b). The third group influences CSC-microtubule (MT) associated functions resulting in errant movement and localization of YFP:CESAs (DeBolt et al., 2007a; Yoneda et al., 2007). These different disruption processes suggest each CBI group targets a different aspect of the complex cellulose biosynthetic process.

A lack of evolved weed resistance in the field suggests CBIs are potentially underutilized tools for weed control (Sabba and Vaughn, 1999; Heap, 2014). CBIs have also been useful research tools in decoding fundamental aspects of cellulose biosynthesis. An exogenous application of a CBI provides spatial and temporal inhibition of cellulose. Resistance screens to CBIs have uncovered key genes in cellulose biosynthesis (Scheible et al., 2001; Desprez et al., 2002). Further, CBIs such as isoxaben have also been effective in linking accessory proteins with CESAs in the CSC (Robert et al., 2005; Gu et al., 2010). Therefore, it is important to extend our range of CBI compounds. Recently, indaziflam (Fig 1A), a herbicide introduced by Bayer Crop Science, was proposed to be a CBI and reported to have a pI50 value of 9.4 (Meyer et al., 2009; Dietrich and Laber, 2012). Indaziflam is labeled for use in turf, perennial crops, and for non-agricultural situations for pre-emergent control of grasses and broadleaf weeds (Meyer et al., 2009; Brosnan et al., 2011). The aim herein was to investigate indaziflam as a CBI and to characterize its inhibitory effect on cellulose biosynthesis.

3.3 Results

3.3.1 Indaziflam Treated Seedlings Exhibit CBI Symptomologies

Dicotyledonous *Arabidopsis thaliana* L. and monocotyledonous *Poa annua* L. were germinated and grown on plates for seven days with various concentrations of indaziflam. Seedlings were grown using either a light (24:0 h light:dark) or dark (0:24 h light:dark) growth regimen to promote root or hypocotyl expansion, respectively. Both *P. annua* and *Arabidopsis* were susceptible to indaziflam and their growth was inhibited in a dose dependent manner (Fig 1B to 1D). The GR₅₀ values (growth reduced by 50%) for light-grown *P. annua*, dark-grown *Arabidopsis*, and light-grown *Arabidopsis* were 671 μ M, 214 μ M, and 200 μ M of indaziflam, respectively (Fig S1; See online version Brabham et al. 2014). The similar GR₅₀ values between the light- and dark-grown

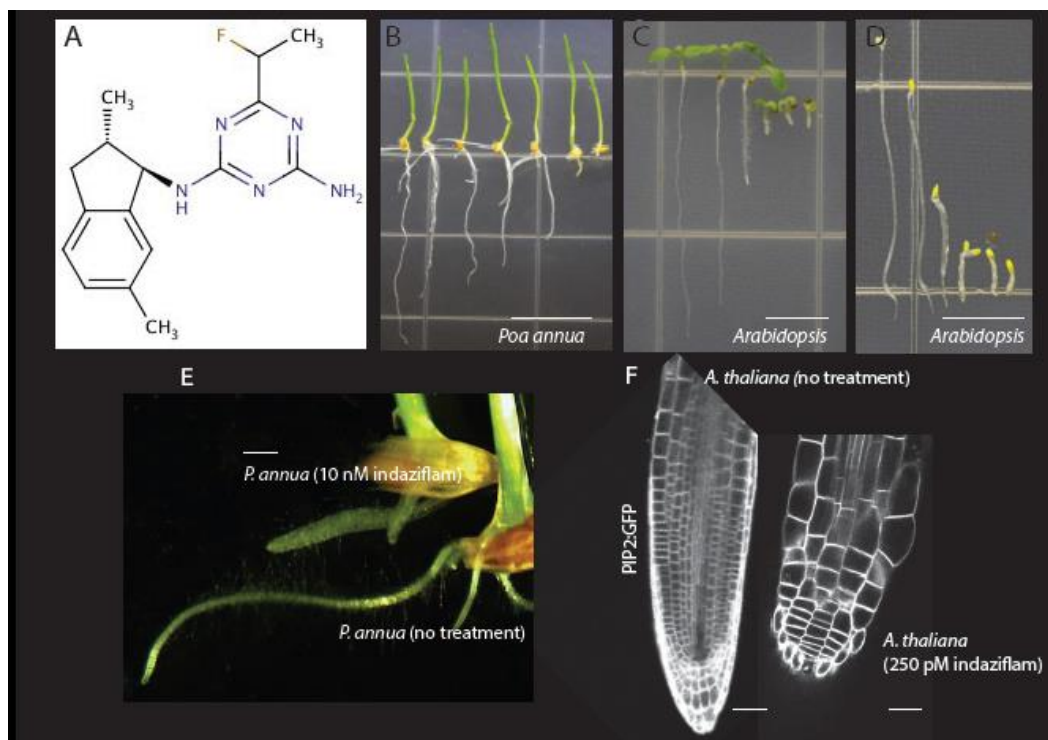


Figure 3.1 Indaziflam is a fluoroalkyltriazine-containing compounds that inhibits elongation in seedlings of *P. annua* and *Arabidopsis*. A, Chemical structure of indaziflam. B to D, Images of 7-d-old seedlings treated with increasing concentrations of indaziflam. B shows light-grown *P. annua* seedlings (indaziflam concentration from left to right are 0, 100, 250, 1,000, 5,000, and 10,000 pM). C and D show light-grown and dark-grown *Arabidopsis* seedlings, respectively (indaziflam concentrations from left to right are 0, 100, 250, 500, 1,000 and 2,500 pM). Indaziflam treatment induced swollen cells. E, representative images of the primary root of *P. annua* grown on plates for 4 d with and without 10 nM indaziflam. F, Transgenic *Arabidopsis* seedlings expressing GFP::PIP2 were examined by laser scanning confocal microscopy and images represent visualization of the primary root grown vertically for 7d on plates without and with 250 pM indaziflam. PIP, plasma membrane intrinsic protein2. Bar = 10 mm in B, 5 mm in C and D, 2 mm in E and 50 μ M in F.

Arabidopsis seedlings suggests the phytotoxic effects of indaziflam do not require light. This eliminated several possible herbicidal modes of action for indaziflam that are dependent on light for toxicity (i.e. photosynthesis, chlorophyll, and pigment inhibitors). Visually, indaziflam treated seedlings exhibited radial swelling (Fig 1E to 1F) and phloroglucinol staining revealed indaziflam caused ectopic lignification, both of which are common characteristics of CBIs (Desprez et al., 2002) (Fig S2; See online version Brabham et al. 2014).

3.3.2 Indaziflam Inhibits Cellulose Biosynthesis

Classification of a herbicide as a CBI has traditionally been based on inhibition of cellulose synthesis in treated plants (Sabba and Vaughn, 1999). Cellulose is polymerized from the substrate UDP-glucose by glucosyltransferase CESA proteins (Delmer et al., 1999) and it can be partitioned from other polysaccharides by treatment with nitric-acid. In crude cell wall extracts from the hypocotyl region of five-day-old etiolated Arabidopsis seedlings, indaziflam reduced the amount of nitric-acid insoluble material (considered crystalline cellulose; Updegraff, 1969) (Fig 2A). This effect was dose dependent as indaziflam at 200 and 400 μM reduced the glucose content of the acid-insoluble fraction by 18% and 51%, respectively, in comparison to the control ($12.7 \mu\text{g mg}^{-1}$). Furthermore, indaziflam inhibited the incorporation of [^{14}C]glucose into the acid-insoluble cellulose fraction within one hour of treatment (Fig 2B). Thus, indaziflam inhibited the production of cellulose soon after treatment (< 1 hour) and in a dose dependent manner. This is consistent with inhibition of cellulose biosynthesis as the primary mode of action for indaziflam.

3.3.3 Isoxaben- and Quinoxiphen-Resistant Plants Are Not Cross-Resistant to Indaziflam

To determine if indaziflam has the same mechanism of action as two other characterized CBIs, we tested if known isoxaben- and quinoxiphen-resistant Arabidopsis mutants were cross-resistant to indaziflam (Fig 3). The mutants used were *cesa3ixr1-1*, *cesa3ixr1-2*, and *cesa1ageusus*. Isoxaben-resistant mutants, *cesa3ixr1-1* and *cesa3ixr1-2* (Heim et al., 1989; Scheible et al., 2001), and the quinoxiphen-resistant mutant, *cesa1ageusus* (Harris

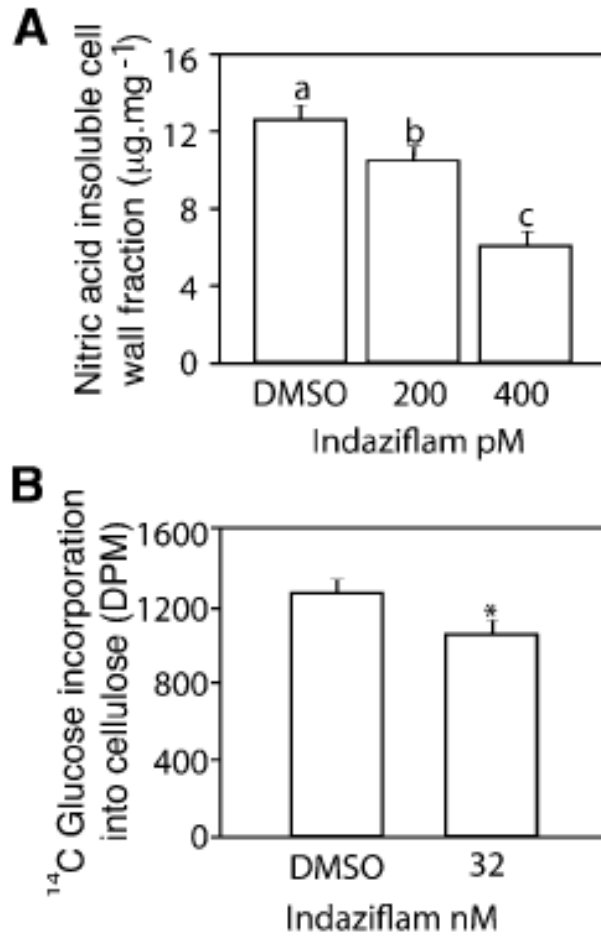


Figure 3.2 Indaziflam treatments quantitatively inhibited the production of cellulose. A, The amount of acid-insoluble Glc content (crystalline cellulose) from pooled etiolated hypocotyls regions (5 mg dry weight) of 5—old dark grown *Arabidopsis* seedlings after treatment with indaziflam at 0 (0.01% DMSO), 200, or 400pM. B, The inhibitory effects of indaziflam on the incorporation of [¹⁴C] Glc into the acid-insoluble cellulose fraction of 3-d-old etiolated dark-grown *Arabidopsis* seedlings after a 1-h treatment. The amount of radioactivity was determined by liquid scintillation spectrometry. In graphs, means were separated using Tukey’s test (a) or a students’ t test (b) and different letters or asterisks indicate a significant difference at an alpha <0.05. Error bars represent +- SE (n=5 for a and b). DPM, disintegrations per minute.

et al., 2012), have point mutations in the C-terminus transspanning membrane domains and not in the cytosolic catalytic domain that confer resistance to their respective herbicide. The results were somewhat inconclusive as to whether the isoxaben- and quinoxiphen-resistant mutants were cross-resistant to indaziflam. There were differences based upon GR50 values in the susceptibility of wildtype and mutants to indaziflam. The isoxaben-resistant mutants *cesa3ixr1-1* ($p < 0.0001$) and *cesa3ixr1-2* ($p < 0.036$) grown in the light both exhibited minor tolerance (< 2 -fold) to indaziflam in comparison to the wild-type. However, these same mutants have a 300-fold and 90-fold level of resistance to isoxaben, respectively (Heim et al., 1989). In the dark, only *cesa3ixr1-1* ($p < 0.0001$) exhibited any tolerance to indaziflam when compared to the wild-type (GR_{50s} 275 vs. 214 μ M). The *cesa1ageusus* mutant and an additional isoxaben resistant mutant, *cesa6ixr2-1* (Desprez et al., 2002)(data not shown), were equally sensitive to indaziflam as wild-type plants whether light- or dark-grown. Our results do not support indaziflam as having the same mechanism of action as quinoxiphen or isoxaben.

3.3.4 Indaziflam Caused Reduced Particle Velocity and Increased Accumulation of CESA Particles at the PM Focal Plane

The question of how the PM localized CSC population responds to indaziflam treatment in living cells is important to determine in order to understand the inhibitory mechanism of indaziflam. To explore this, we examined transgenic Arabidopsis plants expressing both YFP:CESA6 and RFP:TUA5 (Tubulin Alpha 5) (Gutierrez et al., 2009) during short-term exposure to indaziflam. Two questions were initially asked: 1) Does the entire organization of the CSC array change during indaziflam treatment or does the behavior of individual CESA particles change in response to indaziflam? 2) Does indaziflam cause similar or different inhibitory response on the PM localized CSC population compared to previously described CBIs? To address the first question, we imaged the behavior of YFP:CESA6 and RFP:TUA5 in epidermal cells near the apical hook of etiolated Arabidopsis seedlings (Movies S1 and S2; See online version Brabham et al. 2014). Analysis of time-lapse images from seedlings in the absence of indaziflam revealed a dynamic population of YFP:CESA6 labeled particles residing at the PM (Movie S1; See

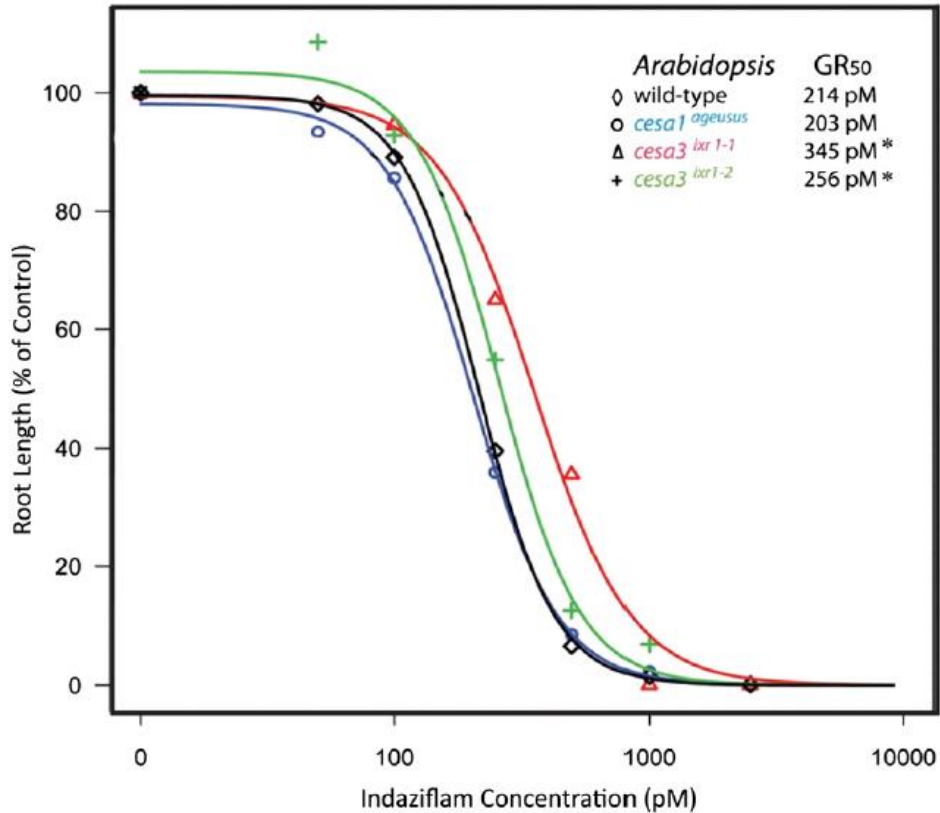


Figure 3.3 Indaziflam dose response and GR₅₀ values of light-grown *Arabidopsis* genotypes. To establish dose responses, seedlings were germinated in the light on agar plates containing indaziflam concentrations ranging from 0 to 10,000 pM. Seedlings root length was measured and standardized as a percentage of the control. The *Arabidopsis* seedlings used in this assay were the Columbia ecotype as the wild type and the mutants previously confirmed resistant to other CBIs. The *cesa3^{ixr1-1}* and *cesa3^{ixr1-2}* mutants are resistant to isoxaben and *cesa1^{ageusus}* is resistant to quinoxifen. The curves and GR₅₀ values were generated by R software using the drc package. Asterisks indicate a significant difference (n=60; p<0.05) in the GR₅₀ values between the mutant and the wild type.

online version Brabham et al. 2014). After indaziflam treatment (500 nM for two hours), a greater population of YFP:CESA6 particles was observed at the PM focal plane (Fig 4A). To quantify this, the number of distinct YFP:CESA6 particles displaying morphology and motility consistent with being membrane localized particles was counted. In the absence of indaziflam, the density of discernable PM localized YFP:CESA6 particles was $0.93 \pm 0.02 \mu\text{m}^{-2}$ (Fig 4B). In contrast, the density of YFP:CESA6 particles in indaziflam treated cells was 30% greater ($1.29 \pm 0.02 \mu\text{m}^{-2}$) (Fig 4B). This response to indaziflam was consistent throughout the hypocotyl cells but was most prominent in expanding cells subtending the apical hook. Thus, indaziflam induced an atypical increase in the population density of CESA particles at the PM, consistent with broad disturbance of array organization.

Individual CESA particles can also be tracked and some aspects of their behavior measured. One measurement is the velocity (positional movement) of PM localized CESA particles. However, the actual movement of CESA particles at the PM is independent of MTs (Paredes et al., 2006; DeBolt et al., 2007a). Thus, a microtubule motor function in propelling CESA particles is unlikely. Rather, the movement of CESA particles has been proposed to be a function of a polymerization force generated by the translocating glucan chain(s) (Diotallevi and Mulder, 2007). The PM movement of CESA particles in untreated cells was bidirectional with an average velocity of $336 \pm 167 \text{ nm} \cdot \text{min}^{-1}$, which is consistent with numerous prior studies (Paredes et al., 2006, Crowell et al., 2009; Gutierrez et al., 2009; Gu et al., 2010; Bischoff et al., 2009; Li et al., 2012). After treatment with indaziflam, YFP:CESA6 velocity was reduced to $119 \pm 95 \text{ nm} \cdot \text{min}^{-1}$ (Fig 5A,B). Thus, indaziflam reduced CESA particle velocity by 65%, which is consistent with a role in inhibiting polymerization.

With the observed atypical increase in CESA density, we asked whether the rate of coincidence between MT and CESA was altered by indaziflam. In the molecular rail hypothesis proposed by Giddings and Staehelin (1988), CESA particles are guided by the underlying cortical MTs. The coincidence between PM CESA particles and MTs is normally around 70 to 80% (Paredes et al., 2006; Li et al., 2012). The average colocalization rate over three experimental runs (total N=544) between YFP:CESA6 particles and RFP:TUA5 after indaziflam treatment was $53 \pm 4\%$. This was considerably

less than the $71\pm 1\%$ colocalization rate (total $N=303$) observed in mock treated cells (summarized in Fig 6, Table 1). This disruption in the colocalization between CESAs and MTs was prominent in expanding cells but was less apparent in cells that had undergone expansion further down the hypocotyl (Fig S3; See online version Brabham et al. 2014). Thus, the increased CESA density after indaziflam treatment appears to contribute to the decreased colocalization between MT and CESA in the region close to apical hook.

3.3.4 Reduced CESA Velocity After Indaziflam Treatment is CSI1 Independent

A primary linker protein between MTs and CSCs has been identified as CSI1 (Gu et al., 2010; Bringmann et al., 2012; Lei et al., 2012; Li et al., 2012). In *csi1* mutants, CESA particles in the PM were found to display reduced velocity and their association with MTs was completely disrupted (Gu et al., 2010; Li et al., 2012). Due to this cellular phenotype being similar to what we observed in wild-type seedlings treated with indaziflam, we explored the impact of indaziflam on the behavior of CESA particles in the *csi1-3* mutant background. The velocity of YFP:CESA6 at the PM focal plane in untreated *csi1-3* was 236 ± 114 nm. min^{-1} and, as expected, was slower than that observed in the untreated. However, upon treatment with indaziflam, YFP:CESA6 velocity in *csi1-3* was further reduced from 236 ± 114 to 125 ± 102 nm min^{-1} . Indaziflam also caused a significant increase in the number of PM localized YFP:CESA6 particles on average to 1.25 particles per μm^{-2} in both *csi1-3* and wild-type seedlings (Fig S5A,B; See online version Brabham et al. 2014). These data suggest the mechanism of action of indaziflam does not depend on a functional CSI1, otherwise the velocity of YFP:CESA6 in the *csi1-3* background should not have been altered.

3.4 Discussion

Indaziflam caused CBI symptomologies, including radial swelling and ectopic lignification, in both *Arabidopsis* and *P. annua* treated seedlings (Fig 1). Furthermore, indaziflam inhibited the production of cellulose in *Arabidopsis* seedlings in a dose dependent manner and within one hour of treatment (Fig 2). Based on these findings, the mode of action of indaziflam is consistent with its classification as a CBI. In

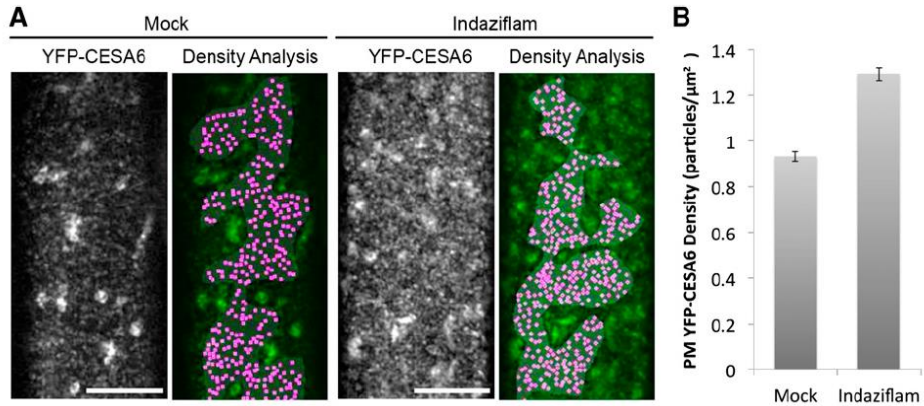


Figure 3.4 Indaziflam treatment induced a higher density of CesAs at the PM. Arabidopsis seedlings expressing YFP:CesA6 were grown in the dark for 3d before imaging. A, Representative images and analysis of the PM-localized YFP:CesA6 particles in the *prc1-1* background are shown. Single optical sections (monochrome) show the distribution of YFP: CesA-labeled puncta upon 2-h 0.01% DMSO mock treatment (left) or 500 nM indaziflam treatment (right). The green/magenta overlay is a spatial count of the puncta that display morphology and motility consistent with PM YFP:CesA particles. A gray mask indicates the region of interest lacking underlying intracellular compartments, and magenta dot indicate local maxima of the fluorescence signal. B, Upon indaziflam treatment, the average density of YFP:CesA6 puncta at the PM increased. N=15 cells from nine seedlings for mock and n=18 cells from 12 seedlings for indaziflam. Error bars at 1 SE from mean. Bar =10uM.

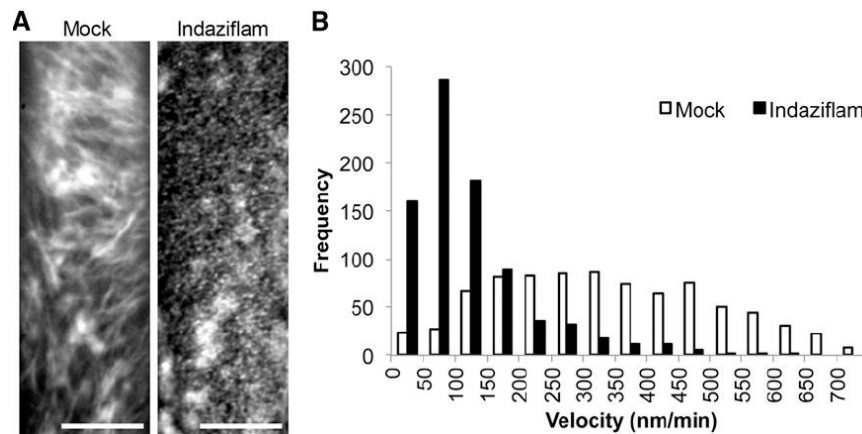


Figure 3.5 Indaziflam reduced the velocity (particle movement rate) of YFP:CesA6 A., Representative time-lapse images of YFP:CesA6 particles in the *prc1-1* background with and without indaziflam treatment (61 frames averaged). B, The histogram depicts the frequency of YFP:CesA6 particles velocities at the PM focal plane after a 2-h treatment with indaziflam or DMSO mock. Velocity was determined from images taken in the epidermal cells of 3-d-old dark-grown hypocotyls. The white bars are the recorded velocity from the mock and the black bars are indaziflam treatment (mean 1 SE) Bar10uM.

characterizing the mechanisms of action of CBIs, it is important to understand the complexity of cellulose biosynthesis. In higher plants, a solitary, hexagonal rosette shaped CSC synthesizes cellulose at the PM (Herth and Weber, 1984; Delmer, 1999). Recent data suggests the CSC consists of 18 to 24 catalytic CESA proteins producing a microfibril with a cross sectional area of around 7 nm² (Jarvis, 2013). Moreover, an incomplete but growing list of accessory proteins that are required for the functionality of CSCs may serve as potential CBI targets. Examples of such accessory proteins are KORRIGAN (endo-1,4-β-D-glucanase)(Lane et al., 2001), COBRA (glycosylphosphatidyl inositol-anchored protein)(Roudier et al., 2006), and CSII (Lei et al., 2011). Thus, there are many potential targets for CBIs and they may be further classified according to the specific mechanism of action. Traditional biochemical methodologies used to illustrate drug molecular mechanisms are not, yet, applicable to CBIs. To date, purification of functionally active cellulose producing CSCs or CESAs has been challenging (Lai-Kee-Him et al., 2002) and insufficiently robust to enable *in vitro* drug affinity binding assays. Further, despite a crystallized bacterial CESA homolog (BCSA) (Morgan et al., 2013), both CESAs and CSCs have sufficiently diverged over time so that CBIs are not toxic to bacteria (Tsekos, 1999; Morgan et al., 2013; Sethaphong et al., 2013). Therefore, determining how a given CBI disrupts cellulose biosynthesis has employed live cell imaging of CESA proteins in the presence of a CBI. (summarized in Fig 6, Table 1). This disruption in the colocalization between CESAs and MTs was prominent in expanding cells but was less apparent in cells that had undergone expansion further down the hypocotyl (Fig S3; See online version Brabham et al. 2014). Thus, the increased CESA density after indaziflam treatment appears to contribute to the decreased colocalization between MT and CESA in the region close to apical hook.

Reduced CESA Velocity After Indaziflam Treatment is CSII Independent

A primary linker protein between MTs and CSCs has been identified as CSII (Gu et al., 2010; Bringmann et al., 2012; Lei et al., 2012; Li et al., 2012). In *csi1* mutants, CESA particles in the PM were found to display reduced velocity and their association with MTs was completely disrupted (Gu et al., 2010; Li et al., 2012). Due to this cellular phenotype being similar to what we observed in wild-type seedlings treated with

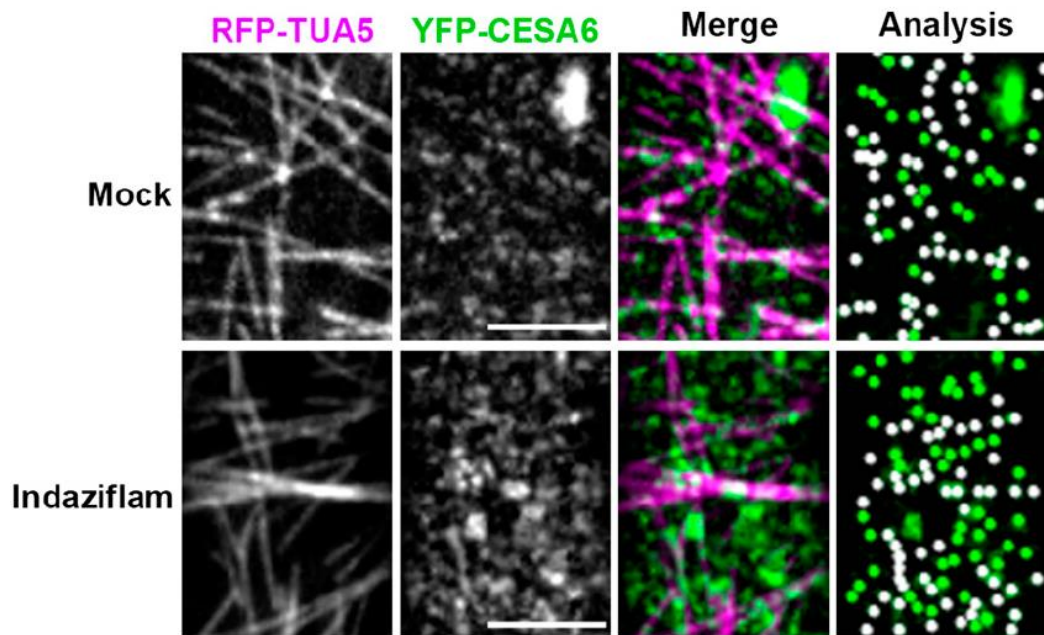


Figure 3.6 Indaziflam treatment decreased the net colocalization between MTs and YFP:CesA6 at the PM. Arabidopsis seedlings expressing both RFP:TAU5 and YFP:CesA6 in *prc1-1* were grown in the dark for 3d before imaging. Representative single optical sections (monochrome) of cortical MTs labeled by RFP:TAU5 (magenta) and PM localization YFP:CesA6 (green) were used for the colocalization analysis Table 1) After 2 h in 0.01% DMSO mock 71%+1% of YFP:CesA6 particles were coaligned with MTs, which was not different from the ratio without any treatment (Li et al. 2012). After 2 h in 500nM indaziflam the colocalization ratio between YFP:CesA6 and RFP:TAU5 decreased to 53%, which was not significantly different from the expected random ratio association of 47%. Bar = 5µM.

indaziflam, we explored the impact of indaziflam on the behavior of CESA particles in the *csi1-3* mutant background. The velocity of YFP:CESA6 at the PM focal plane in untreated *csi1-3* was 236 ± 114 nm. min⁻¹ and, as expected, was slower than that observed in the untreated.

Through confocal microscopy, we demonstrated that indaziflam caused an atypical increase in CESA particle density and reduced, but not paused, velocity at the PM focal plane (Fig 4 and Fig 5). Indaziflam is clearly different from the CBIs quinoxiphen, isoxaben, and thaxtomin-A, which all induce a rapid clearance of CESA particles from the PM focal plane (Paredes et al., 2006; Bischoff et al., 2009; Harris et al., 2012). This corroborates our findings of a lack of cross-resistance to indaziflam in isoxaben- or quinoxiphen-resistant mutants (Fig 3). Similarly, morlin and cobteron (DeBolt et al., 2007a; Yoneda et al., 2007) impact both MT and CESA arrays, which was not the case for indaziflam. Indaziflam effects also share little similarity with those caused by DCB. DCB causes YFP-CESA6 particles to stop moving and hyperaccumulate at single foci in the PM focal plane (Herth, 1984; DeBolt et al., 2007b). While both DCB and indaziflam caused CESA particles to accumulate in the PM, indaziflam, by contrast, induced CESA accumulation in both MT rich and poor regions, while DCB appears to cause accumulation at distinct foci in MT rich regions (DeBolt et al., 2007b). Furthermore, DeBolt et al. (2007b) found that the majority of the accumulated PM localized YFP:CESA6 particles did not exhibit detectable movement 1 h after treatment (max velocity 34 nm min⁻¹). However, in our study, the average particle velocity after

indaziflam treatment was $119 \pm 95 \text{ nm} \cdot \text{min}^{-1}$. In all, the data suggest indaziflam influences a different component of the complex cellulose biosynthetic process than other CBIs.

Interestingly, despite no obvious effect on the cortical MT morphology or motility, CESA-MT coincidence (Paredes et al., 2006) was uncoupled in indaziflam treated cells (Fig 6). Here, the behavior of YFP:CESA6 in indaziflam treated cells resembled the behavior of CESAs in the CSC-MT linker protein, *csi1*, mutant background (Gu et al., 2010). Specifically, in the absence of CSII, CESA particles at the PM were uncoupled from the MT array and exhibited reduced velocity ($236 \pm 114 \text{ nm} \cdot \text{min}^{-1}$). Indaziflam also caused reduced CESA particle velocity and partial uncoupling from the MT array. Thus, utilizing the *csi1-3* mutant we asked does indaziflam interact with CSII. Results for indaziflam treated *csi1-3* were comparable to indaziflam treated wild type cells suggesting the inhibitory mechanism of indaziflam was independent of CSII (Fig S2, Fig S3 and Fig S4; See online version Brabham et al. 2014). Thus, the inhibitory mechanism of indaziflam does not mimic any prior characterized CBI or genetic lesion.

To date, there has yet to be any reported cases of weed species that have evolved field resistance to CBIs (Heap, 2014). The lack of CBI-resistant weeds could be due to several factors. Firstly, CBIs may be used on a relatively small scale because they are mainly registered for use in perennial cropping systems (i.e. orchards and turf), ornamentals, or for total vegetation control. Unlike some other herbicides, such as glyphosate, CBIs are often used in combination with alternative modes of action and this can lower the probability of selecting for resistance to CBIs. Fitness of CBI-resistant weeds may be another factor. Although, no field resistance has been reported, point mutations conferring resistance to isoxaben (Heim et al., 1990) and quinoxiphen (Harris et al., 2012) have been generated in *Arabidopsis* populations treated with the mutagen ethyl-methane-sulfonate. The mutations were mapped to CESA genes (Scheible et al., 2001; Desprez et al., 2002; Harris et al., 2012) and each point mutation was associated with a fitness penalty. Furthermore, plant cells can be habituated to a lethal dose of CBIs by significantly alternating their cell wall composition (Diaz-Cacho et al., 1999; Melida et al., 2010). It is yet to be seen whether the mechanism for *in vitro* CBI habituation

observed in the cell culture system could be mimicked in a developmentally complex multicellular organisms, like a plant, to confer resistance. In lieu of this data, indaziflam is a potent herbicide used at low rates, has long soil residual activity, and has broad spectrum activity on seedlings with type I (eudicots) or type II (Poaceae) cell walls, which is not the case for isoxaben. These properties could result in over reliance on indaziflam alone resulting in an increased selection pressure for indaziflam-resistant weeds. If resistance is managed, indaziflam has the potential to be a valuable alternative mode of action for weed management.

3.5 Materials and Methods

Indaziflam Dose Response and Cross Resistance.

All *Arabidopsis thaliana* seedlings were grown vertically on half-Murashige and Skoog Basal Salt Mixture (PhytoTechnology Laboratories, Shawnee Mission, KS) (MS) agar plates under continuous light or dark conditions. The *Arabidopsis Columbia* ecotype was considered the wild type in all experiments. The CBI-resistant mutants used in conjunction with the dose response assay were isoxaben-resistant (*ixr*) *cesa3ixr1-1*, *cesa3ixr1-2*, *cesa6ixr2-1* (Heim et al., 1989; Scheible et al., 2001), and the quinoxiphen resistant mutant, *cesa1ageusus* (Harris et al., 2012) *Poa annua* were pre-germinated and seedlings (n=12) with a protruding radicle < 1.5 mm were placed in 9-cm wide Petri dishes and grown under constant light. The Petri dishes contained two Whatman filter papers soaked with 4 mL of treatment. Appropriate indaziflam (Specticle 20 WSP [20% w/w ai], Bayer Environmental Science, Research Triangle Park, NC) rates were predetermined prior to experiments. The compatibility and surfactant ingredients present as background in Specticle were not available and were replaced with 0.01% DMSO or dH₂O. Treatments for *Arabidopsis* were indaziflam at 0, 50, 100, 250, 500, 1,000, 10,000 pM and the DMSO concentration in agar media did not exceeded 0.01% v/v. *Poa* treatments were indaziflam at 0, 100, 250, 500, 1,000, 5,000 and 10,000 pM in water. A total of 20 hypocotyl or root lengths from each *Arabidopsis* line and twelve *Poa* roots were measured seven days after treatment. Experiments were replicated in time, thrice. Length data was standardized to percent of the untreated control in each experiment. Percentage data was analyzed in R using the *drc* package to determine and compare

GR50 values (Growth Reduction by 50%)(Knezevic et al. 2007).

Cellulose Assay and Lignin Staining.

Cellulose content in the hypocotyl region of five-day-old dark grown *Arabidopsis* seedlings was determined by boiling 5 mg dry weight of plant in nitric acetic acid (Updegraff, 1969). Treatments were indaziflam at 0, 200 or 400 pM. The insoluble material was quantified colorimetrically for glucose content using the anthrone-sulphuric acid method and back calculated to cellulose (Scott Jr. and Melvin, 1953). For lignin staining, 7-day-old light grown seedlings were incubated in ethanol (70%) for 24 hrs followed by 30 min in a 2% w/v phloroglucinol solution (20% hydrochloric acid). Images were taken with a bright-field stereomicroscope.

[¹⁴C]glucose Cell Wall Incorporation Assay.

An adapted protocol similar to that of Heim et al. (1990) was used to measure the incorporation of radiolabelled glucose into the cellulose fraction of cell wall. Dark grown *Arabidopsis* seedlings were grown for three days in liquid MS media supplemented with 2% (w/v) glucose. After removal from media, seedlings (20 mg fresh weight) were measured and placed in a 1.5 mL Eppendorf tube. This represents one replication. Seedlings were then washed twice with 0.5 mL of glucose-free MS media, centrifuged and the supernatant removed. Next, 0.5 mL glucose-free MS media solution containing [¹⁴C]glucose at 1 uCi mL⁻¹ was added to each tube followed by the addition of treatments. Seedlings were treated for 1 hr in the dark with either DMSO (0.01% v/v) or indaziflam (32 nM). Samples were centrifuged and washed three times to remove unincorporated radioactivity. The material was then boiled in nitric-acetic acid for 30 min, cooled, and centrifuged for 5 min to pelletize insoluble material. A total of 400 uL of supernatant was removed and placed in a 10 mL liquid scintillation vial. The remaining liquid and insoluble material was washed with 0.5 mL of water and centrifuged for 5 min at 10,000 rpm. This was repeated thrice to remove any remaining [¹⁴C]glucose in solution. The pelletized material was resuspended in water and transferred to a liquid scintillation vial. Five mL of scintillation fluid cocktail (Bio-Safe II, Research Products International Corp., Mount Prospect, IL) was added to each vial

with either soluble or insoluble fractions and radioactivity was determined by a liquid scintillation counter.

Confocal microscopy

For live-cell imaging, 3-day-old dark-grown seedlings expressing YFP:CESA6 (Paredes et al., 2006) or YFP:CESA6 – RFP:TUA5 (Gutierrez et al., 2009) were used.

Additionally, to visualize Arabidopsis expansion we examined seedlings expressing the plasma membrane intrinsic protein 2 (PIP2)::GFP (Cutler and Ehrhardt, 2000). Seedlings were mounted in MS liquid medium for 2 hr with or without indaziflam at 500 nM.

Imaging was performed on a Yokogawa CSUX1 spinning disk system featuring a DMI6000 Leica motorized microscope, a Photometrics QuantEM:512SC CCD camera, and a Leica 100x/1.4NA oil objective. An ATOF laser with 3 laser lines (440/491/561 nm) was used to enable faster shuttering and switching between different excitations. Bandpass filters (485/30 nm for CFP; 520/50 nm for GFP; 535/30 nm for YFP; 620/60 nm for RFP) were used for emission filtering. Image analysis was performed using Metamorph (Molecular Devices, Sunnyvale, CA), ImageJ software (version 1.36b) and Imaris (Bitplane, Saint Paul, MN) software.

Chapter 4 TILLING *Brachypodium* Cellulose Synthase A Genes

4.1 Introduction

Grasses have long been under human selection for their energy-dense grain and for their biomass as livestock forage but only recently for biofuels. Despite the economic importance of grasses, many questions remain about their biology and while the dicot *Arabidopsis* is a satisfactory model for many plants, findings in *Arabidopsis* are not always translatable across taxonomic boundaries. As a result, *Brachypodium distachyon* has emerged as a model grass (Draper et al. 2001; Vogel et al. 2010). *Brachypodium* is a temperate, C3, annual grass and belongs to a sister tribe in the same Pooideae subfamily as cereals (e.g. wheat and barley) and forage grasses (e.g. fescue and bluegrass) (Draper et al. 2001; Schneider et al. 2009). Several studies have exemplified *Brachypodium* as a genetic model for grass cell wall development (Christensen et al. 2010), cereal-pathogen interactions (Fitzgerald et al. 2015), and grain development (Hands and Drea 2012).

Functional genomic tools for *Brachypodium* are continuing to be developed (Vogel et al., 2010; Brutnell et al., 2015). One tool that is available is TILLING or Targeting Induced Local Lesion IN Genomes (McCallum et al. 2000, Henikoff et al. 2004). TILLING is a reverse genetic strategy, which isolates point mutations in a gene of interest. The ability to isolate point mutations is of particular interest for cellulose biosynthesis research. Prior studies focused on the cellulose biosynthetic process in *Arabidopsis* have revealed gene redundancy or lethality issues. To overcome this, numerous point mutations have been identified in *AtCesAs* using forward genetics screens. This is an alternative to the qualitative (on/off) outcomes associated with TDNA insertional approach. Identifying TILLING mutants has been accelerated by the capacity to amplify a region of a gene of interest by polymerase chain reaction (PCR) from within a mutagenized seed population and then use next generation sequencing to identify mutations. This approach is referred to as SCAMPRing or sequencing candidate amplicons in multiple parallel reactions (Gilchrist et al. 2013). Development of a TILLING population is a timely and costly process but once developed it is a valuable tool for functional genomic studies.

Grasses, like all vascular land plants, have two types of walls: a primary and a normally lignin-rich secondary cell wall. The primary wall is composed of a highly organized network of polysaccharides (cellulose, hemicellulose, and pectin) plus relatively minor amounts of proteins, elements, and phenolic compounds. The non-cellulosic fraction of primary cell walls differs significantly between grasses and dicots in the relative abundance and type of polysaccharides (Carpita 1996; Vogel 2008). In Eudicots, the primary wall is roughly a 1:1:1 ratio of cellulose, hemicellulose (mainly xyloglucans) and an assortment of pectinaceous polysaccharides. In grasses, like *Brachypodium*, cellulose is still compositionally a third of the primary cell wall but its surrounding wall structure is enriched with arabinoxylans decorated with glucuronic and ferulic acid and mixed linkage glucans (Carpita 2001; Vogel 2008).

Cellulose is the major structural component found in cell walls of grasses and dicots. Thus, the large heteromeric protein complex localized at the plasma membrane responsible for cellulose synthesis has been the subject of intense study. Despite many gains in our understanding of the cellulose biosynthetic machinery in *Arabidopsis* we have a less detailed picture of the process in grasses. From *Arabidopsis* (*At*) research, it is known that 10 CELLULOSE SYNTHASE A (*CesA*) isoforms exist and loss of function experiments have shown 3 different *CesA*s are required to form a fully functional cellulose synthase complex (CSC) in primary (Person et al. 2007; Desprez et al., 2007) or secondary cell walls (Taylor et al. 2003). Genetic studies show that for primary cell walls, *AtCesA1*, *AtCesA3* and the partially redundant role of *AtCesA6*-like (including *AtCesA2*, *AtCesA5*, *AtCesA6*, or *AtCesA9*) are required (Persson et al., 2007; Desprez et al., 2007). By contrast, *AtCesA4*, 7, and 8 are necessary for secondary cell wall cellulose biosynthesis (Taylor et al. 2003). Complete loss of function mutations in *AtCesA1* and *AtCesA3* are pollen gametophyte lethal (Arioli et al., 1998; Persson et al., 2007). The gene orthologs for *CesA* have been identified and characterized in *Brachypodium* (Handakumbura et al. 2013).

In this paper, we introduce a new allele for *BdCesA1* and *BdCesA3* that were identified by TILLING in *Brachypodium* and SCAMPRing to isolate the mutation. Based on expression profiling and phylogenetics, the *BdCesA1* and *BdCesA3* are the orthologs to *AtCesA1* and *AtCesA3*, respectively. The *Bdcesa1*^{S830N} mutation is nested adjacent to

the *CesA* glycotransferase QXXRW motif in the catalytic region and the *cesa3*^{P986S} mutation is localized in the 6th transmembrane domain. Our aim was to not only identify novel mutations and to learn whether mutations in *BdCesA* genes that are broadly expressed in tissues that would support primary cell wall biosynthesis would result in lethality or severe phenotypes as observed in *Arabidopsis* lines, but to also expand the functional genetic resources of *Brachypodium*. The results are described herein.

4.2 Results

4.2.1 Identification of *Brachypodium* Primary Cell Wall *CesAs*.

A phylogenetic and qRT-PCR approach was used to identify *BdCesAs* genes involved in primary cell wall cellulose biosynthesis (Figure 1A-C). The *Brachypodium* referenced genome has 10 predicted *CesAs*. However, *BdCesA10* (Bradi1g36740) is missing catalytic residues required for glucosyltransferase activity (Morgan et al. 2013) and will not be considered a *CesA* here. It is also worth noting that *BdCesA5* (Bradi1g29060) does not have a predicted zinc finger domain believe to be involved in *CesA* protein-protein interactions but we did not exclude it from this analysis. We adopted the *CesA* naming system described by Handakumbura and authors (2013). They classified *BdCesAs* based upon their closest *Arabidopsis* orthologs and our data supports their system (data not shown). To further validate the phylogenetic predictions we quantified the relative gene expression profiles of *CesAs* in coleoptile, root, and shoots tissue from 3 to 4-day old seedlings and from stem internodes of 4-week old plants (Figure 1A-C). Since we are interested in primary cell wall *CesAs*, we calculated the relative fold change values of *CesAs* transcripts from actively growing tissue versus stem tissue, presumably xylem cells, undergoing secondary wall thickening.

The relative expression profile of *CesAs* in coleoptiles, roots, and shoot tissue in general followed a similar pattern. *BdCesA1* (Bradi2g34240), *BdCesA3* (Bradi1g54250), *BdCesA6* (Bradi1g53207) were either the highest or statically similar to the highest expressed *CesAs* (> 2.4 fold) in all organs from 3-4 day old seedlings. *BdCesA9* (Bradi1g36740) mostly followed this trend, except for in shoot tissue (1.2 fold). Handakumbura et al. (2013) found *BdCesA4* (Bradi3g28350), *BdCesA7* (Bradi4g30540), and *BdCesA8* (Bradi2g49912) were involved in secondary cell wall cellulose deposition

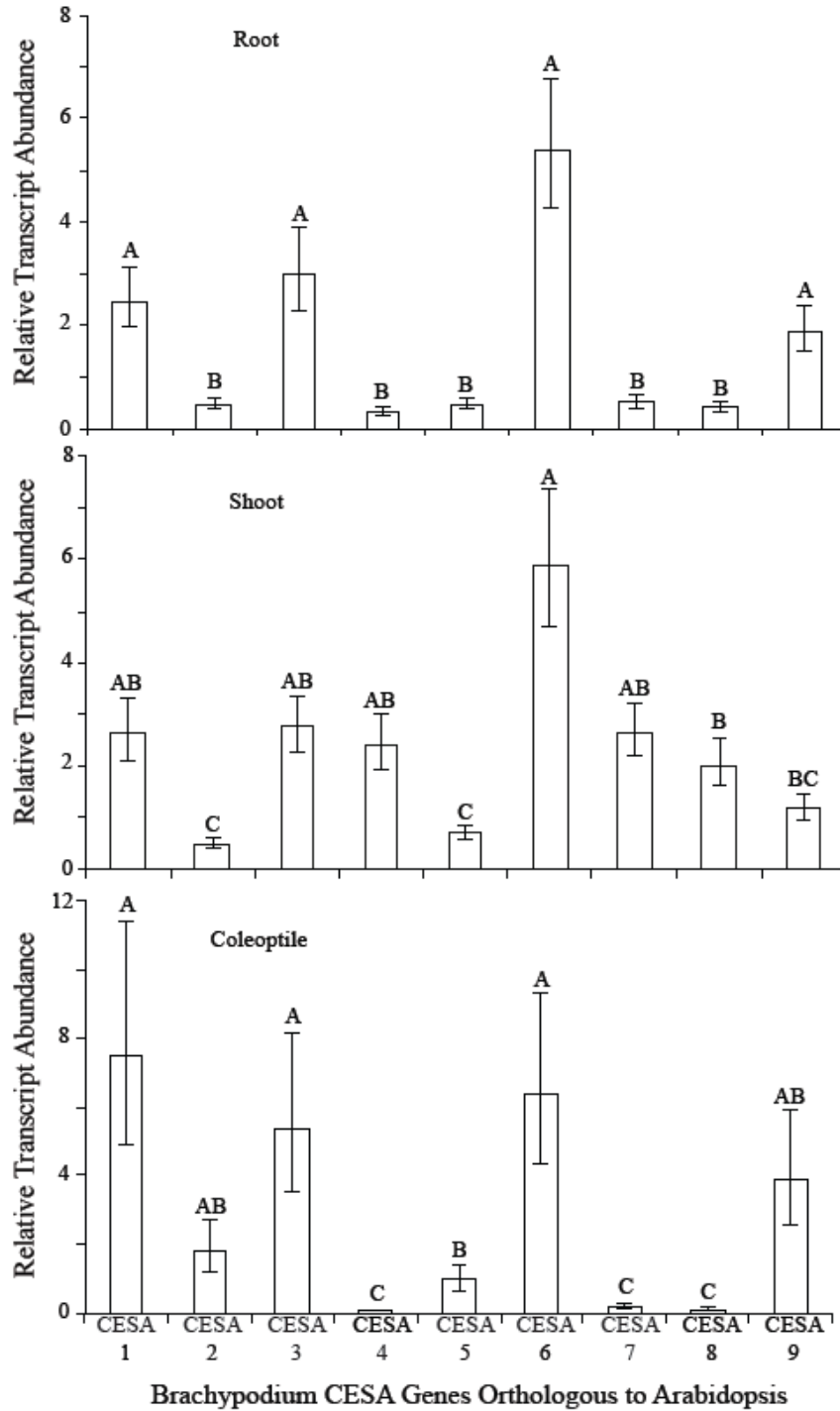


Figure 4.1 Characterizing relative transcript abundance of Brachypodium CesaA genes in 3-4 day old roots, shoots, and coleoptiles to determine primary cell wall CesaA. Fold change values were determined by comparing against gene expression in 3 week old stem tissue. Means followed by a different letter within a tissue type are considered significantly different at alpha 0.01 using Tukeys test.

and, as expected, their expression was significantly reduced in coleoptile and root tissue but not in shoot tissue. The relative transcript abundance of *BdCesA2* (Bradi1g04597) and *BdCesA5* detected in all tissue including stems was low.

Based on these findings and in accordance with Handakumbura et al. (2013), *BdCesA1*, 3, 6, and 9 are involved in primary cell wall cellulose biosynthesis. We can tentatively conclude, based on experimental findings from *Arabidopsis* (Desprez et al. 2007; Persson et al. 2007), *BdCesA1*, 3, and any one of *BdCesA6* or 9 from the *CesA6*-like clade are necessary to form a fully functional cellulose synthase complex during seedling development. We decided to further target *BdCesA1* and *BdCesA3* for TILLING.

4.2.2 Targeting and Identification of *BdCesA1* and *BdCesA3* TILLING Mutants

To identify genomic regions with the highest probability for EMS induced missense and nonsense mutations in our genes of interest, we utilized the web-based tool CODDLE (Codons Optimized to Discover Deleterious Lesion) (Henikoff et al. 2004). Our selected TILLING amplicons for *BdCesA1* and *BdCesA3* were 1,096 and 1,397 bp long, respectively (Figure 2 and Table 1). To identify point mutations, primer pairs were used to amplify our regions of interest using pooled DNA samples from our TILLING population as a template. Using next generation sequencing, a total of 18-point mutations were identified and 13 were located in exons (6 in *BdCesA1* and 7 in *BdCesA3*). Extrapolating these results to the genome scale, we can tentatively expect an average of 1 mutation every 165 bp in our *Brachypodium* TILLING population. Hereafter, we characterized TILLING mutants, specifically focusing on *cesa3*^{P986S} and *cesa1*^{S830N}. However, it is worth noting that homozygous *cesa3*^{W775stop} mutants could not be obtained. This is similar to results from *Arabidopsis* where *Atcesa3* TDNA knockout mutants are gameophyte lethal.

4.2.3 Cellulose Content and Digestibility in *Bdcesa3*^{P986S} and *Bdcesa1*^{S830N} Mutants

To determine the affect of *cesa3*^{P986S} and *cesa1*^{S830N} mutations on cellulose biosynthesis, we measured the cellulose content in leaf, sheath, and stem tissue from mature plants and compared it to the wild-type (Bd21-3). On average, the leaf, sheath, and stem tissue of

Table 4.1 Total number and location of mutations identified in TILLING regions of BdCesA1 and BdCesA3.

BdCesA1		BdCesA3	
SNP ^a	Mutation	SNP	Mutation
G4497A	829 ^{S→N}	C3909T	Intron
G4549A	Silent	G3942A	Intron
C4634T	875 ^{L→F}	G4051A	Intron
C4790T	Intron	G4059A	Intron
C4884T	894 ^{L→F}	G4084A	775 ^{W→STOP}
G4912A	903 ^{G→D}	G4144A	795 ^{W→STOP}
G4984A	927 ^{G→D}	G4168A	Silent
		G4686A	949 ^{V→M}
		G4772A	Silent
		C4791T	985 ^{P→S}
		C4844T	Silent

^a Location of EMS-induced single nucleotide polymorphism (SNP) in the genomic sequence and subsequent amino acid change

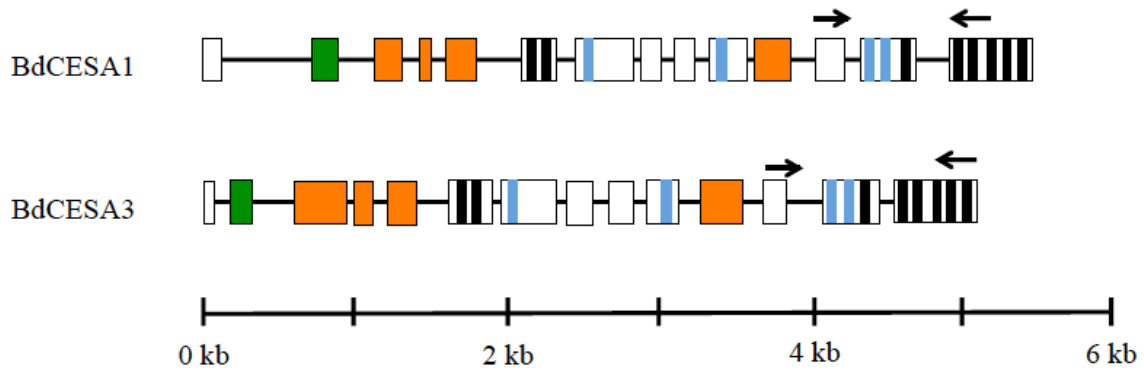


Figure 4.2 Gene structure, protein topology, and TILLING region of *BdCesA1* and *BdCesA3*. Boxes connected by black lines are exons and introns, respectively. Colored boxes or lines within a box represent unique *CesA* protein domains: zinc finger (green box), class specific region (orange boxes), black lines (transmembrane domains), catalytic domains D, D, D, QxxRW (blue lines). The black arrows indicate the location of TILLING forward and reverse primers. The scale represents the length of *CesA* gene in kilobase pairs.

wild-type plants contained 202, 314, and 384 µg of cellulose per mg of alcohol insoluble dry residue (AIR), respectively (Figure 3A). Overall, the mutations *cesa3^{P986S}* and *cesa1^{S830N}* had the most severe effect on stem cellulose content followed by sheath, and leaf tissue. A modest, but significant, 10% reduction in cellulose was detected in the sheath and stem tissue of *cesa3^{P986S}* mutants when compared to wild-type plant tissue. All sampled tissues of *cesa1^{S830N}* mutants had a reduction in cellulose content. In contrast to wild-type plants, *cesa1^{S830N}* mutants had an average of 7% less cellulose in leaf and sheath tissue and a substantial 25% reduction in stem cellulose content.

We further examined how the relative crystalline state of cellulose microfibrils and their interactions with other cell wall components had changed in *cesa3^{P986S}* and *cesa1^{S830N}* mutants. To do this, we measured the accessibility and susceptibility of cellulose found in untreated leaf, sheath, and stem AIR tissue to enzymatic digestion with endo- and exocellulase (Figure 3B). The amount of glucose released in *cesa1^{S830N}* mutants was relatively equal to the wild type in leaf tissue (97%) and numerically less than in stem (87%), and significantly less in sheath tissue (73%). For *cesa3^{P986S}* mutants, the amount of glucose enzymatically released in leaf and sheath tissue was similar (104%) to wild type plants and significantly more (127%) in stem tissue.

4.2.4 Phenotype of *Bdcesa3^{P986S}* and *Bdcesa1^{S830N}* TILLING Mutants

We next wanted to know if the reduction in cellulose detected in *cesa3^{P986S}* and *cesa1^{S830N}* mutants resulted in any phenotypic abnormalities (Figure 4A-F). In Arabidopsis, rapidly expanding tissue is most sensitive to mutations in primary wall *CesAs*. In Brachypodium, under our conditions, no differences in seedling root or coleoptile lengths were detected between mutants and wild-type plants after 7 days of growth in light or dark conditions, respectively (Figure 4C). Furthermore, no obvious differences were seen in vegetative growth through booting (BBCH scale stage 4; Hong et al. 2011)(Figure 4A). However during heading (BBCH stage 5), as inflorescence stems (peduncles) elongated, a measurable difference was observed. Analysis of peduncles on the main stem and the first two primary tillers indicated *cesa1^{S830N}* mutant peduncles were 38% of the wild type (8.2 cm) and *cesa3^{P986S}* peduncles were 20% longer (Figure 4B and 4C). Peduncles were further radial sectioned in order to look at their cell wall

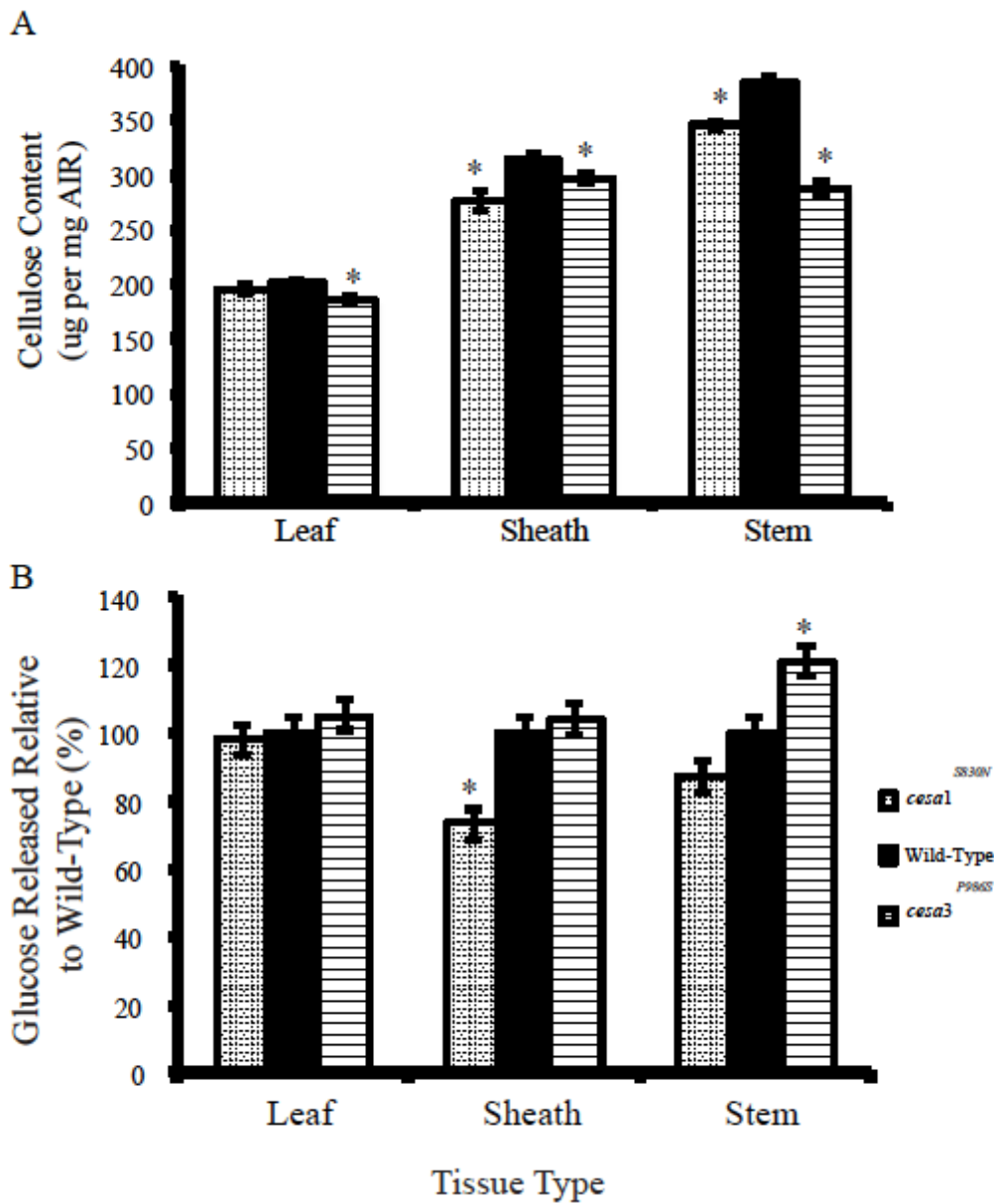


Figure 4.3 Cellulose content in leaf, sheath, and stem from senesced wild type (black), *cesa3*^{P986S} (1 perpendicular line right most), and *cesa1*^{S830N} (left most – combination of parallel and perpendicular lines) mutants (A) and its enzymatic digestibility (B). Asterisks indicate a significant difference from the wild type using Dunnett’s (alpha < 0.01)

structure. However, no obvious cell wall defects like collapsed xylem were observed (Figure 4D-F).

4.2.5 Non-Cellulosic Cell Wall Composition

To see how *cesa3*^{P986S} and *cesa1*^{S830N} mutants compensated for altered cellulose content, we quantified the non-cellulosic cell wall polysaccharides and acetyl bromide soluble lignin (ASBL) fractions of leaf, sheath, and stem from senesced plants (Table 2). To measure non-cellulosic polysaccharides, we hydrolyzed each tissue type in TFA. Across all genotypes and tissue type, the major neutral sugars in decreasing order were: xylose, glucose, arabinose, galactose, rhamnose, and fucose (not shown). This is consistent with arabinoxylans and mixed linkage glucans being the predominant non-cellulosic polysaccharides in grasses while proteoglycans and pectin (galactose, rhamnose, fucose) having only minor roles (Carpita, 1996; Rancour et al. 2012; Cass et al. 2016). The amount of arabinose, glucose, and xylose change was negligible within the stem and sheath tissue of genotypes. However, the amount of arabinose and xylose was significantly increased in leaf tissue of both mutants. Interesting, nearly a 1.4 fold increase in galactose was detected in both *cesa3*^{P986S} and *cesa1*^{S830N} mutants across tissue types. Rhamnose followed this same trend in both mutant stem tissues. In addition, no significant differences were detected in the ASBL fraction found in the stem, sheath, or leaf tissue and on average were 104, 94, and 65 $\mu\text{g mg AIR}^{-1}$, respectively.

4.3 Discussion

In this paper, we introduce a TILLING population as a new community-wide resource for functional genomic research in the grass model *Brachypodium*. Interested parties should visit the Brutnell lab website or another population created by Dalmais et al. (2013) called BRACHYTIL. TILLING is a reverse genetics approach to study protein structure and function by providing researchers with an allelic series of point mutations in their gene of interest. Here, we utilized the *Brachypodium* TILLING population to study CESA proteins important for cellulose biosynthesis during primary cell wall development. *Brachypodium* has 10

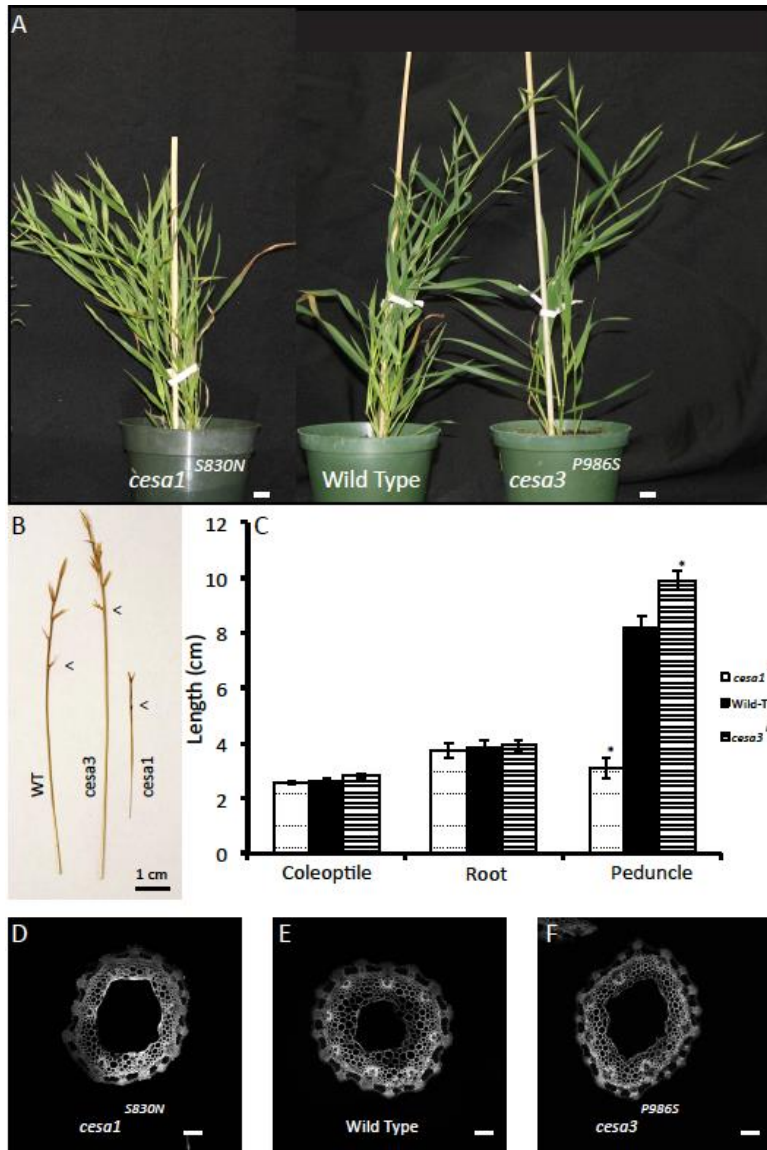


Figure 4.4 Comparing the growth characteristics of wild type, *cesa3*^{P986S}, and *cesa1*^{S830N} mutants. (A) Plants are representative samples of each plant genotype during seed fill growth stages. (B) Representative sample of peduncle length in genotypes. Peduncles were measured up to node (carrots). (C) Measurement of coleoptile (dark grown) and roots (light grown) length after 7 days and peduncle length for each genotype. An asterisk indicates a significant difference from the wild type using Dunnett (alpha = 0.05). (D-F) A representative radial section from peduncles of each genotype. Images were acquired with a confocal microscope at 488 nm. Scale bars (A) 2.54 cm, (B) 1 cm, and (D-F) 1 mm.

Table 4.2 Quantification of non-cellulosic TFA soluble sugars and acetyl bromide soluble lignin content in the stem, sheath, and leaf of wild type and TILLING mutants.

	Rhamnose ^b	Arabinose	Galactose	Glucose	Xylose	ABSL
	μg mg ⁻¹					
Stem^a						
Wild Type	1.9 ± 0.1 ^c	36 ± 1.7	7.8 ± 0.1	50 ± 2.0	147 ± 4.6	103 ± 2.4
<i>cesa3</i> ^{P986S}	2.4 ± 0.1*	41 ± 1.8	12 ± 0.1*	53 ± 1.9	132 ± 5.0	108 ± 2.5
<i>cesa1</i> ^{S830N}	2.4 ± 0.1*	40 ± 1.7	11 ± 0.1*	56 ± 2.0	149 ± 4.2	100 ± 2.3
Sheath						
Wild Type	2.5 ± 0.1	50 ± 3.2	12 ± 1.1	42 ± 1.6	140 ± 4.6	96 ± 2.8
<i>cesa3</i> ^{P986S}	2.6 ± 0.1	51 ± 3.1	15 ± 1.1*	47 ± 1.2	149 ± 4.1	99 ± 2.7
<i>cesa1</i> ^{S830N}	2.8 ± 0.1	53 ± 3.2	17 ± 1.1*	43 ± 1.4	146 ± 4.8	88 ± 2.9
Leaf						
Wild Type	5.2 ± 0.1	44 ± 5.7	17 ± 1.0	62 ± 5.0	103 ± 4.4	63 ± 2.8
<i>cesa3</i> ^{P986S}	4.6 ± 0.1	55 ± 5.8*	22 ± 1.2*	54 ± 5.0	144 ± 4.7*	64 ± 2.9
<i>cesa1</i> ^{S830N}	4.6 ± 0.1	51 ± 5.7*	20 ± 1.0	58 ± 4.6	124 ± 4.4*	67 ± 2.9

^a Tissue from 6 biological reps was measured in triplicate for each genotype for neutral sugars and only 4 biological reps for acetyl bromide soluble lignin (ABSL).

^b Fucose and mannose values are not shown (< 1.4 μg mg⁻¹).

^c Values are mean ± 1 standard error. Means were separated with Dunnetts and an asterisk indicates means were significantly different than the wild type at an alpha value of 0.01.

predicted *CesA* genes, but only 8 are full-length. In accordance with Handakumbura et al. (2013), we found *BdCesA1*, *BdCesA3*, *BdCesA6*, and *BdCesA9* are highly expressed in rapidly dividing and elongating tissue from 3-4 day old seedlings. Based on research in *Arabidopsis* (Desprez et al. 2007; Persson et al. 2007), we tentatively concluded *BdCesA1*, *BdCesA3*, and any one from the *CesA6*-like clade (*BdCesA6* or *BdCesA9*) are required to form 1 fully functional heterotrimeric polyunit in the hexameric cellulose synthase complex during seedling development (Nixon et al. 2016). We focused our TILLING efforts on *BdCESA1* and *BdCESA3* because loss of function mutation of these genes in *Arabidopsis* is pollen gametophyte lethal. We also found this to be partially true in our study as homozygous *Bdcesa3*^{W775stop} TILLING mutants could not be obtained (data not shown). This makes TILLING an especially powerful tool for studying the structure and function of CESAs. A screen of the *Brachypodium* TILLING population, revealed a total of 18-point mutations and 13 were located in exons (6 in *BdCESA1* and 7 in *BdCESA3*). In this paper we focused on *cesa3*^{P986S} and *cesa1*^{S830N}.

4.3.1 Biosynthesis and Crystallinity of Cellulose in TILLING Mutants. First, we feel it is important to the reader to understand where these mutations are located and how they could disrupt the functionality of CESAs. The *cesa3*^{P986S} missense mutation is located near the middle of the 6th out of 8 transmembrane domains while the serine to asparagine substitution at 830 in *cesa1* is located in the cytosolic catalytic loop just after (10 amino acids past) the important glycotransferase motif QXXRW and before the beginning of the 3rd transmembrane region. These mutations have the potential to disrupt the catalysis and extrusion of a single glucan chain through the transmembrane pore in CESAs and further alter the crystallization of glucan chains into a cellulose microfibril.

To test this, we measured the amount of cellulose and its digestibility by cellulases in the *Bd21-3* wild type and mutants. In the wild type, we found, on average, the leaf, sheath, and stem tissue from senesced mature plants contained 202, 314, and 384 µg of cellulose per mg of AIR, respectively. This data is consistent with the literature (Christensen et al. 2010; Rancour et al. 2012; Cass et al. 2016). The *cesa1*^{S830N} mutant had an average of 7% less cellulose in leaf and sheath tissue and a 25% reduction in stem cellulose content. After accounting for this reduction, the amount of glucose released

from enzymatic digestion of cellulose was, on average, 20% less in sheaths and stems in comparison to wild type. This could indicate a reduction in cellulose susceptibility to enzymatic attack because of pleiotropic cell wall modifications and/or their interaction with cellulose. Phenolic compounds, mostly lignin and ferulic acid, in grasses are known to have a deleterious effect on enzymatic cellulose saccharification (Li et al. 2008; de Oliveira et al. 2015 and referenced there in). However, we did not detect an increase in ABSL lignin content in either mutant. Since we did not directly measure ferulic acid, we cannot exclude it from having a possibility role in hindering cellulose digestion.

In *cesa3*^{P986S} mutant plants, a 10% reduction in cellulose was detected in sheath and stem tissue and this cellulose was more susceptible (16%) to enzymatic digestion relative to wild type tissue. The location of this mutation in a transmembrane region would suggest translocation of the glucan chain and ultimately hybridization of glucan chains into a crystalline like state is altered. In Arabidopsis, mutations in the 4th transmembrane (*cesa1*^{A903I}) and in the putative “gated loop” between the 5th and 6th transmembranes (*cesa3*^{T942I}) also significantly decreased cellulose crystallinity (Harris et al. 2009; Harris et al. 2012; Slabaugh et al. 2014). Changes in cell wall architecture can also lead to increased saccharification. For example, Marriot et al. (2014) found a mutant called *sac1* that had reduced xylose content and the authors hypothesized the increased saccharification was because of a reduction in ferulic acid attachment sites on arabinoxylans.

4.3.2 Tilling Mutant Phenotype and Cell Wall Compensation. Cellulose is required for anisotropic growth and tissue undergoing rapid cellular expansion is most sensitive to cell wall defects (Brabham and Debolt 2012; Carpita and McCann 2015). For example, disrupting CesaA expression or protein function in Arabidopsis can result in swollen seedling tissue, smaller leaves, and shorter inflorescence stems (Williamson et al. 2001; Burn et al. 2002; Persson et al. 2007). In our Brachypodium mutants, grown under laboratory conditions, no obvious morphological defects were observed during vegetative growth stages. At maturity, inflorescence height was noticeable shorter (62%) in *cesa1*^{S830N} plants in comparison to the wild type and closer examination revealed

peduncles failed to properly elongate. In contrast, *cesa3^{P986S}* mutants had a 20% longer peduncle in comparison to the wild type.

It was surprising to us that no growth abnormalities were detected in seedlings or in vegetative growth in our conditions. This could indicate a compensatory response in cell wall architecture occurred in mutants and we tested this by measuring the TFA hydrolysable non-cellulosic cell wall fraction of mature plant tissue. In leaves, both *cesa3^{P986S}* and *cesa1^{S830N}* mutants presumably compensated for weakened cell wall integrity by significantly increasing arabinoxylan content. A major compensatory response in sheath and stem from either mutant was not detected. A subtle (~1.4 fold increase) change was measured in galactose (~1.4 fold increase) in both tissue types but this monosaccharide accounted for less than 5% of the total non-cellulosic cell wall fraction. Thus the lack of a reduced growth mutant phenotype in vegetative tissue and the longer peduncle in *cesa3^{P986S}* mutants is still surprising. Taken as a whole, the unique characteristic of grass cell wall may be better able to withstand genetic manipulation for improved saccharification than dicots but this hypothesis needs further testing to validate.

4.4 Materials and Methods

Plant Material and Growth. The Brachypodium line Bd21-3 was used in all experiments. Bd21-3 seed were originally EMS-mutagenized by the Brutnell laboratory at the Danforth Center (St. Louis, Missouri) to create a TILLING population. The Brutnell lab also screened and identified TILLING mutants using our TILLING primers and subsequently sent us the mutants for characterization. TILLING primers were designed using the web-based tool CODDLE (Codons Optimized to Discover Deleterious Lesion; Henikoff et al. 2004). In all experiments, seeds were sterilized with 30% household bleach for 15 min and subsequently washed three times with sterile distilled water and kept at 4 C for 2 d or 3 weeks. The 3-week cold treatment sufficiently vernalized seeds to promote rapid flowering. For all measurement studies, plants were pre-germinated and seedlings with a protruding radicle < 1mm were selected for use. To measure coleoptile (dark grown) or root (light grown) length at 7 days after germination, seedlings were placed on agar (11 g L⁻¹) plates and grown vertically in growth chambers at 22 C with a 14-h photoperiod. Plates of dark grown plants were wrapped in aluminum foil. After 7

days, tissue length were measured. Seedlings were left in the growth chamber for an additional week and transferred to soil pots and growth was maintained under 24-hr supplemental lighting at room temperature. Peduncle length from the primary and 1st 2 tiller stems were measured and further sectioned with a vibratome or by a hand-held razor to observed cell walls. Sections were stained in ammonium and fluorescence was visualized at 488 nm wavelength with a Olympus confocal microscope.

Identification of Brachypodium CESAs. The protein sequences of Arabidopsis and Rice CESAs were blasted against the Brachypodium genome (Phytozome) and putative BdCESAs were checked for domains specific to CESAs glycotransferases (Carroll and Specht, 2011). Handakumbura et al. (2013) named BdCESAs after their closest Arabidopsis orthologs. We conducted a phylogentic analysis in Mesquite (100 bootstraps) using the class specific protein region (D to QxxRW motif) from Arabidopsis and Brachypodium to confirm their results. Our results matched, thus we used their naming system.

Expression of Putative CESAs. For qRT-PCR, we followed the rules provided by Udvardi et al. (2008). Shoot and root tissue of light grown and coleoptile tissue from dark grown 3 to 4 day old seedlings and the bottom 4 internodes (secondary cell wall tissue) from 3 week old plants were harvested and stored at -80 C for later RNA extraction. During harvest, shoot tissue (coleoptile removed) was only harvested if the first leaf had not developed a collar and for elongating coleoptile tissue the encapsulated shoot was removed. Tissue was pooled within sectioning group from multiple biological samples until roughly 100 mg of tissue was collected. This was considered one biological replication. RNA was extracted from each sample following the RNAeasy Kit manual (Quaigen) instructions. After synthesis of cDNA, regular PCR was conducted using GADPH intron spanning primers for each sample to check for RNA contamination. Quantitative RT-PCR primers are listed in Table 5.1. Ten ng/uL of cDNA was used in an individual tube run⁻¹. Relative fold change was determined using the delta-delta method with our control gene being GADPH and standardized against gene expression in stems.

Data was logged transformed to meet basic ANOVA assumptions. Means were separated at an alpha value of 0.01 using Tukeys test and back transformed for presentation.

Cell Wall Analysis. Senesced plants were harvested and sectioned into leaf, sheath, and stem tissue then dried for 1 week at 60 C. Tissue was either milled or sectioned into pieces (>3mm) with a scalpel. To obtain alcohol insoluble crude cell wall residue (AIR), tissue was washed with 70% ethanol and placed in a 70 C water bath for 1 hr. This was repeated twice, except the final ethanol wash was left over night, followed by a brief acetone wash at room temperature. Dried AIR tissue was subsequently used for cell wall analyses.

To measure cell wall sugars, 3 to 5 mg of AIR was weighed out in triplicates for each biological sample and placed into glass tubes. There were 6 biological samples genotype⁻¹. To determine non-cellulosic neutral sugar monosaccharides, material was autoclaved at 121 C for 90 min with 2 N trifluoroacetic acid (TFA). Afterwards, TFA was evaporated off for 2 two days under vacuum and samples were resuspended in 500 uL water, vortexed, and spun at 2000 rfc for 5 min. The supernatant was removed and placed into a 2 mL eppendorf tube and the pH was adjusted to a basic pH (9-11) using 10 M NaOH and then subsequently filtered into HPLC vials. Myo-inositol was used as an internal standard. Neutral sugars (fucose, rhamnose, arabinose, galactose, glucose, mannose, xylose) were identified and quantified by pulsed electrochemical detection using a Dionex ED50 apparatus. Sugars were separated using a CarboPAC-PA1 anion-exchange column following the protocol described by Mendu et al. (2011).

The TFA insoluble residue was washed with 70% ethanol then acetone and dried overnight. The residue was then boiled in nitric acetic acid for 30 min and washed twice with water and once with acetone to remove solubilized sugars. The acid insoluble residue (considered crystalline cellulose) was hydrolyzed in 67% sulfuric acid for 1 hr and quantified colorimetrically using the anthrone-sulfuric acid method (Foster et al. 2010).

Lignin content in tissue types for each genotype was determined using a modified acetyl bromide method (Fukushima and Hatfield 2001 and 2004; Chang et al. 2008). Briefly, 5 mg of AIR tissue was placed in a 10 mL glass screw-cap tubes and 1 mL of

fresh acetyl bromide:glacial acetate acid mixture (25:75 v/v) was added. Tubes were then placed in a hot water bath (50 C) for 2 hr with occasional shaking. After samples had cooled to room temperature, 4 mL of glacial acetic acid was added, vortexed, centrifuged at 2000 rcf for 15 min, and 150 uL of supernatant was transferred to an eppendorf tube. In each tube, a freshly made absorbance solution was added (1.1 mL), capped, and inverted a few times. The 1.1 mL absorbance solution contained 200 uL of 1.5 M NaOH, 150 uL of 0.5 M hydroxylamine hydrochloric acid, and 750 uL of glacial acetic acid. Samples were transferred to quartz cuvette and absorbance was measured at 280 nm. A non-tissue blank was included at the start of the experiment. To calculate total acetyl bromide soluble lignin (ABSL) content in AIR tissue, absorbance values were divided by the extinction coefficient 18.126 (average slope value of bromegrass from Fukushima and Hatfield 2001), multiplied by the dilution factor 33.33 (0.150 mL/5 mL), divided by the starting AIR weight, and finally multiplied by 1000 to get ug ABSL mg⁻¹. Each tissue type was replicated 3 times per biological rep and there were 4 biological replications genotype⁻¹. For all cell wall components, data was checked for normality and means were separated at an alpha value of 0.01 using Dunnetts test.

Microscale Enzymatic Saccharification. Enzymatic saccharification of leaf, sheath, and stem AIR tissue from Bd21-3 and mutant plants was conducted following a microscale version of the National Renewable Energy Laboratory (NREL) protocol low solids enzymatic saccharification of lignocellulosic biomass (Harris et al. 2009). Briefly, 5 to 6 mg of AIR tissue was placed in to 500 mL of an equal enzymatic mixture of Celluclast (cellulase from *Trichoerma reesei*) and Novozyme 188 (cellobiase from *Aspergillus niger*) for 24hrs. All enzymes were purchased from Sigma-Aldrich (St. Louis, MO USA). During the 24-hr period, samples were placed in an eppendorf box and shaken horizontally in an Innova 4300 incubator/shaker at 50 C while shaking at 300 rpm using a 1-inch orbit. Enzyme blanks and Whatman #1 filter paper were included as negative and positive controls. Afterwards, tubes were centrifuged briefly and 150uL was extracted and placed into a 96 well plate. Glucose content (g L⁻¹) was measured electrochemically in a YSI 2900 Biochemistry Analyzer. Here, the hydrogen peroxide by-product from the oxidation of glucose with glucose oxidase was used to create a current. This value was

converted into glucose content using a standard curve. The amount of glucose detected in the blank was initially subtracted from sample values. Next, these values were divided by the amount of tissue weight (mg) in each tube and then converted percent glucose extracted from cellulose and expressed as percent of the wild type. Three biological samples for each tissue type for a genotype were used for to obtain values and this was repeated in time. Data was check for normality and means were separated at an alpha value of 0.01 using Dunnetts.

Chapter 5 Probing Plant Cell Wall Biology in Grasses: A Function of Chemical Genetics and Herbicide Selectivity

5.1 Introduction

Cellulose is a major structural component found in plant cell walls and is required for anisotropic cell enlargement. It is made up of multiple coalesced strands of β -1,4 linked glucose molecules that are synthesized, intertwined, and finally deposited into the cell wall by a plasma membrane bound multi-protein complex referred to as the cellulose synthase complex (CSC) (Kimura et al. 1999; Somerville 2006). The catalytic subunits in this complex are the CELLULOSE SYNTHASE A (CesA) proteins and each CesA extrudes one glucan chain. The CSC is empirically thought to be a hexamer of heterotrimeric CesA subunits in an equimolar ratio (Gonneau et al. 2014; Hill et al. 2014; Nixon et al. 2016; Vandavasi et al. 2016). In *Arabidopsis thaliana* (L.), 10 CesA isoforms exist and traditional genetic experiments have shown CesA1, CesA3, and one representative from the CesA6 clade (2, 5, 6, 9) are collectively required to form a fully functional CSC in rapidly dividing and elongating cells (Desprez et al. 2007; Persson et al. 2007) This process appears to be evolutionary conserved amongst Angiosperms (Tseko 1999; Carroll and Spect 2011). A number of CSC-specific and -nonspecific accessory proteins are necessary for CSC assembly, trafficking, localization, and PM motility as well as cellulose crystallization (Gu et al. 2010; Mansoori et al. 2014; Vain et al. 2014; Worden et al. 2015; Zhang et al. 2015).

Chemical biology has become an extremely valuable tool for plant biologists in simplifying the complexity associated with cellulose biosynthesis (Paredes et al. 2006; Gutierrez et al. 2009; Brabham and Debolt, 2012; Worden et al. 2015). Chemical biology is an adjustable and reversible approach using inhibitors of protein function rather than complete reliance on traditional genetic approaches (Spring 2005). Further exploitation of this methodology depends on identifying mutants with increased or decreased sensitivity to the tested inhibitor. It is assumed that mutations in the select mutants are located in proteins that have some role in the pathway or function of interest. This has been shown to be a fair assumption with compounds that inhibit cellulose biosynthesis (CBIs). More specifically, high levels of resistance to isoxaben, quinoxiphen, and flupoxam have been

identified in ethyl methanesulfonate (EMS) mutagenized *Arabidopsis* populations and mapped to amino-acid-changing point mutations in *CesA1*, *CesA3*, or *CesA6* (Heim et al. 1989; Scheible et al. 2001; Desprez et al. 2002; Harris et al. 2012; Shim 2014; Tatento et al. 2015). Interestingly, none of the tested point mutations are known to confer cross-resistance to the other compounds (Heim et al. 1998; Sabba and Vaughn 1999; Harris et al. 2012). It also been observed, except for quinoxiphen, that these compounds have a greater efficacy on dicots than on grass seedlings. For example, isoxaben, when used as a herbicide is labeled for use in established turf, perennial crops, and non-cropland for annual broadleaf weed control, but not for weedy grasses (Shaner 2014). In addition, the triazole carboxamides, flupoxam and triazofenamide, were at one time being considered for pre- and post-emergence use in cereals and rice but are not currently (Heim et al. 1998).

In agriculture, weeds can evolve resistance or be inherently tolerant to herbicides through several target- and non-target-site mechanisms. Non-target-site mechanisms prevent the herbicide of interest from reaching phytotoxic levels at the site of action (ex: meristems). This can be accomplished by reducing the amount of herbicide absorbed and/or translocated to the site of action, herbicide metabolism, or compartmentalization (ex: vacuoles). Gene amplification/duplication of the herbicide target and genetic mutations (point mutations / deletions / insertions) that lower the binding affinity of the herbicide are considered target-site mechanisms. Unique biological characteristics at the cellular, organ, or in whole plant can also lead to increased tolerance (Hall et al. 1994; Powles and Preston 2006, Gaines et al. 2010).

The tolerance exhibited by grasses to isoxaben has been investigated, but is not fully understood. Tolerance is presumed to be a target-site mechanism because differences in isoxaben metabolism or uptake could not sufficiently explain the isoxaben tolerance observed in wheat and creeping bentgrass (Cabanne et al. 1987; Corio-Costet et al. 1991; Heim et al. 1993). The biological differences in the non-cellulosic fraction of grass cell walls versus that found in dicots could be another potential and untested tolerance mechanism. The primary wall is a compositional matrix of cellulose, hemicellulose, pectin, aromatics, and proteins.

Primary cell walls can be classified as type I or II walls. The typical type I cell walls found in dicots, gymnosperms, and non-Commelinoid monocots species contains 25% cellulose, 35% hemi-cellulose, 30% pectin, and 10% proteins on a dry weight basis. The type II wall of rushes, sedges, and grasses in the Commelinoid order is roughly composed of 25% cellulose, 65% hemi-cellulose, and < 5% pectin, phenolics, and proteins (Carpita and Gibeaut 1993; Carpita 1996; Vogel 2008). Furthermore, the composition in the non-cellulose fraction differs considerable between type I and II primary walls. Type I walls are rich in xyloglucans in a cross-linking pectin matrix. Conversely, the hemi-cellulose composition in type II walls is mainly phenolic crossed linked arabinoxylans with growth stage dependent amounts of mixed linked glucans (MLG) and minor amounts of xyloglucans (Carpita and Gibeaut 1993; Scheller and Ulvskov 2010; Fincher 2009). MLG is made up of β -1,4 linked glucose molecules with a β -1,3 linkage normally every 3 to 4 repeating units of β -1,4 glucans. The β -1,3 linkage introduces a “kink” in the polysaccharide chain and reduces the ability of MLG to completely hybridize with other polysaccharides and gives MLG an overall gel like behavior (Fincher 2009). MLG content in vegetative tissue is highest in elongating tissue and rapidly declines as tissue ages (Carpita 1996; Christenson et al. 2010, Vega-Sanchez et al. 2012; Riksfardini et al. 2015). Genes in the cellulose synthase-like F (CslF) or H (CslH) families have been implicated in MLG production (Burton et al. 2006; Burton et al. 2008; Doblin et al. 2009).

If labeled for agricultural use, CBIs are used as pre-emergent herbicides and have a narrow window of opportunity to effectively control seedlings. Herein, the focus of this research is to elucidate the tolerance mechanism of grasses to isoxaben utilizing *Brachypodium* as our model grass. We propose isoxaben tolerance in grasses is due to the unique compensatory response of grass cell walls to CBIs instead of known target and non-target site mechanisms.

5.2 Results

5.2.1 Grasses Are Tolerant to a Chemical Diverse Subclass of CBIs.

Grasses are tolerant to a selective number of CBIs, mainly isoxaben and the triazole carboxamides of flupoxam and triazofenamide (Cabanne et al. 1987; Heim et al.

1998; Sabba and Vaughn 1999). To quantify and compare the sensitivity of grass and dicot seedlings to isoxaben, we conducted a dose response experiment using *Brachypodium* and annual bluegrass to represent grasses and the dicot representatives were *Arabidopsis* and soybean (Figure 1). At 7 days after treatment, root growth in all seedlings was inhibited in a dose dependent manner and at higher rates roots were severely stunted and swollen. The level of susceptibility from most to least was *Arabidopsis* > soybean > *Brachypodium* > annual bluegrass. The rate at which root growth was reduced by 50% (GR_{50}) for *Arabidopsis* was 3.1 nM. Based on GR_{50} values, soybean, *Brachypodium*, and annual bluegrass were 31-fold, 91-fold, and 160-fold more tolerant to isoxaben in comparison to *Arabidopsis*, respectively. In comparison to soybean (GR_{50} 93 nM), *Brachypodium* was nearly 3-fold more tolerant and annual bluegrass was 5.3-fold more tolerant. Analysis of this data indicates grasses exhibit a high level of tolerance to isoxaben and tolerance is independent of seed size.

In the dicot *Arabidopsis*, resistance to isoxaben and flupoxam is conferred by point mutations in *CesAs* (reviewed in Tatento et al. 2015). Next, we asked whether reduced grasses activity is a common characteristic of CBIs that target CESAs. To test this, we utilized quinoxiphen. Resistance to quinoxiphen can be conferred by three different point mutations mapped to *CesA1* in *Arabidopsis* (Harris et al. 2012; Tatento et al. 2015), but its phytotoxicity to grasses is not known. A dose response experiment was conducted as above to address this question (data not shown). Growth of *Arabidopsis* and soybean seedlings was severely inhibited at rates greater than 1 μ M and 10 μ M quinoxiphen, respectively. Quinoxiphen at 100 μ M did not reduce root length of annual bluegrass and *Brachypodium* by more than 25%. However, these results may not be completely reliable because quinoxiphen became increasingly difficult to solubilize in DMSO as rates exceeded 50 μ M. Together, the CBI tolerance detected in the tested grasses raises an interesting question about grass cellulose biosynthesis, but first we wanted to exclude the possibility that known target-site and non-target site mechanisms could explain tolerance. For this, we used *Brachypodium* and isoxaben as our model grass and CBI.

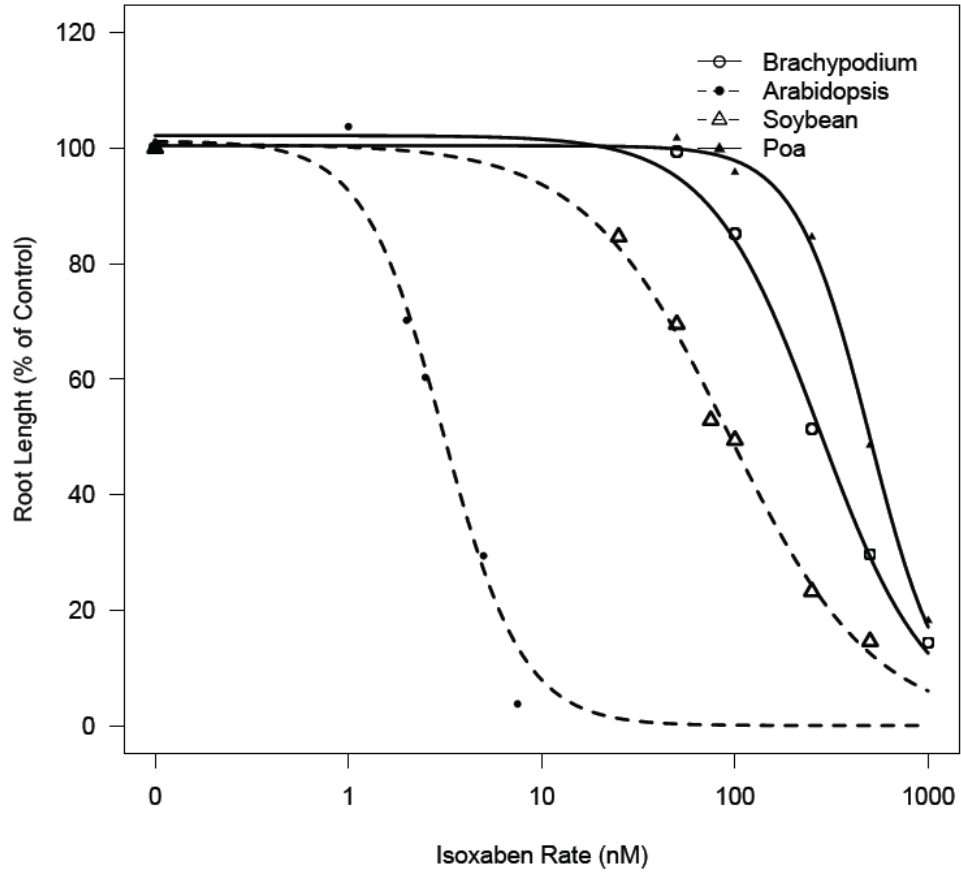


Figure 5.1 Isoxaben root growth inhibition curves of Brachypodium, annual bluegrass, Arabidopsis, and soybean seedlings after 7 days on treatment. The graph depicts the tolerance levels of grasses (solid lines) to isoxaben in comparison to dicots (dash lines).

5.2.2 Brachypodium Does Not Sufficiently Metabolize Isoxaben.

Brachypodium seedlings are nearly 100-fold more tolerant than Arabidopsis to isoxaben and this level of tolerance would suggest the most likely tolerance mechanisms are metabolism and/or target-site based. We first tested if 6-day old Brachypodium seedlings could metabolize 1 μM of ^{14}C -isoxaben (Figure 2A-C). After 72 hours of treatment, roots adsorbed 12% of the total radioactivity and 49% was translocated to shoot tissue. In roots and shoots 80% of the radioactivity was detected in the form of the parent compound and only 20% as an unknown metabolite (Figure 2.B). This data support the idea that grasses do not sufficiently metabolize isoxaben to explain tolerance compared to dicots. Therefore, we hypothesized that differences in the binding affinity of isoxaben to Cesa target site in dicots versus grass CesAs is the tolerance mechanisms.

5.2.3 Known Resistance Conferring Point Mutations Are Not Found in BdCesAs.

In Arabidopsis (At), 7 amino point mutations in *AtCesA3* and 2 in *AtCesA6* confer resistance to isoxaben (summarized in Tatento et al. 2015). The exact inhibitory mechanism or affinity of isoxaben to CesAs is not known but it assumed *CesA3* and/or *CesA6* are the molecular targets. To determine if the aforementioned point mutations are naturally found in the Brachypodium *CesA* orthologs, we first had to identify them (Figure 3A). The Brachypodium reference genome has 8 predicted full-length and 2 truncated *BdCesAs*. Handakumbura et al. (2013), through phylogenetic and gene expression analysis, named them after their closest Arabidopsis orthologs. Interestingly, Brachypodium has an additional copy of *CesA3* (*BdCesA2* and *BdCesA3*) and only half the number (2) of a full length *CesA* (*BdCesA6* and *BdCesA9*) in the *CesA6* clade. To further validate their naming system, we quantified the relative gene expression profiles of *CesAs* in coleoptile tissue from 3 to 4 day old dark grown seedlings (Figure 3A). Analysis of our results indicate *BdCesA3* and *BdCesA6* or *BdCesA9* are the putative isoxaben targets. An increase in the number of *CesA3*-like cellular targets, or gene amplification, is probably not a viable tolerance mechanism because *BdCesA2* does not appear to be highly expressed (Figure 3A; and Handakumbura et al. 2013). Alignment of the *BdCesA3* protein sequence with an isoxaben-susceptible and –resistant form of *AtCesA3* revealed *BdCesA3* does not contain the expected point mutations (Figure 3B).

A Amount and Partittioning of ¹⁴ C-Isoxaben in 9 Day Old Brachypodium		
	Root	Shoot
	----- % -----	
Total ¹⁴ C Extracted *	12	
Partitioning of ¹⁴ C Extracted	51	49
Form of ¹⁴ C-Isoxaben		
Metabolite A	18	21
Parent Molecule	82	79

* > 90% of total radioactivity was recovered

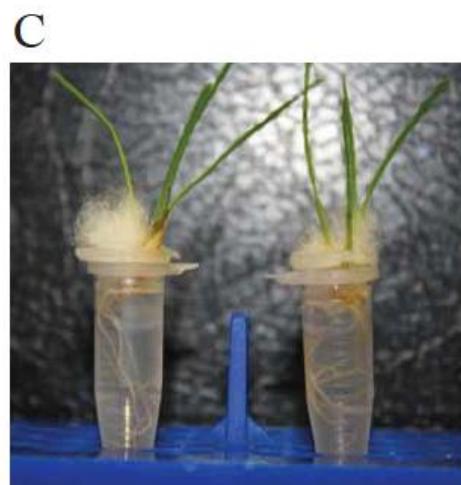
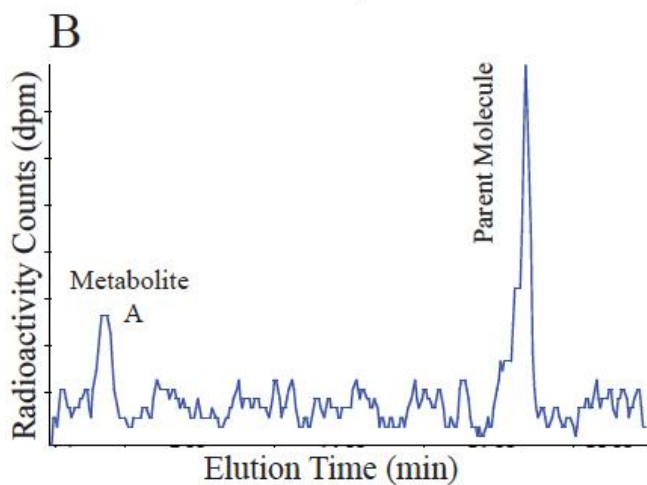


Figure 5.2 A) Brachypodium does not sufficiently metabolize radiolabeled isoxaben after 72 hours of treatment. B) A representative chromatograph of ¹⁴C-Isoxaben metabolites from root extracts. C) A representation of experimental setup.

The same was observed with BdCesA6 and BdCesA9 in comparison to a susceptible and resistant protein sequence of AtCesA6 (Figure 3B). This would indicate BdCesAs do not contain known resistance conferring point mutations. However, we cannot eliminate the possibility that other amino acid changes detected in BdCesAs reduce the binding affinity of isoxaben. We are currently working to compliment *AtCesA6^{prc1-1}* or *AtCesA3^{je5}* mutants with their respective Brachypodium orthologs to test for this possibility

5.2.4 CSLF6 Mutants are Hypersensitive to Isoxaben.

After investigating expected isoxaben tolerance mechanisms, the question of interest was whether cellulose biosynthesis had sufficiently evolved in grasses after divergence from dicots. A review of the literature strongly indicates the biosynthetic machinery required for cellulose production is conserved amongst Angiosperms (Tseko 1999; Carroll and Spect 2011; Handakumbura et al. 2013). So, in rethinking the phytotoxic affects of these compounds, we suspected rapidly expanding tissue is the most susceptible to CBI treatment because of the weakened state of cell walls and not the loss of cellulose per se. The inability of the cell wall to resist the massive turgor pressure exerted on it by the encapsulated cell results in isotropic cell expansion and stunted seedlings growth. In realizing this, we decided to investigate grass-specific non-cellulosic primary cell wall components and their role in isoxaben tolerance (Figure 4A-E). We focused our efforts the hemi-cellulose polysaccharide made up of β -(1,3)(1,4) linked glucose molecule called mixed linkage glucans (MLG). In vegetative tissue, MLG content is highest in cell walls when seedlings are most sensitive to CBIs (Christenson et al 2010; Vega-Sanchez et al. 2012; Riksfardini et al. 2015) and could presumably partially compensate for the loss of cell wall integrity. *Cellulose synthase-like F6 (CslF6)* appears to be the major isozyme involved in MLG synthesis (Burton et al. 2006; Burton et al. 2008; Christenson et al 2010; Vega-Sanchez et al. 2012). To test the role of MLG in isoxaben tolerance, a putative *Bdcslf6* (Bradi3g16307) T-DNA insertional mutant was identified from the JGI Brachypodium collection (Bragg et al. 2012) (Figure 4A-E). The T-DNA is predicted to be located in an intron after the first exon and semi-quantitative PCR for CSLF6 transcript revealed this gene is transcribed in 2-3 day old seedlings (data not shown). Quantitative RT-PCR was conducted to determine if *CslF6* is still expressed at the same

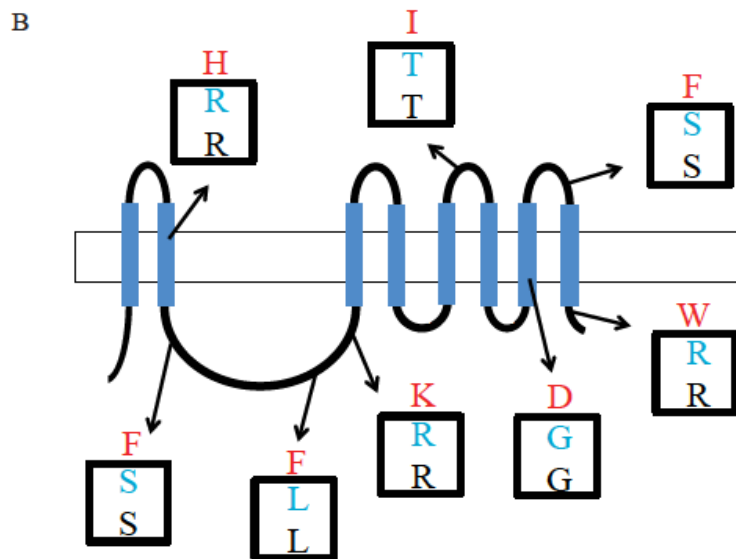
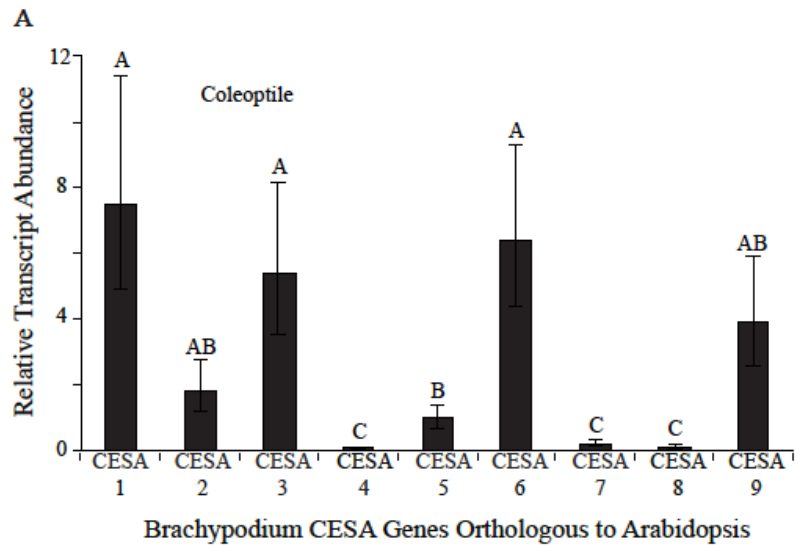


Figure 5.3 The putative isoxaben targets in Brachypodium do not contain expected resistance conferring point mutations found in Arabidopsis. A) Characterizing relative transcript abundance of Brachypodium *CesA* genes in 3-4 day old coleoptiles to identify isoxaben targets. Fold change values were determined by comparing against gene expression in 3 week old stem tissue. Means followed by a different letter are considered significantly different at alpha at 0.05 using tukeys. B) Combined results from protein alignment of BdCesA3 with an isoxaben-resistant and -susceptible Arabidopsis Cesa3 sequence and BdCesA6 and 9 with an Arabidopsis resistant- and -susceptible form of Cesa6. The red letters outside boxes are the amino acid change detected in isoxaben resistant Arabidopsis plants. Inside boxes, blue letters are the amino acid found in susceptible (wild type) Arabidopsis and black letters are the amino acids found in Brachypodium.

magnitude in putative *cslf6* plants in comparison to wild type (Figure 4A). In 2-3 day old wild type seedlings, the relative expression of *CsIF6* was 94% of the *GAPDH* control, but only 84% of *GAPDH* in *cslf6* plants. Moreover, glucose content in the TFA hydrolysable cell wall fraction was significantly reduced by 66% in 2-3 day old *cslf6* mutants in comparison to wild type (Figure 4B). This is not a direct measurement of MLG content because glucose from glucuronoarabinoxylans or xyloglucans (glucose backbone with xylose substitutions) found in grass primary cell walls can contaminate this pool (Carpita and Gibeaut 1993; Fincher 2009; Christensen et al. 2010). *Bdcslf6* mutants also display spontaneous lesions in mature leaf tissue (Figure 4C) similar to that observed in rice *cslf6* mutants (Vega-Sanchez et al. 2012). Analysis of the collective data indicates that the MLG content is significantly reduced in this mutant.

To determine if MLG played a role in grass tolerance to isoxaben, a dose response experiment was conducted to quantify and compare the isoxaben GR₅₀ values of *cslf6*, *cesa1*^{S830N} mutants to wild type seedlings (Figure 4D and E). A *cesa1*^{S830N} mutant with reduced cellulose content (thesis Chapter 3) was included and was expected to be overly sensitive to isoxaben. At 7 days after treatment, the GR₅₀ root inhibition values for wild type, *cesa1*^{S830N}, and *cslf6* were 261, 248, and 123 nM of isoxaben, respectively (Figure E). Interestingly, *cslf6* mutants, but not *cesa1*^{S830N} mutants, were hypersensitive to isoxaben than the wild type. This suggests MLGs positively influence the overall mechanical strength of cell walls, but we were expecting a greater increase (> 5 fold) in isoxaben sensitivity than 2.1 fold detected in *cslf6* mutants.

5.3 Discussion

Cellulose biosynthesis inhibitors (CBIs) are useful compounds for weed control and for dissecting cellulose biosynthesis. In this paper, weed science and plant biology data was used to investigate the tolerance mechanisms of grasses to the CBI isoxaben. However, we also quickly realized that grasses are tolerant to a chemically diverse subclass of CBIs that have an affinity for primary cell wall CesAs (Figure 1A; data not shown). This CBI subclass contains isoxaben, quinoxiphen, and the triazole carboxamides, flupoxam and triazofenamide. Resistance to these compounds has been mapped to point mutations on *AtCesA1*, *AtCesA3*, and *AtCesA6* in Arabidopsis. In dose response experiments, we

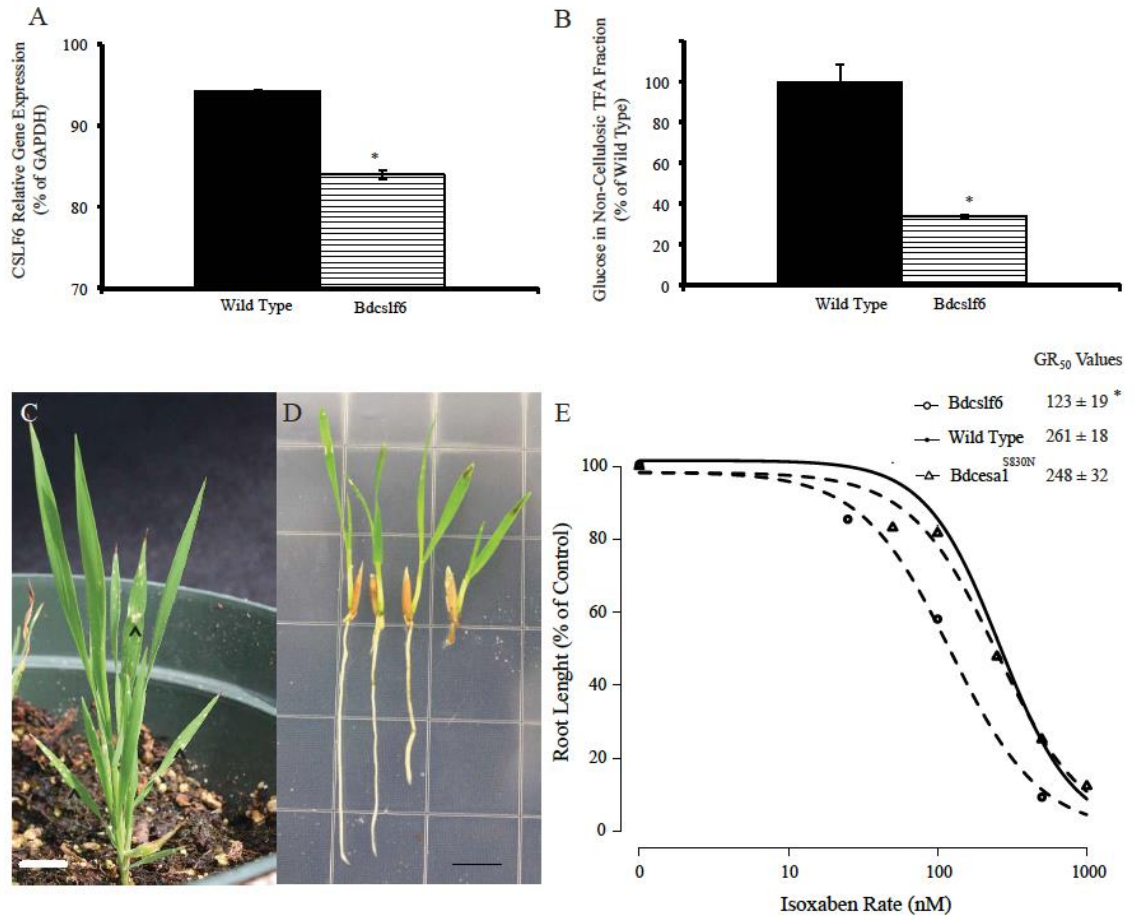


Figure 5.4 Characterization of *Brachypodium csf6* mutants gene expression, glucose content, and susceptible to isoxaben. A) Relative transcript abundance of *CSLF6* in 2-3 day old wild type (black) and *csf6* mutants. Transcripts were standardized to control gene expression (*GAPDH*). B) An indirect measurement of mixed linkage glucan content. Glucose content in TFA hydrolysable non-cellulosic cell wall fraction from 2-3 day old type (black) and *csf6* mutants standardized to the wild type. C) The picture is a representative image of *csf6* mutants and the spontaneous lesions the contain (carats). D) A representative seedlings from the isoxaben dose response (left to right 0, 50, 100, 500nM). E) Isoxaben dose response curves and GR₅₀ values for *Brachypodium* wild-type (solid line), *Bdcslf6* (dash line and circles), and *Bdcasal*^{S830N} mutants (dash line with triangles). All scale bars = 1 cm and asterisks indicate a significant difference at alpha value of 0.05.

found grasses (Brachypodium and annual bluegrass) were at least 50-fold or 3-fold more tolerant to isoxaben and quinoxiphen compared to Arabidopsis or soybean seedlings, respectively.

Based on the high level of tolerance exhibited by grasses in comparison to Arabidopsis, the most likely tolerance mechanisms were predicted to be herbicide metabolism or differences binding affinity to target-site CesAs. To test these mechanisms, we used Brachypodium as our model grass and isoxaben as our model CBI. We found Brachypodium did not appreciably metabolize isoxaben 3 days after the initial treatment (Figure 2). This result agrees with Cabanne et al. 1987, Corio-Costet et al. 1991, and Heim et al. 1993 who also found differences in uptake and translocation of isoxaben between grass and dicot seedlings was minor. We next investigated target-site resistance. In Arabidopsis, 7 amino acid changing point mutations in *AtCesA3* and 2 in *AtCesA6* confer resistance to isoxaben (summarized in Tatento et al. 2015). These mutations presumably reduce the binding affinity of isoxaben to its CesA targets. To determine if Brachypodium naturally contained these amino acid changes, we identified the Arabidopsis CesA3 and CesA6 orthologs. BdCesA3 and BdCesA6 or BdCesA9 were identified as the putative isoxaben targets (Figure 3A; Handakumbura et al. 2013). The Brachypodium orthologs did not contain the same amino acid substitutions as resistant Arabidopsis (Figure 3B). To test if other amino acid changes in BdCesAs confer tolerance to isoxaben, we are currently complimenting *AtCesA6^{prc1-1}* or *AtCesA3^{je5}* mutants with their respective Brachypodium orthologs.

It was next hypothesized that grass-specific cell wall components could compensate for the loss of cellulose caused by isoxaben. A targeted hypersensitive screen with a MLG deficient *Bdcslf6* mutant was conducted to determine the role of MLG in grass tolerance (Figure 4). This approach was taken because MLG content is highest in rapidly elongated tissue (Christenson et al 2010; Vega-Sanchez et al. 2012; Riksfardini et al. 2015); which is also when cells are most sensitive to CBI treatment. A *cesa1^{S830N}* mutant was also included and expected to be hypersensitive to isoxaben because Arabidopsis mutants involved cellulose biosynthesis in primary cell walls are hypersensitive to CBIs (Somerville 2006; Debolt et al. 2007; Xia et al. 2014). Interestingly, we found *Bdcesa1^{S830N}* mutants had the same isoxaben sensitivity as wild

type plants, but *Bdcslf6* mutants were 2.1 times more susceptible (Figure 4E). This raises interesting questions about grass cell wall biology, especially during cellular elongation.

Implications for Grass Cell Wall Biology

In the primary cell walls of grasses (type II) and non-grass species (type I), cellulose is the major structural component and is required for anisotropic growth (Caprita and Gibeaut 1993). However, it takes a concerted effort from the entire cell wall to loosen and allow cells to elongate while still maintaining its structural integrity. This process is complex and differs significantly between type I and II wall and we have less understanding of this process in type II grass cell walls.

One elegant way to study this process is to habituate cell cultures to CBIs. In this method, cells are forced to manipulate their cell wall characteristics to compensate for the loss of cellulose. This data can be used to make inferences about the underlying importance of non-cellulosic polysaccharides. In type I cell walls, for example, and also for a proof of concept, the cellulose-xyloglucan-pectin matrix shares the load-bearing and loosening functions of the cell wall (Dick-Perez et al. 2011; Wang et al. 2015). In CBI habituated *Arabidopsis* (Manfield et al. 2004), bean (Encina et al. 2002; Garcia-Angulo et al. 2006), and tomato (Shedletzky et al. 1992) cell cultures, cellulose is replaced with an extensive crossed-linked pectin network. This response is also characteristic of *Arabidopsis* mutants with reduced cellulose in their primary cell walls (Peng et al. 2001; Mouille et al. 2003).

In type II primary cell walls, cell elongation is dependent on the cellulose-hemicellulose network. When habituated to the CBI dichlobenil (DCB), maize callus became enriched with arabinoxylans and crossed linked with ferulates (Melida et al. 2009; Melida et al. 2011). Shedletzky et al. (1992) found a similar response in barley cells but there was also an increase in MLG content from 9 to 17% of the cell wall. Melida and authors (2009) proposed that the increase in MLG content in barley, but not maize, was a founder effect of cell origin. Barley cell cultures were generated from MLGs rich endosperm tissue and maize cells were generated from immature embryos (Shedletzky et al. 1992; Melida et al. 2009). Another plausible scenario is MLG are

evolutionary more important in barley and other species in the Pooideae subfamily than species in the Panicoideae subfamily.

Regardless, the precise role of MLG in primary cell walls is still in question. Our finding that *Bdcslf6* mutants were more sensitive to isoxaben would indicate MLGs have a structural role in cell elongation. In rice seedlings, a MLG deficiency in *Oscslf6* mutants indicated MLGs were important for cell wall flexibility but not tensile strength (Vega-Sanchez et al. 2012; Smith-Moritz et al. 2015). This was later shown to be an artifact of altered cellulose microfibril organization in expanding coleoptile and mesophyll tissue (Smith-Moritz et al. 2015). Interestingly, a *xxt1 xxt2* xyloglucan deficient *Arabidopsis* mutant has a subtle cell expansion phenotype that was attributed to altered cellulose arrangement and microtubule patterning (Xiao et al. 2016). The correct deposition and orientation of cellulose in the cell wall is critical for guiding cell elongation (Caprita and Gibeaut 1993; Somerville 2006). The similarity between *cslf6* and *xxt1 xxt2* mutants could indicate MLG may mimic the role of xyloglucan in dicots.

Collectively, it appears the wall-strengthening strategy of grass cell walls is to increase the number phenolic linked arabinoxylans. The fact that *Bdcesa1^{S830N}* cellulose mutants were not hypersensitive to isoxaben indicates other non-cellulosic cell wall components can partially compensate for the loss of cellulose and still maintain and promote cell elongation. Moreover, Shedletzky et al. (1992) found that when dicots were habituated to isoxaben their compensatory response of an increased pectin-crosslinking network resulted in considerably weaker walls in comparison to non-habituated cells, however, the opposite was detected with habituated grass cell walls. We hypothesize grass tolerance to this CBI subclass is due to the pre-emergent nature of CBIs and the ability of grass cell walls to maintain enough strength to allow roots to sufficiently elongate and escape the herbicide treated zone. Further research is needed to test this theory. It would be of interest to test the susceptibility of ferulic acid or arabinose *Brachypodium* mutants to isoxaben. One other obvious question remains, if grasses can partially compensate for the loss of cellulose, then why don't grasses exhibit a higher level of tolerance to other CBIs?

5.4 Material and Methods

Plant Material. *Arabidopsis* (*Arabidopsis thaliana* L. ecotype-Columbia), and annual bluegrass (*Poa annua* L.), soybean (*Glycine max* L.; variety AG 4135 Monsanto Co. St. Louis, MO), *Brachypodium* (ecotype 21-3) and mutants seeds were surface sterilized for 15 min with 30% household bleach and subsequently washed three times with sterilized distilled water and kept at 4 C for 2 d. Seeds were placed on agar (11 g L⁻¹) square petri dish plates and grown vertically in growth chambers at 22 C with a 16-photoperiod, except for soybean. Soybean were grown horizontally in agar (6 g L⁻¹) plates. *Brachypodium* wild type, mutants, annual bluegrass and soybean seedlings were pre-germinated and seedlings with a protruding radicle < 1 mm were selected for experimentation.

Dose Response Experiments. *Arabidopsis*, *Brachypodium* 21-3, *Brachypodium* mutants, annual bluegrass, and soybean seedlings were grown as described above on agar plates with a range of isoxaben concentrations (0, 1 nM, 2.5, 5, 7.5, 25, 50, 75, 100, 250, 500 nM, 1 μM) or quinoxiphen (0.25 μM, 0.5, 0.75, 1, 5, 10, 50, 100 μM). Compounds were dissolved in DMSO and DMSO (0.05% v/v) alone the untreated control. At 7 days after treatment, root length was either directly measured or photographs of the plates were taken and pixel number root⁻¹ was converted into cm in ImageJ (Schneider et al. 2012). The latter was possible because of the grid pattern on square plates used in this experiment. Root lengths are expressed as a percentage of the untreated control. Each experiment was repeated at least 3 times. Dose response curves and GR₅₀ values were generated in R using the drc package (Knezevic et al. 2007).

Isoxaben Metabolism Experiment. *Brachypodium* 21-3 was grown as above and seeds that germinated on the same day were transferred to petri dishes containing two sheets of Whatmann filter paper and water (4mL) for an additional 4 days. On the 5th day after germination, roots of 6 seedlings were placed in a 2 ml eppendorf tube that contained 1.8 mL of ½ strength Hoaglands solution (pH 5.7-8). A cotton ball was used as a support structure. This system was derived from Conn et al. (2013). Seedlings were acclimated to hydroponic conditions for 24 hours. The next day, seedlings in eppendorf tube were

transferred to a new tube that contained a fresh solution of ½ strength Hoagland and 1 μM ^{14}C -isoxaben. Radiolabeled isoxaben (specific activity 27.1 mCi/mmol) was kindly provided by Dow AgroScience. Seedlings were grown in treatment solutions for 72 hours. Tubes were checked twice daily and refilled with ½ strength Hoagland as needed and further shaken. Plants were grown under a 16 hr photoperiod with supplemental lighting ($0.25 \mu\text{mol m}^{-2} \text{sec}^{-1}$) at 25 C. The experiment had 2 to 3 tubes of seedlings and was repeated 3 times giving a total of 8 samples. There were total of 3 runs overtime and 2 to 3 reps run⁻¹ (n=8). At 72 hrs after treatment, seedlings were removed from solution and roots plus seed coat were thoroughly methanol (100%) washed to remove residual radioactivity. The wash was collected in scintillation vials, as was the remaining solution in treatment tubes. Afterwards, seedlings were sectioned into seed coat, root+crown and shoot. Fresh weights of roots and shoots were recorded and tissue was frozen in liquid nitrogen and stored at -20 C.

To extract isoxaben and its potential metabolites, plant material was ground in liquid nitrogen using a mortar and pestle. The pulverized tissue was transferred to a round bottom 50 mL centrifuge tube with the help of methanol (3 mL) and centrifuged for 10 min at 7650 rcf. The supernatant was removed and retained. A second 3 mL of methanol was added to the pellet, vortexed, and centrifuged again. The second supernatant was added brought up to a total volume of 6 mL. The pellet was also retained. The combined supernatants were concentrated to 1 ml in a rotary evaporator and filtered (0.45 μM filter) into a 1.5 mL HPLC vial (William 2014). The radiolabeled compounds in the extracts were separated using an HPLC coupled to a radioactivity detector (Radiomatic Flo-One Beta Series A-500). Compounds were eluted on a C18 4.6 X 250 mm column (GL Sciences Inc) following the protocol of Corio-Costet et al. (1999). Compound peak area was calculated as a percentage of total radioactivity recovered from extracts. Radioactivity associated with insoluble fractions (tissue pellet, seed coat, cotton swab) was recovered by combustion in a Packard oxidizer to capture $^{14}\text{CO}_2$. The leftover Hoagland solution, wash, and oxidizer fractions were all diluted with 15 mL scintillation cocktail (Biosafe II) followed by liquid scintillation counting. In each replication, greater than 90% of total radioactivity from ^{14}C -isoxaben was recovered.

Brachypodium Cesa Expression. We initially utilized the results from Handakumbura et al. (2013) to identify *Brachypodium* (Bd) *Cesa*s. Quantitative RT-PCR was used next to determine the putative orthologs of *Arabidopsis* (At) *Cesa3* and *AtCesa6* in *Brachypodium*. The coleoptile tissue (encapsulated shoot tissue removed) from 3 day old dark grown seedlings and the bottom 4 internodes (secondary cell wall tissue) from 3 week old plants were harvested and stored at -80 C for later RNA extraction. Tissue was pooled within a sectioning group from multiple biological samples until roughly 100 mg of tissue was collected. This was considered one biological replication. RNA was extracted from each sample following the protocol from the RNAeasy Kit manual (Quaigen). After synthesis of cDNA, regular PCR was conducted using GAPDH intron spanning primers for each sample to check for RNA contamination. RT-PCR primers are listed in Table 5.1. Ten ug of cDNA was used in an individual run. Relative fold change was determined using the delta-delta method with our control gene being *GADPH* and standardized against gene expression in stems. Data was log transformed to meet basic ANOVA assumptions. Means were separated using Tukey's multiple comparison test and back transformed for presentation.

Cloning BdCESAs and Construction of Transgenic Lines. Full length cDNA of *BdCesa3* and *BdCesa9* were PCR amplified with Pfusion from coleoptile tissue. After PCR cleanup, A overhangs were added to each product with Taq polymerase, TA cloned into pCR2.1 (ThermoFisher Scientific), and sequenced. For the complementation assay, ATTB sites were added to TA cloned products and Gateway cloned in to pMDC43 plasmid. The 35S promoters were replaced with the endogenous promoter of *AtCesa3* or *AtCesa6* promoter (~2 kb) before gateway cloning (Desprez et al. 2007). All primers used are listed in the supplemental table. Constructs were introduced into *Agrobacterium* by electroporation and *AtCesa6^{prc1-1}* or *AtCesa3^{je5}* were floral dipped with the potential complementary construct. Transgenic plants were selected on hygromycin.

Hypersensitivity Screen. *Brachypodium* T-DNA insertion lines in the predicted genomic region of *CsIF6* (Bradi3g16307) were ordered from the Western Regional Research Center now named the JGI *Brachypodium* collection (Bragg et al. 2012).

To identify and confirm T-DNA insertion into *CsIF6*, DNA was harvested from segregating transgenic seedlings lines and initially checked for any TDNA event using hygromycin primers. Hygromycin positive plants were then screened for TDNA insertion into *CsIF6* using gene specific primer (806 bp) (560 bp 5' and 3' of the predicted TDNA insertion site and a TDNA left border primer). All predicted insertion events were derived from a pJJ2LBA vector backbone thus the T3 TDNA primer was used from Bragg et al. (2012). Line JJ12353 was identified as a putative *csIf6* mutant. Two hemizygous plants of JJ12353 were self-pollinated and homozygous TDNA mutants from the next generation were identified by PCR. To amass enough seed for experimentation, 2 additional breeding cycles were needed. To confirm *CsIF6* gene function is disrupted, quantitative RT-PCR was used to compare transcript levels in 2-3 day old mutant seedlings. This was performed following a similar method as described in the Brachypodium *CesA* expression experiment, except *CsIF6* CT values were initially standardized to the control *GAPDH*. A one-tailed t-test was used to compare expression values between mutant and wild type. Primers used in the experiment are listed in table 5.1.

A indirect measurement was used to determine glucose content in 2-3 day old light grown *csIf6* and wild type seedlings. To obtain alcohol insoluble crude cell wall residue (AIR), tissue was washed with 70% ethanol and placed in a 70 C water bath for 1 hr. This was repeated twice, except the final ethanol wash was leftover night, followed by an acetone wash at room temperature. Dried AIR tissue was subsequently ground in a mortal and pestle and de-starched with alpha-amylase for 4 hours. This was repeatedly washed with water (>5x), once with acetone, and dried. This tissue (1-2mg) was hydrolyzed in 2 N trifluoroacetic acid (TFA) at 121 C for 60 min to measured non-cellulosic neutral sugar monosaccharides. Afterwards, TFA was evaporated off for 2 two days under vacuum and samples were resuspended in 500 uL water, vortexed, and spun at 2000 rfc for 5 min. The supernatant was removed and placed into a 2 mL eppendorf tube and the final pH adjusted to basic pH (9-11) using 10 M NaOH. The solution was subsequently filtered (0.45 uM filter) into HPLC vials. Myo-inositol before TFA hydrolysis, was added as an internal standard. The myo-inositol concentration after TFA was evaporated off and 500 mL of water was 200 mM. Neutral sugars (fucose, rhamnose, arabinose, galactose, glucose, mannose, xylose) were identified and quantified by pulsed

electrochemical detection using a Dionex ED50 apparatus. Monosaccharaides were separated using a CarboPAC-PA1 anion-exchange column following the protocol described by Mendu et al. (2011). Glucose levels were converted to percent of total quantified monosaccharaides and then percent of glucose in wild type seedlings. A one-tailed t-test was used to compare values at an alpha value of 0.05.

Table 5.1 List of primers used in all experiments

Primer Name	Gene Number	Use	Forward primer	Reverse primer
CESA1	Bradi2g34240	qRT-PCR	TAAGCAAGGCAATGGC AAAGGTCC	ATGTGGTTCATGGCGAGA GGATGA
CESA2	Bradi1g04597	qRT-PCR	TGACGGCAATGAGCTT CCTCGT	ATGGCGCCAGCTTTCTGT GGT
CESA3	Bradi1g54250	qRT-PCR	GGTATCTCCTACGCCA TCAACAGTGG	CTGCTTACCATAAGACC CTTGAGGA
CESA4		qRT-PCR		
CESA5	Bradi1g29060	qRT-PCR	GAGAATCCACCCACTT CCTTATG	GGTGCAAACCTCCTGT CT
CESA6		qRT-PCR		
CESA7	Bradi4g30540	qRT-PCR	TGCAAAGTGGGACGAG AAGAAGGA	TCGCCTCGTCGTTTATTGG GACAT
CESA8	Bradi2g49912	qRT-PCR	TTCGGTTTCTCTCAGG CCTTTCT	AGTGCCAGCTCATAATTC CAGCGA
CESA9	Bradi1g02510	qRT-PCR	ACCGTGACAACCAAGG CTGGA	AAATGCCAGCCACTACCC CGA
GAPDH		qRT-PCR		
CESA1	Bradi2g34240	Tilling	AAACGCTTTGGCCAGT CTCCGATATT	CCACCAGGTTAATCACAA GCACAGTGG
CESA3	Bradi1g54250	Tilling	AGAGATTTGGACAGTC CGCAGCTTTTG	TTCTAGCAGTTGATGCCA CAGGTTTG
GAPH intron spanning		cDNA quality check	ATGGGCAAGATTAAGA TCGGAATCAACGG	AGTGGTGCAGCTAGCATT TGAGACAAT
Hyg Forward (1000bp)		TDNA check	ATGAAAAAGCCTGAAC TCACCGCGAC	CTATTTCTTTGCCCTCGGA CGAGTGC
BdCslf6 TDNA	Bradi3g16307	TDNA mutant	TTGTTTCATCAGGATTA GGAG	CCTAATATGCTAGTACTCT ACATA
T3- TDNA neg ori LB		TDNA	CAA TTT CAC ACA GGA AAC AGC T	
T3- TDNA pos ori LB		TDNA	AGC TGT TTC CTG TGT GAA ATT G	
CES9 cDNA	Bradi1g02510	cloning	ATGGAGGCCAGCGCCG GGCTG	CTAGTTGCAATCCAGACC ACACTGCTC
CESA3 cDNA	Bradi1g54250	cloning	ATGGACGTCGACGCGG GTGCCGT	CTAGCAGTTGATGCCACA GGTTTGGAT
CESA6 cDNA	Bradi1g53207	cloning	ATGGAGGCGAGCGCGG GGCTGGTG	TTAGTTGCAATCCAGACC ACATTGCTCC
CSLF6 cDNA	Bradi3g16307	cloning	ATGGCGCCAGCGGTGC CGGC	TCACGGCCAGAGGTAGTA GCCGTGC

Table 5.1 Continued

CSLF6	Bradi3g16307	qRT-PCR	GATCTTCAGGAGGGACA TCTCATT	ATTGGAGTGATCATGAG TGGAGTC
pAtcesa3 kpn R		promoter	gcg gta cct tgt cac tta gtt gct tcc a	
pAtcesa3 pme F		promoter	gcc gtt taa acc act taa aca aca aaa a	
pAtcesa6 hind F		promoter	ccc aag ctt aaa atc aac aag caa aat a	
pATcesa6 kpn R		promoter	gcg gta ccattt gtc tga aaa cag aca c	

References

- Amikam, D., and Galperin, M.Y. 2006. PilZ domain is part of the bacterial c-di- GMP binding protein. *Bioinformatics* 22: 3–6.
- Armstrong, J. I., Yuan, S., Dale, J. M., Tanner, V. N., and Theologis, A. 2004. Identification of auxin transcriptional activation by means of chemical genetics in *Arabidopsis*. *Proc. Natl. Acad. Sci. U.S.A.* 101:14978–14983.
- Bashline, L., Li, S., Anderson, C.T., Lei, L., and Gu, Y. 2013. The endocytosis of cellulose synthase in *Arabidopsis* is dependent on μ 2, a clathrin-mediated endocytosis adaptin. *Plant Physiol.* 163:150–160.
- Baskin, T.I. 2005. Anisotropic expansion of the plant cell wall. *Annu. Rev. Cell Dev. Biol.* 21: 203–222.
- Baskin, T. I., Betzner, A. S., Hoggart, R., Cork, A., and Williamson, R. E. 1992. Root morphology mutants in *Arabidopsis thaliana*. *Plant Physiol.* 19: 427–437.
- Bassel, G. W., Fung, P., Chow, T. F., Foong, J. A., Provart, N. J., and Cutler, S. R. 2008. Elucidating the germination transcriptional program using small molecules. *Plant Physiol.* 147: 143–155.
- Brabham, C. and DeBolt, S. 2012. Chemical genetics to examine cellulose biosynthesis. *Front Plant Sci.* 3: 309.
- Brabham, C., Lei, L., Gu, Y., Stork, J., Barrett, M., and DeBolt S. 2014. Indaziflam Herbicidal Action: A Potent Cellulose Biosynthesis Inhibitor. *Plant Physiol.* 166: 1177–1185.
- Bragg, J. N., Wu, J., Gordon, S. P., Guttman, M. E., Thilmony, R., Lazo, G. R., Gu, Y. Q., and Vogel, J. P. 2012. Generation and characterization of the western regional research center *Brachypodium* T-DNA insertional mutant collection. *PLoS ONE* 7: e41916.
- Bischoff, V., Cookson, S.J., Wu, S., Scheible, W.R. 2009 Thaxtomin A affects CESA-complex density, expression of cell wall genes, cell wall composition, and causes ectopic lignification in *Arabidopsis thaliana* seedlings. *J Exp. Bot.* 60: 955-965

- Bischoff, V., Nita, S., Neumetzler, L., Schindelasch, D., Urbain, A., Eshed, R., Persson, S., Delmer, D., Scheible, W. R. 2010. TRICHOME BIREFRINGENCE and its homolog AT5G01360 encode plant-specific DUF231 proteins required for cellulose biosynthesis in Arabidopsis. *Plant Physiol.* 153: 590–602.
- Blum, M., Boehler, M., Randall, E., et al. 2010. Mandipropamid targets the cellulose synthase-like PiCesA3 to inhibit cell wall biosynthesis in the oomycete plant pathogen, *Phytophthora infestans*. *Molecular Plant Pathol.* 11: 227–243.
- Blum, M., Gamper, H. A., Waldner, M., Sierotzki, H., and Gisi, U. 2012. The cellulose synthase 3 (CesA3) gene of oomycetes: Structure, phylogeny and influence on sensitivity to carboxylic acid amide (CAA) fungicides. *Fungal Biol.* 116: 529–542.
- Bringmann, M., Li, E., Sampathkumar, A., Kocabek, T., Hauser, M.T., and Persson, S. 2012. POM- POM2/CELLULOSE SYNTHASE INTERACTION1 is essential for the function association of cellulose synthase and microtubules in Arabidopsis. *Plant Cell* 24:163-177.
- Brosnan, J.T., McCullough, P.E., and Breeden, G.K. 2011. Smooth crabgrass control with indaziflam at various spring timings. *Weed Tech* 25: 363-366
- Brown, R. M. Jr. 1996. The biosynthesis of cellulose. *J. Macromol. Sci.* 10:1345–1373.
- Brutnell, T. P., Bennetzen, J. L., and Vogel, J. P. 2015. *Brachypodium distachyon* and *Setaria viridis*: Model genetic systems for the grasses. *Annu. Rev. Plant Biol.* 66: 465-485.
- Burk, H., Zhong, R., and Ye, Z. H. 2007. The katanin microtubule severing protein in plants. *J. Integr. Plant Biol.* 49: 1174–1182.
- Burn, J. E., Hocart, C. H., Birch, R. J., Cork, A. C., and Williamson, R. E. 2002. Functional analysis of the cellulose synthase genes *CesA1*, *CesA2*, and *CesA3* in Arabidopsis. *Plant Physiol.* 129: 797-807.
- Burton, R.A., Jobling, S.A., Harvey, A.J., Shirley, N.J., Mather, D.E., Bacic, A., and Fincher, G.B. 2008. The genetics and transcriptional profiles of the cellulose synthase-like HvCsIF gene family in barley (*Hordeum vulgare* L.). *Plant Physiol.* 146: 1821–1833.

- Burton, R.A., Wilson, S.M., Hrmova, M., Harvey, A.J., Shirley, N.J., Medhurst, A., Stone, B.A., Newbiggin, E.J., Bacic, A., and Fincher, G.B. 2006. Cellulose synthase like CslF genes mediate the synthesis of cell wall (1,3;1,4)-b-D-glucans. *Science* 311: 1940– 1942.
- Cabanne, F., Lefebvre, A., Scalla, R., 1987. Behaviour of the herbicide EL-107 in wheat and rape grown under controlled condition. *Weed Res.* 27: 135-142.
- Carpita, N. C. and Gibeaut, D. M. 1993. Structural models of primary cell walls in flowering plants: consistency of molecular structure with the physical properties of the walls during growth. *Plant J.* 3: 1-30.
- Carpita, N. C. and McCann, M. C. 2015. Characterizing visible and invisible cell wall mutant phenotypes. *J. Exp. Bot.* doi: 10.1093/jxb/erv090.
- Carpita N. C. and McCann, M.C. 2008. Maize and sorghum: genetic resources for bioenergy grasses. *Trends Plant Sci.* 13: 415–420.
- Carpita, N. C. 1996. Structure and biogenesis of the cell walls of grasses. *Annu. Rev. Plant Physiol. Plant Mol. Biol.* 47: 445-476.
- Carpita, N.C. 2011. Update on mechanisms of plant cell wall biosynthesis: how plants make cellulose and other (1–4)- β -D-glycans. *Plant Physiol.* 155: 171–184.
- Carroll, A., and Specht, C. D. 2011. Understanding plant cellulose synthases through a comprehensive investigation of the cellulose synthase family sequences. *Front Plant Sci.* 2: 5.
- Cass, C. L., Lavell, A. A., Santoro, N., Foster, C. E., Karlen, S. D., Smith, R. A., Ralph, J., Garvin, D. F., and Sedbrook, J. C. 2016. Cell Wall Composition and Biomass Recalcitrance Differences Within a Genotypically Diverse Set of *Brachypodium distachyon* Inbred Lines. *Front Plant Sci.* 7: 708.
- Chang, X. F., Chandra, R., Berleth, T. and Beatson, R. P. 2008. Rapid, microscale, acetyl bromide-based method for high-throughput determination of lignin content in *Arabidopsis thaliana*. *J. Agri. Food Chem.* 56: 6825-6834.
- Chen, S., Ehrhardt, D.W., and Somerville, C.R. 2010. Mutations of cellulose synthase

- (CESA1) phosphorylation sites modulate anisotropic cell expansion and bidirectional mobility of cellulose synthase. *Proc. Natl. Acad. Sci. U.S.A.* 107: 17188–17193.
- Christensen, U., Alonso-Simon, A., Scheller, H. V., Willats, W. G.T., and Harholt, J. 2010. Characterization of the primary cell walls of seedlings of *Brachypodium distachyon*- A potential model plant for temperate grasses. *Phytochemistry* 71: 62-69.
- Conn, S. J., Hocking, H., Dayod, M., Xu, B., Athman, A., Henderson, S., Aukett, L., Conn, V., Shearer, M. K., Fuentes, S., Tyerman, S. D., and Gilliam, M. 2013. Protocol: optimising hydroponic growth systems for nutritional and physiological analysis of *Arabidopsis thaliana* and other plants. *Plant Methods* 9:4.
- Corio-Costet, M.F., Agnese, M.D., and Scalla, R. 1991. Effects of Isoxaben on Sensitive and Tolerant Plant Cell Cultures I. Metabolic fate of isoxaben. *Pestic. Biochem. Physiol.* 40: 246–254.
- Crowell, E.F., Bischoff, V., Desprez, T., Rolland, A., Stierhof, Y.D., Schumacher, K., Gonneau, M., Höfte, H., and Vernhettes, S. 2009. Pausing of golgi bodies on microtubules regulates secretion of cellulose synthase complexes in *Arabidopsis*. *Plant Cell* 21: 1141-1154.
- Cutler, S.R., Ehrhardt, D.W., Griffiths, J.S., and Somerville, C.R. 2000. Random GFP cDNA fusions enable visualization of subcellular structures in cells of *Arabidopsis* at a high frequency. *Proc. Natl. Acad. Sci. USA* 97: 3718–3723.
- Davis, J.K. 2012. Combining polysaccharide biosynthesis and transport in a single enzyme: dual function cell wall glycan synthases. *Front Plant Sci.* 3:138.
- Diaz-Cacho, P., Moral, R., Encina, A., Acebes, J.L., and Alvarez, J. 1999. Cell wall modification in bean (*Phaseolus vulgaris*) callus cultures tolerant to isoxaben. *Physiol. Plantarum* 107: 54-59.
- Dietrich, H. and Laber, B. 2012. Inhibitors of cellulose biosynthesis. In Kramer W, Schirmer U, Jeschke P, Witschel M, eds, *Modern Crop Protection Compounds*, Ed 2 Vol 1. Wiley-VCH Verlag and Co. KGaA, Weinheim, p356

- Diotallevi, F. and Mulder, B. 2007. The cellulose synthase complex: A polymerization driven supramolecular motor. *Biophysical J.* 92: 2666-2673.
- Dalmais, M., Antelme, S., Ho-Yue-Kuang, S., Wang, Y., Darracq, O., d'Yvoire, M. B., Cezard, L., Legee, F., Blondet, E., Oria, N., Troadec, C., Brunaud, V., Jouanin, L., Hofte, H., Bendahmane, A., Lapierre, C., and Sibout, R. 2013. A TILLING platform for function genomics in *Brachypodium distachyon*. *PLOS One* 8: e65503.
- Delmer, D. P., Read, S. M., and Cooper, G. 1987. Identification of a receptor protein in cotton fibers for the herbicide 2,6-dichlorobenzonitrile. *Plant Physiol.* 84, 415–420.
- de Oliveira, D. M., Finger-Teixeira, A., Mota, T. R., Salvador, V. H., Moreira-Vilar, F. C., Molinari, H. B. C., Mitchell, R. A. C., Marchiosi, R., Ferrarese-Filho, O., and dos Santos, W. D. 2015. Ferulic acid: a key component in grass lignocellulose recalcitrance to hydrolysis. *Plant Biotechnol. J.* 13: 1224-1232.
- De Rybel, B., Audenaert, D., Vert, G., Rozhon, W., Mayerhofer, J., Peelman, F. 2009. Chemical inhibition of a subset of *Arabidopsis thaliana* GSK3-like kinases activates brassinosteroid signaling. *Chem. Biol.* 16: 594–604.
- Desprez, T., Juraniec, M., Crowell, E. F., Jouy, H., Pochylova, Z., Parcy, F., Hofte, H., Gonneau, M., and Vernhettes, S. 2007. Organization of cellulose synthase Complexes involved in primary cell wall synthesis in *Arabidopsis thaliana*. *Proc. Natl. Acad. Sci. USA.* 104: 15572-15577.
- Debolt, S., Gutierrez, R., Ehrhardt, D. W., and Somerville, C. 2007. Nonmotile Cellulose Synthase Subunits Repeatedly Accumulate within Localized Regions at the Plasma Membrane in *Arabidopsis Hypocotyl* Cells following 2,6-Dichlorobenzonitrile Treatment. *Plant Physiol.* 145: 334-338.
- Desprez, T., Vernhettes, S., Fagard, M., Refregier, G., Desnos, T., Aletti E. 2002. Resistance against herbicide isoxaben and cellulose deficiency caused by distinct mutations in same cellulose synthase isoform CESA6. *Plant Physiol.* 128: 482–490.
- Dick-Pérez, M., Zhang, Y., Hayes, J., Salazar, A., Zabolina, O. A., and Hong, M. 2011. Structure and interactions of plant cell-wall polysaccharides by two- and three-

- dimensional magic-angle-spinning solid-state NMR. *Biochemistry* 50: 989–1000.
- Doblin, M. S., Pettolino, F. A., Wilson, S. M., Campbell, R., Burton, R. A., Fincher, G. B., Newbigin, E., and Bacic, A. 2009. A barley *cellulose synthase-like CSLH* gene mediates (1,3;1,4)- β -d-glucan synthesis in transgenic *Arabidopsis*. *Proc. Natl. Acad. Sci. U.S.A.* 106: 5996–6001.
- Drakakaki, G., Van de Ven, W, and Pan S, et al. 2012. Isolation and proteomic analysis of the SYP61 compartment reveal its role in exocytic trafficking in *Arabidopsis*. *Cell Res.* 22: 413–424.
- Drakakaki, G., Robert, S., Szatmari, A., Brown, M. Q., Nagawa, S., Damme, D. V., 2011. Clusters of bioactive compounds target dynamic endomembrane networks in vivo. *Proc. Natl. Acad. Sci. U.S.A.* 108: 17850–17855.
- Draper, J., Mur, L. A. J., Jenkins, G., Ghoshbiswas, G. C., Bablak, P., Hasterok, R., and Routledge, A. P. M. 2001. *Brachypodium distachyon*. A new model systems for functional genomics in grasses. *Plant Physiol.* 127: 1539-1555.
- Encina, A., Sevillano, J. M., Acebes, J. L., and Alvarez, J. 2002. Cell wall modifications of bean (*Phaseolus vulgaris*) cell suspensions during habituation and dehabituation to dichlobenil. *Physiol. Plant* 114: 182–91.
- Endler, A., Kesten, C., Schneider, R., Zhang, Y., Ivakov, A., Froehlich, A., Funke, N., and Persson, S. 2015. A Mechanism for Sustained Cellulose Synthesis during Salt Stress. *Cell* 162: 1353–1364.
- Fernandes, N., Thomas, L.H., Altaner, C.M., Callow, P., Forsyth, V.T., Apperley, D.C., Kennedy, C.J., and Jarvis, M.C. 2011. Nanostructure of cellulose microfibrils in spruce wood. *Proc. Natl. Acad. Sci. USA* 108:
- Fincher, G. B. 2009. Revolutionary times in our understanding of cell wall biosynthesis and remodeling in the grasses. *Plant Physiol.* 149: 27-37.
- Fitzgerald, T. L., Powell, J. J., Schneebeil, K., Hsia, M. M., Gardiner, D. M., Bragg, J. N., McIntyre, C. L., Manners, J. M., Ayliffe, M., Watt, M., Vogel, J. P., Henry, R.J., and Kazan, K., 2015. *Brachypodium* as an emerging model for cereal-pathogen interactions. *Ann. Bot.* 115: 717-731.
- Foster, C. E., Martin, T. M., and Pauly, M. 2010. Comprehensive compositional analysis

- of plant cell walls (lignocellulosic biomass) Part II: Carbohydrates. *J. Vis. Exp.* 37: 1837.
- Fukushima, R. S. and Hatfield, R. D. 2004. Comparison of the acetyl bromide spectrophotometric method with other analytical lignin methods for determining lignin concentration in forages samples. *J. Agri. Food Chem.* 52: 3713-3720.
- Fukushima, R. S. and Hatfield, R. D. 2001. Extraction and isolation of lignin for utilization as a standard to determine lignin concentration using the acetyl bromide spectrophotometric method. *J. Agri. Food Chem.* 49: 3133-3139.
- Gaines, T. A., W. Zhang, D. Wang, B. Bukun, S. T. Chisholm, D. L. Shaner, S. J. Nissen, W. L. Patzoldt, P. J. Tranel, A. S. Culpepper, T. L. Grey, T. M. Webster, W. K. Vencill, R. D. Sammons, J. Jiang, C. Preston, J. E. Leach, and P. Westra 2010. Gene amplification confers glyphosate resistance in *Amaranthus palmeri*. *Proc. Natl. Acad. Sci. USA.* 107:1029-1034.
- García-Angulo, P., Alonso-Simón, A., Encina, A., Álvarez, J.M., and Acebes JL. 2012. Cellulose biosynthesis inhibitors: Comparative effect on bean cell cultures. *Int. J. Mol. Sci.* 13: 3685–3702.
- Garcia-Angulo, P., Willats, W. G. T., Encina, A. E., Alonso-Simon, A., Alvarez, J. M., and Acebes, J. L., 2006. Immunocytochemical characterization of the cell walls of bean cell suspensions during habituation and dehabituation to dichlobenil. *Physiol. Plant* 127:87–99.
- Giddings, T.H. and Staehelin, L.A. 1988. Spatial relationship between microtubules and plasma-membrane rosettes during the deposition of primary wall microfibrils in *Closterium* sp. *Planta* 173: 22-30.
- Gilchrist, E. J, Sidebottom, C. H. D., Koh C. S., MacInnes, T., Sharpe, A. G., and Haughn, G. W. 2013. A mutant *Brassica napus* (Canola) population for the identification of new genetic diversity via TILLING and next generation sequencing. *PLOS One* 8: e84303.
- Gonneau, M., Desprez, T., Guillot, A., Vernhettes, S., and Höfte, H. 2014. Catalytic Subunit Stoichiometry within the Cellulose Synthase Complex. *Plant Physiol.* 166: 1709–1712.
- Grenville-Briggs, L.J., Anderson, V.L., Fugelstad, J. 2008. Cellulose synthesis in

- Phytophthora infestans is required for normal appressorium formation and successful infection of potato. *Plant Cell* 20: 720–738.
- Griffiths, J., Šola, K., Kushwaha R, et al. 2015. Unidirectional movement of cellulose synthase complexes in Arabidopsis seed coat epidermal cells deposit cellulose involved in mucilage extrusion, adherence and ray formation. *Plant Physiol.*
- Grossmann, K., Tresch, S., and Plath, P. 2001. Triaziflam and diaminotriazine derivatives affect enantioselectively multiple herbicide target sites. *Z Naturforsch., C: J. Biosci* 56: 559–569.
- Gutierrez, R., Lindeboom, J. J., Paredez, A. R., Emons, A. M. C., and Ehrhardt, D. W. 2009. Arabidopsis cortical microtubules position cellulose synthase delivery to the plasma membrane and interact with cellulose synthase trafficking compartments. *Nat. Cell Biol.* 11: 797–743.
- Gu, Y., Kaplinsky, N., Bringmann, M., Cobb, A., Carroll, A., Sampathkumar, A., Baskin, T.I., Persson, S., and Somerville, C.R. 2010. Identification of a cellulose synthase-associated protein required for cellulose biosynthesis. *Proc. Natl. Acad. Sci. USA.* 107: 12866–12871.
- Hall, L. M., Holtum, J. A. M., and Powles, S. B. 1994. Mechanisms responsible for cross and multiple resistance. p. 243-261. Powles, S. and Holtum, J., eds. *Herbicide resistance in plants: biology and biochemistry*. CRC Press. Boca Raton, Florida.
- Haigler, C. H., and Brown, R. M. Jr. 1986. Transport of rosettes from the Golgi apparatus to the plasma membrane in isolated mesophyll cells of *Zinnia elegans* during differentiation to tracheary elements in suspension culture. *Protoplasma* 134: 111–120.
- Handakumbura, P. P., Matos, D., A., Osmont, K. S. Harrington, M. J., Heo, K., Kafle, K., Kim, S. H., Baskin, T. I., and Hazen, S. P. 2015. Perturbation of *Brachypodium distachyon*. Cellulose synthase A4 or 7 results in abnormal cell walls. *BMC Plant Biol.* 13: 131-146.
- Hands, P. and Drea, S. 2012. A comparative view of grain development in *Brachypodium distachyon*. *J. Cereal Sci.* 56: 2-8.
- Harris, D., Stork, J., and DeBolt, S. 2009. Genetic modification of cellulose synthase

- reduces crystallinity and improves biochemical conversion to fermentable sugars. *GCB Bioenergy* 1: 51-60.
- Harris, D. M., Corbin, K., Wang, T., Gutierrez, R., Bertolo, A. L., Petti, C., Smilgies, D.M., Estevez, J. M., Bonetta, D., Urbanowicz, B., Ehrhardt, D.W., Somerville, C., Rose, J. C. K., Hong, M., and DeBolt, S. 2012. Cellulose microfibril crystallinity is reduced by mutating C-terminal transmembrane region residues CESA1A-V903 and CESA3T-I942. *Proc. Natl. Acad. Sci. USA.* 109: 4098-103.
- Heap I (2014) The international survey of herbicide resistant weeds.
- Heim, D.R., Skomp, J.R., Tschabold, E.E., and Larrinua, I.M. 1990 Isoxaben inhibits the synthesis of acid insoluble cell wall materials in *Arabidopsis thaliana*. *Plant Physiol.* 93: 695-700
- Heim, D. R., Bjelk L. A., James, J., and Larrinua, I. M. 1993. Mechanism of Isoxaben Tolerance in *Agrostis palustris* var. Penncross. *J. Exp. Bot.* 44:1185-1189.
- Heim, D.R., Larrinua, I.M., Murdoch, M.G., and Roberts, J.L. 1998. Triazofenamide is a cellulose biosynthesis inhibitor. *Pestic. Biochem. Physiol.* 59: 163–168.
- Heim, D. R., Roberts, J. L., Pike, P. D., and Larrinua I. M. 1989. Mutation of a locus of *Arabidopsis thaliana* confers resistance to the herbicide isoxaben. *Plant Physiol.* 90: 146–150.
- Henikoff, S., Till, B. J., and Comai, L. 2004. TILLING. Traditional mutagenesis meets functional genomics. *Plant Physiol.* 135: 630-636.
- Herth, W. and Weber, G. 1984. Occurrence of the putative cellulose-synthesizing “Rosettes” in the plasma membrane of *Glycine max* suspension culture cells. *Naturwissenschaften* 71:153-154
- Herth, W. 1987. Effects of 2,6-DCB on plasma membrane rosettes of wheat root cells. *Naturwissenschaften* 74: 556-557.
- Hill, J.L., Hammudi, M.B., Tien, M. 2014. The *Arabidopsis* Cellulose Synthase Complex: A Proposed Hexamer of CESA Trimers in an Equimolar Stoichiometry. *Plant Cell* 26: 4834–4842.
- Hoffman, J. C., and Vaughn, K. C. 1996. Flupoxam induces classic club root morphology but is not a mitotic disrupter herbicide. *Pestic. Biochem. Physiol.* 55: 49–53.

- Hong, S. Y., Park, J. H., Cho, S. H., Yang, M. S. and Park, C. M. Phenological growth stages of *Brachypodium distachyon*: codification and description. *Weed Res.* 51: 612-620.
- Huang, Y.B. and Fu, Y. 2013. Hydrolysis of cellulose to glucose by solid acid catalysts. *Green Chem.* 15: 1095–1111.
- Jacob-Wilk, D., Kurek, I., Hogan, P., and Delmer, D. P. 2006. The cotton fiber zinc-binding domain of cellulose synthase A1 from *Gossypium hirsutum* displays rapid turnover in vitro and in vivo. *Proc. Natl. Acad. Sci. U.S.A.* 103: 12191–12196.
- Jarvis, M. 2013. Cellulose Biosynthesis: Counting the Chains. *Plant Physiol.* 163: 1485-1486.
- Kiedaisch, B., Blanton, R., and Haigler, C. 2003. Characterization of a novel cellulose synthesis inhibitor. *Planta* 217: 922–930.
- Kimura, S., Laosinchai, W., Itoh, T., Cui, X., Linder, C., and Brown, R. 1999. Immunogold labeling of rosette terminal cellulose-synthesizing complexes in the vascular plant *Vigna angularis*. *Plant Cell* 11: 2075–2086.
- King, R.R., Calhoun, L.A. 2009. The thaxtomin phytotoxins: sources, synthesis, biosynthesis, biotransformation and biological activity. *Phytochemistry* 70: 833–841.
- Knezevic, S.Z., Streibig, J.C., and Ritz, C. 2007. Utilizing R software package for dose-response studies: the concept and data analysis. *Weed Technol.* 21: 840–848.
- Kudo, N.K., Furuta, S.F., Taniguchi, M.T., Endo, T.E., and Sato, K.S. 1999. Synthesis and Herbicidal Activity of 1, 5-Diarylpyrazole Derivatives. *Chem. Pharm. Bull.* 47: 857–868.
- Lai, K., Him, J., Chanzy, H., Mueller, M., Putaux, J.L., Imai, T., and Bulone, V. 2002. In vitro versus in vivo cellulose microfibrils from plant primary wall synthases: structural differences. *J. Biol. Chem.* 277: 36931-36939.
- Lei, L., Li, S., Du, J., Bashline, L., and Gu, Y. 2013. CELLULOSE SYNTHASE

- INTERACTIVE3 Regulates Cellulose Biosynthesis in Both a Microtubule-Dependent and Microtubule-Independent Manner in Arabidopsis. *Plant Cell* 25: 4912–23.
- Lei, L., Li, S., and Gu, Y. 2012 Cellulose synthase interactive protein 1 (CSII) mediates the intimate relationship between cellulose microfibrils and cortical microtubules. *Plant Signaling Behav.* 7: 1-5.
- Li, S., Bashline, L., Lei, L., and Gu, Y. 2014. Cellulose synthesis and its regulation. *The Arabidopsis book / American Society of Plant Biologists* 12: e0169.
- Li, S., Lei, L., Somerville, C.R., and Gu, Y. 2012. Cellulose synthase interactive protein 1 (CSII) links microtubules and cellulose synthase complexes. *Proc. Natl. Acad. Sci. USA* 109: 185-190.
- Li, X., Weng, J. K., and Chapple, C. 2008. Improvement of biomass through lignin modification. *Plant J.* 54: 569-581.
- Luo, Y., Scholl, S., Doering, A. 2015. V-ATPase activity in the TGN/EE is required for exocytosis and recycling in Arabidopsis. *Nat. Plants*.
- Manfield, I. W., Orfila, C., McCartney, L., Harholt, J., Bernal, A. J., Scheller, H. V. 2004. Novel cell wall architecture of isoxaben-habituated Arabidopsis suspension-cultured cells: Global transcript profiling and cellular analysis. *Plant J.* 40: 260–75.
- Mansoori, N., Timmers, J., Desprez, T., Alvim-Kamei, C.L, Dees, D.C.T., Vincken, J-P. 2014. KORRIGAN1 Interacts Specifically with Integral Components of the Cellulose Synthase Machinery. *PLoS ONE* 9: e112387.
- Marriotta, P. E., Siboutb, R., Lapierreb, C., Fangeld, J. U., Willatsd, W. G. T., Hofte, H., Gómez, L. D., and McQueen-Masona, S. J. 2015. Range of cell-wall alterations enhance saccharification in *Brachypodium distachyon* mutants. *Proc. Natl. Acad. Sci. USA.* 111: 14601-14606.
- McCallum, C. M., Comai, L., Greene, E. A., and Henikoff, S. 2000. Targeting induced local lesions in genomes (TILLING) for plant functional genomics. *Plant Physiol.* 123: 439-422.
- Melida, H., Alvarez, J., Acebes, J. L., Encina, A., and Fry, S. C. 2011. Changes in

- cinnamic acid derivatives associated with the habituation of maize cells to dichlobenil. *Mol. Plant* 4: 869-878.
- Melida, H., Garcia-Angulo, P., Alonso-Simon, A., Encina, A., Alvarex, J., and Acebes, J. L. 2009. Novel type II cell wall architecture in dichlobenil-habituated maize calluses. *Planta*. 229: 617-631.
- Melida, H., Garcia-Angulo, P., Alonso-Simon, A., Alvarez, J.M., Acebes, J.L., and Encina, A. 2010. The phenolic profile of maize primary cell wall changes in cellulose deficient cell cultures. *Phytochemistry* 71: 1684-1689.
- Mendu, V., Griffiths, J., Persson, S., Stork, J., Voiniciuc, C., Downie, A. B., Haughn, G., and DeBolt, S. 2011. Subfunctionalization of cellulose synthases in seed coat epidermal cells mediate secondary radial wall synthesis and mucilage attachment *Plant Physiol.* 157: 441-53.
- Meyer, D.F., Hanrahan, R., Michel, J., Monke, B., Mudge, L., Norton, L., Olsen, C., Parker, A. Smith, J. and Spak, D. 2009 Indaziflam/BCS-AA10717-A new herbicide for pre-emergent control of grasses and broadleaf weeds for turf and ornamentals. WSSA Annual Meeting,
- Mizuta, S., and Brown, R. M. 1992. Effects of 2,6-dichlorobenzonitrile and tinopal LPW on the structure of the cellulose synthesizing complexes of *Vaucheria hamata*. *Protoplasma* 166, 200–207.
- Mizuta, S., and Brown, R.M. Jr. 1992. High resolution analysis of the formation of cellulose synthesizing complexes in *Vaucheria hamata*. *Protoplasma* 166: 187–199.
- Morgan, J. L. W., Strumillo, J., and Zimmer, J. 2013. Crystallographic snapshot of cellulose synthesis and membrane translocation. *Nature* 493: 181-186.
- Morgan, J.L., McNamara, J.T., and Zimmer, J. 2014. Mechanism of activation of bacterial cellulose synthase by cyclic di-GMP. *Nat. Struct. Mol. Biol.* 21: 489–496.
- Mouille, G., Robin, S., Lecomte, M., Pagant, S., and Hofte, H. 2003. Classification and identification of *Arabidopsis* cell wall mutants using fourier-transform infrared (FT-IR) microspectroscopy. *Plant J.* 35: 393-404.

- Mueller, S. C., and Brown, R. M. Jr. 1982. The control of cellulose microfibril deposition in the cell wall of higher plants. *Planta* 154: 489–500.
- Nixon, T. B., Mansouri, K., Singh, A., Du, J., Davis, J. K., Lee, J., Slabaugh, E., Vandavasi, V. G., O’Neill, H., Roberts, E. M. Roberts, A. W., Yingling, Y. G. and Haigler, C. H. 2016. Comparative structural and computational analysis supports eighteen cellulose synthases in the plant cellulose synthesis complex. *Sci. Reports* 6: 28696.
- Orologas, N., Delivopoulos, S. G., Dim-poulou, A., and Tsekos, I. 2005. Effects of 2,6-dichlorobenzonitrile on plasma membrane cellulose synthesizing complexes and cellulose localization in cells of the red alga *Erythrocladia subintegra*. *Phycologia* 44: 465–476.
- Ovecka, M., Berson, T., Beck, M., Derksen, J., Samaj, J., Baluska, F. 2010. Structural sterol are involved in both the initiation and tip growth of root hairs in *Arabidopsis thaliana*. *Plant Cell* 22: 2999–3019.
- Paredez, A. R., Somerville, C. R., and Ehrhardt, D. W. 2006. Visualization of cellulose synthase demonstrates functional association with microtubules. *Science* 312: 1491–1495.
- Park, S., Fung, P., Nishimura, N., Jensen, D. R., Fujii, H., Zhao, Y., et al. 2009. Abscisic acid inhibits type 2C protein phosphatases via the PYR/PYL family of START proteins. *Science* 324: 1068–1071.
- Pear, J. R., Kawagoe, Y., Schreckengost, W. E., Delmer, D. P., and Stalker, D. M. 1996. Higher plants contain homologs of the bacterial *celA* genes encoding the catalytic subunit of cellulose synthase. *Proc. Natl. Acad. Sci. U.S.A.* 93, 12637–12642.
- Peng, L., Hocart, C. H., Redmond, J. W., and Williamson, R. E. 2000. Fractionation of carbohydrates in *Arabidopsis* root cell walls shows that three radial swelling loci are specifically involved in cellulose production. *Planta* 211: 406-414.
- Persson, S., Paredez, A., Carroll, A., Palsdottir, H. Poindexter, P., Khitrov, N., Auer, M., and Somerville, C. R. 2007. Genetic evidence for three unique components in primary cell-wall cellulose synthase complexes in *Arabidopsis*. *Proc. Natl. Acad. Sci. USA.* 104: 15566-15571.
- Powles, S. B. and C. Preston. 2006. Evolved glycosate resistance in plants: Biochemical

- and genetic basis of resistance. *Weed Technol.* 20:282-289.
- Purushotham, P., Cho, S. H., Diaz-Moreno, S., Kumar, M., Nixon, B. T., Bulone, V., and Zimmer, J. 2016. A single heterologously expressed plant cellulose synthase isoforms is sufficient for cellulose microfibril formation in vitro. *Proc. Natl. Acad. Sci. USA.* 113: 11360-11365.
- Rajangam, A. S., Kumar, M., Aspeborg, H., Guerriero, G., Arvestad, L., Pansri, P., et al. 2008. MAP20, a microtubule-associated protein in the secondary cell walls of hybrid aspen, is a target of the cellulose synthesis inhibitor 2,6-dichlorobenzonitrile. *Plant Physiol.* 148, 1283–1294.
- Rancour, D. M., Marita, J. M., and Hatfield, R. D. 2012. Cell wall composition throughout development for the model grass *Brachypodium distachyon*. *Front Plant Sci.* 3: 226.
- Riksfardini, A. E., Collins, H. M., Byrt, C. S., Betts, N., Henderson, M., Shirley, N. J., Schewrdt, J., Lahnstein, J., Fincher, G. B., and Burton, R. A. 2015. Distribution, structure and biosynthetic gene families of (1,3;1,4)-B-glucan in *Sorghum bicolor*. *J. Integr. Plant Biol.* 57: 429-445.
- Robert, S., Chary, S.N., Drakakaki, G., Li, S., Yang, Z., Raikhel, N.V., and Hicks, G.R. 2008. Endosidin1 defines a compartment involved in endocytosis of the brassinosteroid receptor BRI1 and the auxin transporters PIN2 and AUX1. *Proc. Natl. Acad. Sci. USA.* 105: 8464–8469.
- Robert, S., Bichet, A., Grandjean, O., Kierzkowski, D., Satiat-Jeunemaitre, B., Pelletier, S., et al. 2005. An Arabidopsis endo-1,4-β-D-glucanase involved in cellulose synthesis undergoes regulated intracellular cycling. *Plant Cell* 17, 3378–3389.
- Robert, S., Raikhel, N. V., and Hicks, G. R. 2009. Powerful partners: Arabidopsis and chemical genomics. *Arabidopsis Book* 7:e0109. doi: 10.1199/tab.0109
- Rojas-Pierce, M., Titapiwatanakun, B., Sohn, E. J., Fang, F., Larive, C. K., Blakeslee, J., et al. 2007. Arabidopsis glycoprotein19 participates in the inhibition of gravitropism by gravacin. *Chem. Biol.* 14, 1366–1376.
- Ross, P., Mayer, R., and Benziman, M. 1991. Cellulose biosynthesis and function in bacteria. *Microbiol. Rev.* 55: 35–58.

- Roudier, F., Fernandez, A.G., Fujita, M., Himmelspach, R., Borner, G.H.H., Schindelman, G., Song, S., Baskin, T.I., Dupree, P., Wasteneys, G. O, and Benfey, P.N. 2005. COBRA, an Arabidopsis extracellular glycosyl-phosphatidylinositol-anchored protein, specifically controls highly anisotropic expansion through its involvement in cellulose microfibril orientation. *Plant Cell* 17: 1749–1763.
- Sabba R. P. and Vaughn K. C. 1999. Herbicides that inhibit cellulose biosynthesis. *Weed Sci.* 14: 757–763.
- Sanderfoot, A.A., Kovaleva, V., Bassham, D.C., and Raikhel, NV. 2001. Interactions between syntaxins identify at least five SNARE complexes within the Golgi/prevacuolar system of the Arabidopsis cell. *Mol. Biol. Cell* 12: 3733–3743.
- Santiago, J., Dupeux, F., Round, A., Antoni, R., Park, S., Jamin, M., et al. 2009. The abscisic acid receptor PYR1 in complex with abscisic acid. *Nature* 462, 665–668.
- Saxena, I. M., and Brown, R. M. Jr. 2005. Cellulose biosynthesis: current views and evolving concepts. *Ann. Bot.* 96, 9–21.
- Scheible, W. R., Fry, B., Kochevenko, A., Schindelasch, D., Zimmerli, L., Somerville, S., et al. 2003. An Arabidopsis mutant resistant to thaxtomin A, a cellulose synthesis inhibitor from *Streptomyces* species. *Plant Cell* 15, 1781–1794.
- Scheible, W. R., Eshed, R., Richmond, T., Delmer, D., and Somerville C. 2001. Modifications of cellulose synthase confer resistance to isoxaben and thiazolidinone herbicides in Arabidopsis *Ixr1* mutants. *Proc. Natl. Acad. Sci. USA.* 98: 10079-10084.
- Scheller, H. V. and Ulvskov, P. 2010. Hemicelluloses. *Ann. Rev. Plant Biol.* 61: 263-289.
- Schneider, C. A., Rasband, W. S., and Eliceiri, K. W. 2012. NIH Image to ImageJ: 25 Years of Image Analysis. *Nat. Methods* 9:671-675.
- Schneider, J., Doring, E., Hilu, K. W., and Roser, M. 2009. Phylogenetic structure of the grass subfamily Pooideae based on comparison of plastid *matK* gene-3' *trnK* exon and nuclear ITS sequences. *Taxon* 58: 405-424.
- Scott, T.A. Jr. and Melvin, E.H. 1953. Determination of dextran with anthrone. *Anal. Chem.* 25:1656-1661.

- Sethaphong, L., Haigler, C.H., Kubicki, J.D., Zimmer, J., Bonetta, D., Debolt, S., and Yingling, Y.G. 2013. Tertiary model of a plant cellulose synthase. *Proc. Natl. Acad. Sci. USA.* 100:7512-7517.
- Shaner, D. L. 2014. *Herbicide handbook*. 10th ed. Weed Science Society of Amer. Lawrence, KS. P. p 273.
- Shedletzky, E., Shmuel, M., Trainin, T., Kalman, S., and Delmer D. 1992. Cell Wall Structure in Cells Adapted to Growth on the Cellulose-Synthesis Inhibitor 2,6-Dichlorobenzonitrile : A Comparison between Two Dicotyledonous Plants and a Gramineous Monocot. *Plant Physiol.* 100: 120–130.
- Shim I. 2014. *Forward Genetic Analysis of Cellulose Biosynthesis Inhibitor Resistance Wall Hydrolysis Sensitivity*. University of Ontario Institute of Technology.
- Slabaugh, E., Sethaphong, L., Xiao, C., Amick, J., Anderson, C. T., Haigler, C. H., and Yingling, Y. G. 2014. Computational and genetic evidence that different structural conformations of a non-catalytic region affect the function of plant cellulose synthase. *J. Exp. Bot.* 65: 6645–6653.
- Smith-Moritz, A. M., Hao, Z., Fernandez-Nino- S. G., Fangel, J. U., Verherbruggen, Y., Holman, H. N., Willats, W. G. T., Ronald, P. C., Scheller, H. V., Heazlewood, J. L. and Vega-Sanchez, M. E. 2015. Structural characterization of a mixed-linkage glucan deficient mutant reveals alteration in cellulose microfibril orientation in rice coleoptile mesophyll cell walls. *Front Plant Sci.* 6:628.
- Somerville, C. 2006. Cellulose synthesis in higher plants. *Annu. Rev. Cell Dev. Biol.* 22: 53-78.
- Somerville, C, Bauer S, Brininstool G, et al. 2004. Toward a Systems Approach to Understanding plant cell walls. *Science* 306: 2206–2211.
- Sorek, N., Sorek, H., Kijac A., Szemenyei, H.J., Bauer, S., Hematy, K., Wemmer, D.E., and Somerville, C.R. 2014. The Arabidopsis COBRA protein facilitates cellulose crystallization at the plasma membrane. *J. Biol. Chem.* 289: 34911–34920.
- Spring, D. R., 2005. Chemical genetics to chemical genomics: small molecules offer big insights. *Chem. Soc. Rev.* 34: 472-482.
- Surpin, M., Rojas-Pierce, M., Carter, C., Jicks, G. R., Vasquez, J., and Raikhel, N. V.

2005. The power of chemical genomics to study the link between endomembrane system components and the gravitropic response. *Proc. Natl. Acad. Sci. U.S.A.* 102: 4902– 4907.
- Tatento, M., Brabham, C., and Debolt, S. 2015. Cellulose biosynthesis inhibitors- a multifunctional toolbox. *J. Exp. Bot.* 67: 533-542.
- Taylor, N.G., Howells, R. M., Huttly, A. K., Vivkers, K., and Turner, S. R. 2003. Interactions among three distinct Cesa proteins essential for cellulose synthase. *Proc. Natl. Acad. Sci. USA.* 100: 1450-1455.
- Tegg, R.S., Shabala, S.N., Cuin, T.A., Davies, N.W., and Wilson, C.R. 2013. Enhanced resistance to the cellulose biosynthetic inhibitors, thaxtomin A and isoxaben in *Arabidopsis thaliana* mutants, also provides specific co-resistance to the auxin transport inhibitor, 1-NPA. *BMC Plant Biol.* 13: 76.
- Toth, R., and van der Hoorn, R. A. L. 2009. Emerging principles in plant chemical genetics. *Trends Plant Sci.* 15: 81–88.
- Tsekos, I. 1999. The sites of cellulose synthesis in algae: diversity and evolution of cellulose-synthesizing enzyme complexes. *J. Phycol.* 35: 635–655.
- Udvardi, M., K., Czechowshi, T., and Scheible, W-R. 2008. Eleven golden rules of quantitative RT-PCR. *Plant Cell* 20:1736-1737.
- Updegraff, D.M. 1969. Semimicro determination of cellulose in biological. *Materials Anal. Biochem.* 32: 420-424.
- Vain T, Crowell EF, Timpano H, et al. 2014. The cellulase KORRIGAN is part of the Cellulose Synthase Complex. *Plant Physiol.* 165, 1521–1532.
- Vandavasi, V. G., Putnam, D. K., Zhang, Q., Petridis, L., Heller, W. T., Nixon, T. B., Haigler, C. H., Kalluri, U., Coates, L., Langan, P., Smith, J. C., Meiler, J., and O'Neill, H. 2016. A Structural Study of CESA1 catalytic domain of *Arabidopsis thaliana* Cellulose Synthase Complex: Evidence for CESA trimmers. *Plant Physiol.* 170: 123-135.
- Vega-Sanchez, M., E., Verherthbruggen, Y., Christensen, U., Chen, X., Sharma, V., Varanasi, P., Jobling, S. A., Talbot, M., White, R. G., Joo, M., Singh, S., Auer, M., Scheller, H. V., and Ronald, P. C. 2012. Loss of cellulose synthase-like F6

- function affects mixed-linkage glucan deposition, cell wall mechanical properties, and defense response in vegetative tissue of rice. *Plant Physiol.* 159: 56-59.
- Vidaurre, D., and Bonetta, D. 2012. Accelerating forward genetics for cell wall reconstruction. *Front Plant Sci.* 3:119.
- Vogel, J. P. and the International Brachypodium Initiative. 2010. Genome sequencing and analysis of the model grass *Brachypodium distachyon*. *Nature* 463: 763-768.
- Vogel, J. 2008. Unique aspects of the grass cell wall. *Curr. Opin. Plant Biol.* 11: 201-207.
- Wang, T., and Hong, M. 2016. Solid-state NMR investigations of cellulose structure and interactions with matrix polysaccharides in plant primary cell walls. *J. Exp. Biol.* 67: 503–514.
- Wang, T., Park, Y. B., Cosgrove, D. J., and Hong, M. 2015. Cellulose-Pectin Spatial Contacts Are Inherent to Never-Dried *Arabidopsis thaliana* Primary Cell Walls: Evidence from Solid-State NMR. *Plant Physiol.* 168: 871-841.
- Xiao, C., Zhang, T., Zheng, Y., Cosgrove, D. J., and Anderson, C. T. 2016. Xyloglucan deficiency disrupts microtubule stability and cellulose biosynthesis in *Arabidopsis*, altering cell growth and morphogenesis. *Plant Physiol.* 170: 243-249.
- Xia, Y., Brabham C., Stork, J., Strickland, J., Ladak, A., Gu, Y., Wallace, I., and Debolt, S. 2014. Acetobixan, an inhibitor of cellulose synthesis identified by microbial bioprospecting. *PLoS ONE* 9: e95245.
- Williams, A. P. 2014. Plant growth regulators and herbicides for management of *Poa annua*: Impact of biotypes and behavior of flurprimidol in turfgrass species. University of Kentucky.
- Williamson, R. E., Burn, J. E., Birch, R., Baskin, T. I., Arioli, T., Betzner, A. S., and Cork, A. 2001. Morphology of *rsw1*, a cellulose-deficient mutant of *Arabidopsis thaliana*. *Protoplasma* 215: 116–127.
- Wightman, R., Marshall, R., and Turner, S. R. 2009. A cellulose synthase containing compartment moves rapidly beneath sites of secondary wall synthesis. *Plant Cell Physiol.* 50, 584–594.
- Worden, N, Wilkop, TE, Esteva, Esteve V, et al. 2015. CESTRIN, inhibits cellulose

- deposition and interferes with the trafficking of cellulose synthase complexes and their associated proteins KORRIGAN1 and POM2/CSII. *Plant Physiol.* 167: 381–393.
- Yoneda, A., Higaki, T., Kutsuna, N., Kondo, Y., Osada, H., Hasezawa, S., and Matsui, M. 2007. Chemical genetic screening identifies a novel inhibitor of parallel alignment of cortical microtubules and cellulose microfibrils. *Plant Cell Physiol.* 48: 1393-1403.
- Yoneda, A., Ito T, Higaki, T., Kutsuna, N., Saito, T., Ishimizu ,T., Osada, H., Hasezawa, S., Matsui, M., and Demura, T. 2010. Cobtorin target analysis reveals that pectin functions in the deposition of cellulose microfibrils in parallel with cortical microtubules. *Plant J.* 64: 657–667.
- Zhang, Y. Nikolovski, N., Sorieul, M., Velloso, T., McFarlane, H. E., Dupree, R., Kesten, C., Schneider, R., Driemeier, C., Lathe, R., Lampugnani, E., Yu, X., Ivakov, A., Doblin, M. S., Mortimer, J. C., Brown, S. P., Persson, S., and Dupree, P. 2016. Golgi-localized STELLO proteins regulate the assembly and trafficking of cellulose synthase complexes in Arabidopsis. *Nat. Commun.* 7: 11656.
- Zhao, Y., Dai, X., Blackwell, H. E., Schreiber, S. L., and Chory, J. 2003. SIR1, an upstream component in auxin signaling identified by chemical genetics. *Science* 301, 1107–1110.
- Zhong, R., Burk, D. H., Morrison, W. H., and Ye, Z. H. 2002. A kinesin like protein is essential for oriented deposition of cellulose microfibrils and cell wall strength. *Plant Cell* 14: 3101–3117.
- Zhu, J., Gong, Z., Zhang, C., Song, C., Damsz, B., Inan, G., Koiwa, H., Zhu, J., Hasegawa, P.M., and Bressan, R.A. 2002. OSM1/SYP61: A Syntaxin Protein in Arabidopsis Controls Abscisic Acid Mediated and Non Abscisic Acid Mediated Responses to Abiotic Stress. *Plant Cell* 14: 3009–3028.

Vita

1. PLACE OF BIRTH: Trenton, Illinois

2. EDUCATION:

Purdue University - Master of Science (2008 – 2011)

Western Illinois University - Bachelor of Science (2006 – 2008)

3. RESEARCH EXPERIENCE

Graduate Research Assistant University of Kentucky (2011 – Present)

Graduate Research Assistant Purdue University (2008-2011)

Pioneer Hi-Bred Pat Intern (Summer 2007)

Pioneer Hi-Bred Research Assistant (2004-2007)

5. PUBLICATIONS

Tateno, M., **Brabham***, C., and Debolt, S. 2015. Cellulose biosynthesis inhibitors-multifunctional toolbox. *J. Exp. Botany*. (accepted)

Brabham, C., Stork, J. and Debolt, S. (2015). [¹⁴C] Glucose Cell Wall Incorporation Assay for the Estimation of Cellulose Biosynthesis. *Bio-protocol* 5(18): e1589.

Brabham*, C., Lei, L., Gu, Y., Stork, J., Barrett, M., and Debolt, S. 2014. Indaziflam herbicidal action: a potent cellulose biosynthesis inhibitor. *Plant Phys*.

Xia, Y, **Brabham**, C., Stork, J., Strickland, J., Ladak, A., Gu, Y., Wallace, I., and Debolt, S. 2014. Acetobixan, an inhibitor of cellulose synthesis identified by microbial bioprospecting. *PLoS ONE* 9(4): e95245.

Brabham, C. and Debolt, S. 2013. Chemical genetics to examine cellulose biosynthesis. *Front. Plant Sci.* 3:309.

Brabham, C. B., Gerber, C. K., and Johnson, W. G. 2011. Fate of glyphosate-resistant giant ragweed (*Ambrosia trifida*) in the presence and absence of glyphosate. *Weed Sci.* 59:506-511.

Brabham, C. B., Johnson, W. G., Loux, M. M., and Dobbels, T. 2011. Control of glyphosate-resistant and glyphosate-sensitive giant ragweed in soybean with adjuvants, fomesafen, and glyphosate tank mixtures. *Crop Management* 10(1): DOI:10.1094/CM-2011-0422-02-RS.

Brabham, C. B. and Johnson, W. G. 2010. Efficacy of Ignite and Flexstar tank mixtures on giant ragweed and common lambsquarters. Crop Management doi:10.1094/CM-2010-1227-01-RS.